Master's thesis

NTNU
Norwegian University of Science and Technology
Faculty of Information Technology and Electrical Engineering
Department of Electric Power Engineering

Katrine Hansen Reisænen

# An Artificial Neural Network-Based Power Management in Hybrid Microgrid

Master's thesis in Energy and Environmental Engineering
Supervisor: Mohammad Amin
June 2021

NTNU
Norwegian University of Science and Technology

Katrine Hansen Reisænen

# An Artificial Neural Network-Based Power Management in Hybrid Microgrid

Master's thesis in Energy and Environmental Engineering
Supervisor: Mohammad Amin
June 2021

Norwegian University of Science and Technology
Faculty of Information Technology and Electrical Engineering
Department of Electric Power Engineering

NTNU
Kunnskap for en bedre verden

# Abstract

This thesis analyzes a hybrid microgrid with an artificial neural network (ANN) power management strategy. The ANN will work as a centralized controller. The purpose is to see if an ANN can control the power flow of distributed energy resources, loads, energy storage systems and the microgrids connection to the main grid. Today, the power system is going through significant changes. More and more renewable energy sources have to be injected into the power system to secure a sustainable future, and the power delivery has to be reliable. One solution is microgrids. Microgrids are systems with small energy sources, loads and energy storage units, and they can connect and disconnect to the main grid as it pleases. However, because microgrids contain uncontrollable renewable energy sources and small loads, the changes in power flow can change rapidly. The rapid changes in load and generated power can lead to an unstable system and poor power quality. Therefore, an artificial neural network centralized controller is presented as a microgrid power management method. ANNs are inspired by neurons in the brain and is trained to learn patterns. The training is performed by samples of inputs and targets from an optimal power flow (OPF) algorithm. Simulations were done for both ANN and OPF as a centralized controller in MATLAB/Simulink, and the results were examined and compared. The results showed that the centralized controller with the ANN managed to keep a good power-sharing between DERs and the grid. But the power quality and dynamic response were poor, and the limitations in the system were not withheld. Improvements in the low-level control and converters were suggested. Comparing the ANN and OPF showed that the ANN managed to follow the same trends as the OPF, but a significant error occurred in some places. Improvements as changing the architecture and training method were suggested. Further research should improve both the microgrid and ANN performance and include this power management in broader systems.

*Key Words:* Hybrid Microgrid, Microgrid Power Management, Optimal Power Flow, Artificial Neural Networks, Tertiary Control

# Sammendrag

Denne oppgaven analyserer et hybrid mikronett med et kunstig nevralt nettverk som styrer kraftflyten. Kraftflyten er analysert og det kunstige nevrale nettverket er sammenlignet med en optimal kraftflyt-algoritme. Hensikten med dette er for å se om kunstige nevrale nettverk kan bidra til å kontrollere kraftflyten av distribuert elproduksjon, laster og mikronettets tilkobling til hovednettet. I dag gjennomgår kraftsystemet store endringer. For å sikre en bærekraftig fremtid må mer og mer fornybare ressurser kobles til kraftsystemet og energiforsyningen må være pålitelig. En løsning på dette er mikronett. Mikronett er et system som inneholder små energikilder, små laster og energilagringssystemer. Det kan i tillegg kobles av og på hovednettet, alt etter hva som er praktisk og økonomisk. Men fordi mikronettet inneholder ukontrollerbare energikilder og små laster vil kraftflyten endre seg fort og drastisk. For å sikre et stabilt og pålitelig mikronett er et kunstig nevralt nettverk implementert for å styre kraftflyten. Kunstige nevrale nettverk er inspirert av nevroner i hjernen. Disse har evnen til å lære og å se sammenhenger. Læringen til dette nettverket skjer gjennom inn-verdier og ut-verdier fra den optimale kraftflyt-algoritmen. For å sjekke hvor godt det kunstige nettverket fungerer, har det blitt gjort simuleringer i MATLAB/Simulink der det nevrale nettverket fungerer som en sentralisert kontroller. Resultatene er analysert og sammenlignet med den optimale kraftflyt metoden. Resultatene viser at det nevrale nettverker klarer å styre kraftflyten bra. Dessverre er kvaliteten og den dynamiske responsen dårlig, og begrensinger ikke tatt hånd om. Forbedringer i lav-nivå kontroll og konverter er foreslått. Det nevrale nettverket følger den optimale kraftflyten bra, men noen store feil oppstår av og til. Forslag til forbedringer er å endre på arkitekturen eller treningsmetoden. Videre forskning burde fokusere på å forbedre mikronettet, det nevrale nettverket og sette det inn i et større system.

*Stikkord:* Hybrid Mikronett, Strømstyring, Optimal Kraftflyt, Kunstige Nevrale Nettverk, Tertiær Kontroll

# Preface

This thesis is the final chapter of the five year Master of Science program Energy and Environmental engineering at the Norwegian University of Science and Technology (NTNU). My specializations has been in electric power systems and is done for the Faculty of Information Technology and Electrical Engineering.

Prior to this thesis, in the autumn 2020, a specialization project was done. My project had focus on the stability of a system dominated by power electronics, and has formed a basis prior to writing this thesis

My supervisor through this last year of studying is Associate Professor Mohammad Amin.

# Acknowledgements

These last five years of studying has been an experience with a lot of ups and downs. I want to give a big thanks to my friends and classmates that have been a part of it. Experiencing good times and bad times together has been a part of making these years great.

I also want to thank my family for being a great support, even though they have no idea what I am writing about or learning.

Lastly, I want to thank my supervisor Mohammad Amin for his great help and guidance during this thesis and the last year. He has always been available when needed and always has a good answer to my questions.

June 2021, Trondheim

Katrine Hansen Reisænen

# Contents

# List of Tables

# List of Figures

# Abbreviations

**ANN** - Artificial Neural Network

**CL** - Constant Load

**DER** - Distributed Energy Resource

**ESS** - Energy Storage System

**EV** - Electrical Vehicle

**MPPT** - Maximum Power Point Tracking

**MSE** - Mean Square Error

**OPF** - Optimal Power Flow

**PCC** - Point of Common Coupling

**PWM** - Pulse Width Modulation

**PV** - Photo Voltaic

**SI** - Solar Irradiance

**SOC** - State of Charge

**SUDC** - Self-Synchronized Universal Droop Controller

**VL** - Variable Load

**VSC** - Voltage Source Converter

# Chapter 1

# Introduction

## 1.1 Background and Motivation

### 1.1.1 Future Power Systems

Today's power electricity production comes from a variety of sources. The three most used energy sources are coal, gas and hydropower [1]. Typical for these three sources is that they can generate much power with large generators, and they are predictable. Unfortunately, only hydropower is renewable. Non-renewable resources have to be replaced by renewable to secure a sustainable future. In the last ten years, the use of renewable sources as wind, solar and hydro has increased, fig.1.1.

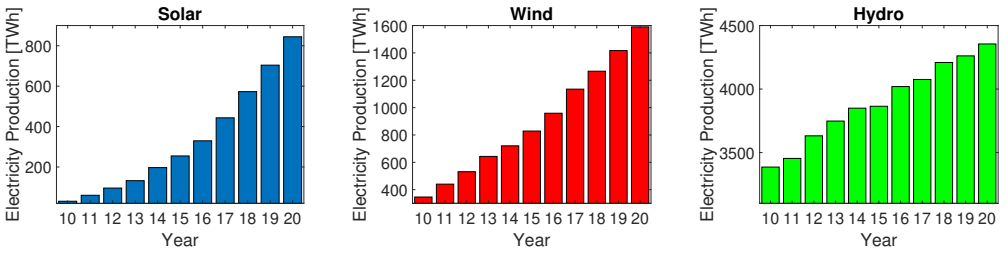


**(a)** **(b)** **(c)**

**Figure 1.1:** Plots of worldwide energy production from 2010 to 2020 from: (a) Solar; (b) Wind;(c) Hydro [1].

The traditional power grid is going through significant changes due to the rising use of renewable energy sources, the development of energy storage systems, and the customer's ability to buy and sell power [2]. At the same time is the standard of living increasing. Furthermore, the need for electricity is increasing [3]. Thus, the power delivery has to be

reliable and have good quality.

Microgrids are small systems with energy sources and loads. One of the main characters of a microgrid is being self-sufficient when disconnected to the grid [4]. Microgrids often contain loads, distributed energy resources (DERs) and energy storage systems (ESS). Distributed energy resources are small generation units located close to the user, such as solar PV, windmills or fuel cells. Energy storage systems, such as batteries, secures the delivery of power when the power sources can not deliver enough. When faults or disturbances in the main grid occur, the microgrid can disconnect and supply itself. That means that the microgrid is very reliable. In addition, to have a reliable power delivery, the microgrid can consider energy prices and buy and sell power when the prices are favourable. Fig.1.2 shows an example microgrid. However, the microgrid has some issues.

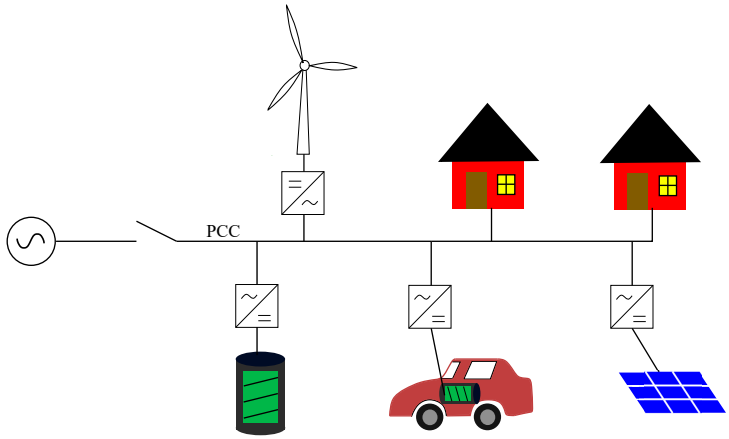


**Figure 1.2:** Example microgrid in islanded mode. Wind and solar power sources, batteries and electric vehicles (EV) are to secure power delivery, and houses and also the EV are the loads.

### 1.1.2 Microgrids Power Management

Because a microgrid consists of small energy sources, it has low inertia. Due to the low inertia, it is challenging to maintain a good energy balance and stability. The energy sources can also be hard to predict and rely on, as the power production can change quickly. A quick change in power production can, for example, be wind power if the wind suddenly calms down. A power management strategy is needed to balance the power and load. In this thesis, a centralized controller is proposed to balance the load in a hybrid microgrid. A centralized controller takes in measured values from the microgrid units, processes them, and gives an output [5]. In this case, the output is the reference values to the controllers of the different converters. Fig.1.3 shows an example of how a centralized controller works.

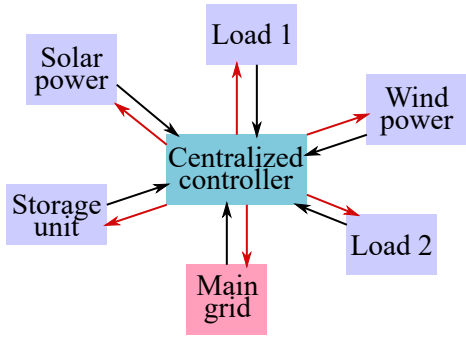


**Figure 1.3:** A centralized controller receives information from loads, sources, storage units and the main grid and sends information back.

### 1.1.3 Optimal Power Flow

Optimal power flow is based on controlling the power flow to optimize a specific parameter [6]. For example, the primary goal can be to minimize the costs or to minimize the power losses. When calculating the optimal power flow, system constraints and operating limits have to be considered. Constraints can, for example, be AC voltage limits and power flow limits. Different types of programming can be used for optimal power flow, for example, linear programming and different types of non-linear programming. In this thesis, optimal power flow is used as a centralized controller to control the power flow in the microgrid by taking in measured values and giving out references to the grid switch, power reference of the VSC and the current reference to the EV. The purpose is to keep the power losses at a minimum while being connected to the grid for a minimum amount of time and keep the microgrid stable.

### 1.1.4 Artificial Neural Networks

In the human brain, there are millions and millions of neurons. The neurons are connected and decide how a human thinks. Throughout the years, the neurons in our brains learn new things, patterns and way of thinking. The idea behind artificial neural networks is to have a computer that learns and can solve tasks like a human brain [7]. For example, an ANN can predict the weather based on experience and training.

A simple ANN consists of an input layer, hidden layers and one output layer. The numbers of inputs and outputs can vary. In each hidden layer, there are a number of neurons. The neurons take in values from the input or other hidden layers, multiply them with weights and add a bias. The output goes through an activation function and to another hidden layer or the output. To get an ANN to work as pleased, it has to go through a training process. The training process changes the value of the weights and bias to get the wanted output. Fig.1.4 shows a neural network with two inputs, one hidden layer with

three neurons, and two outputs. In this thesis, the ANN is used as a centralized controller. The training process is performed with samples from the optimal power flow. The goal is to have an ANN centralized controller that works well as a power management strategy and works as good as an OPF centralized controller. Having an ANN as a centralized controller can give some advantages. It is good at predictions, have a low computing time, can see complex, non-linear relationships between parameters, and can still work even though one input is missing [8].

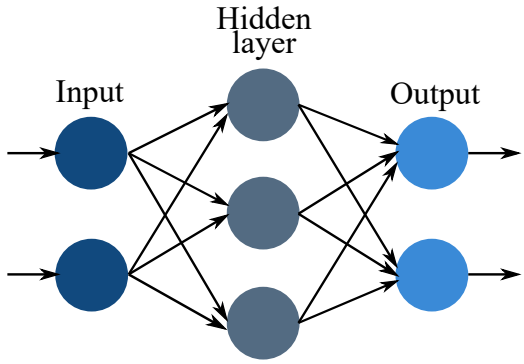


**Figure 1.4:** An ANN with two inputs, one hidden layer with three neurons and an output layer with two outputs.

### 1.1.5 Problem Statement

This thesis focuses on using an artificial neural network as a centralized controller for power management of a hybrid microgrid. The goal is to secure that loads have a stable and sufficient energy supply. Simulations are done in Simulink/MATLAB to see how the ANN works as a power management strategy. The power from and to all the units are examined and compared to an OPF algorithm. The simulations are done with one base case scenario, one scenario with abnormal change in load, one scenario with abnormal change in solar irradiance, and one with fully discharged batteries.

### 1.1.6 Related Work

Some research combining neural network and microgrid control has been performed. In [9] is PI-controllers replaced by ANN to control the frequency in an interconnected microgrid. The results have shown that the ANN gave better results than the original controller. [10] also proposes ANN instead of PID controllers, showing improvements in frequency. [11] proposes a system with a PV inverter control of ANN. The ANN gave less total harmonic distortion and a better voltage and current quality. [12] proposes ANN to update the voltage and frequency parameters when a fault occurs in the network, with good results. Furthermore, [13] uses ANN to forecast and predict solar power to handle

the insecurity that comes with it. [14] is predicting the renewable energy sources and the load to switch on and off different sources to maintain a power balance in the system. This research is closest to this thesis.

## 1.2 Objectives

This thesis is focusing on microgrid power management using an artificial neural network. An ANN is made and trained with samples from an optimal power flow algorithm, verified and tested in Simulink/MATLAB. This research result gives a clue if ANN can work as a power management strategy and is suitable for optimizing power flow in a microgrid. The main objectives of this thesis are:

- To analyze the power management of a hybrid microgrid controlled by an artificial neural network.
- To analyze the artificial neural network performance compared to an optimal power flow algorithm.

## 1.3 Purpose

This thesis aims to see if artificial neural networks can optimize the power flow in a hybrid microgrid as a centralized controller. It will be examined if the ANN follows the OPF model and if the microgrid's performance regarding to power sharing, quality and behaviour is intact. The results are given by simulations in MATLAB/Simulink.

## 1.4 Scope of the Thesis

A few assumptions have been made to focus on the main objective and limit the difficulty in this thesis. Following assumptions and simplifications has been made:

- The electric vehicle in the microgrid does not charge or discharge when it is disconnected.
- When analyzing the microgrid's performance, plots of power going in and out of the units are presented, the same yields for the voltages and current.
- When simulating in Simulink, only 24 seconds are simulated, where each second accounts as an hour.

## 1.5 Contribution

This thesis has contributed to the research of artificial neural networks as a centralized controller in a microgrid. The contributions of the thesis include:

- In chapter 2, general information about microgrids are presented, including the microgrid used for further simulations.
- In chapter 3, the control system and converter are described, including values for the example microgrid.
- In chapter 4, an optimal power flow method for the hybrid microgrid is presented. The OPF model is presented as a centralized controller for a microgrid and is simulated in Simulink. The results are presented in plots and discussed.
- In chapter 5, an artificial neural network is presented as a centralized controller in a microgrid. The ANN is trained using inputs and targets from the OPF algorithm presented in chapter 4. Simulations are done to see if the ANN manages to follow the criteria to be a sufficient power management strategy. The performance of the ANN is compared to the OPF algorithm. The results are presented and discussed.

## 1.6 Structure

This thesis first gives an overview of microgrids and the microgrid model used in this thesis. Then, the converters and control systems are explained to give a bigger picture of how the centralized controller works and which references are needed. Furthermore, the optimal power flow and artificial neural networks are presented in their chapters as a centralized controller and results are given. Lastly, a conclusion is made. Each chapter starts with a short introduction of the topic in the chapter.

*Chapter 2:* Includes general and basic information about microgrids. It explains the different types of microgrids and which resources that are common to have. It also goes through control methods used today and the pros and cons of using them. This chapter sets the microgrid and different types of control systems in a bigger perspective to see the need for a more robust control system. The microgrid used for simulations in this thesis is presented. In the end, the per-unit values are presented.

*Chapter 3:* This chapter includes the topology of the converters and its control system needed. The chapter goes through the topology of the voltage source converter and the control system used: the self-synchronized universal droop controller and the pulse width modulation. The chapter also goes through the DC-DC converters: the bidirectional converter and step-up converter, and the control systems used: current control, voltage control and fuzzy logic.

*Chapter 4:* This chapter explains optimal power flow and the type of OPF used here. An OPF algorithm is presented and simulated using MATLAB/Simulink. The results from the simulations are presented.

*Chapter 5:* Artificial neural networks are explained, and a model is presented. The ANN is trained using inputs and targets from the OPF method, and the mean square error verifies the network. Simulations are done in MATLAB/Simulink to see how the ANN works as a power management strategy. The outputs of the ANN is also compared to the OPF algorithm. The results are presented and discussed.

*Chapter 6:* Lastly, the results and work in this thesis are concluded. Further work is presented.

# Chapter 2

# Microgrids

## 2.1 Introduction

A microgrid is in [15] defined as *"a cluster of loads, Distributed Generation (DG) units and ESSs operated in coordination to reliably supply electricity, connected to the host power system at the distribution level at a single point of connection, the Point of Common Coupling (PCC)."* This chapter gives an overview of microgrids and their operation. It explains the different modes and types of a microgrid. Furthermore, the energy sources and loads are described. Then, microgrids' control and power management are explained. Lastly, the microgrid model for further use in this thesis is described, together with the sources, loads and energy storages.

## 2.2 Grid Connected Mode and Islanded Mode

Microgrids can work both by themselves and also when connected to the grid. This feature is one of the main characteristics of microgrids. When the microgrid is disconnected from the main grid, it is in islanded mode (often termed stand-alone mode or autonomous mode). Furthermore, when the microgrid is connected to the main grid, it is in grid-connected mode. This connection/disconnection usually happens with a switch [16].

The reasons to keep the microgrid disconnected from the grid are usually [16][17]:

- Because of maintenance or economics (pre-planned).
- Because of fault, disturbances, or voltage fluctuations in the main grid (unplanned).

With the ability to disconnect from the grid, the microgrid is considered to enhance

energy security, improve power quality, reduce emissions and losses, and improve the system's economics [17][18]. For example, when the power prices are very high, the microgrid can discharge batteries by delivering power to the grid or its loads. Furthermore, when the power prices are low, the microgrid can charge the batteries.

## 2.3 Energy Sources and Loads

A microgrid mainly contains distributed energy resources (DERs, often termed distributed generation units), energy storage systems, and loads.

### 2.3.1 Distributed Energy Resources

Distributed energy resources (DER) are small energy generators often located near the user [19]. Examples of DERs are photovoltaic (PV), wind power, gas turbines, and fuel cells [20]. Because the DERs are placed closer to the consumer, the power losses are lower [21]. The DERs are on a smaller scale and are easier to control.

### 2.3.2 Energy Storage Systems

Energy storage systems are included to enhance reliability in the microgrid [22]. Energy storage systems are essential if the DERs are hard to predict, for example, if the microgrid only contains PV and wind power. The ESS allows charging when the power production in the microgrid is high, or the power prices are low, and discharge if the power production is low or the prices are high. Types of ESS can, for example, be electrochemical batteries, supercapacitors, and flywheel energy storage. Lithium-ion batteries are the most used because of their relatively low energy-weight ratio and low energy loss when not in use [23].

### 2.3.3 Loads

The loads in microgrids can both constant and variable, and they can also be DC or AC. For example, one type of load can be an electric vehicle, and another can be a house.

## 2.4 Types of Microgrid

Microgrids can be of different types, sizes and have different applications. When it comes to types, there are three of them: AC microgrid, DC microgrid, and hybrid (AC/DC)microgrid [24][25].

**AC microgrid:** Consist of one AC bus, practical with many AC loads and sources.

**DC microgrid:** Consist of one DC bus, practical with many DC loads and sources.

**Hybrid microgrid:** Consist of one DC bus and one AC bus. Practical with variable types of loads and sources.

When choosing the type of microgrid, the loads and sources have to be considered. For example, if there are only DC loads and sources, one will choose the DC microgrid. Usually, a hybrid microgrid would be chosen to avoid many AC/DC converters when having various sources. Fewer converters reduce both costs and losses within the microgrid. Because of this, the rest of the thesis is focusing on the hybrid microgrid. For further readings, see [26]. Fig.2.1 shows an AC microgrid, a DC microgrid, a hybrid microgrid with one DC load and source and one AC load and source. It can be observed that the hybrid microgrid demands three converters, and the others need four.

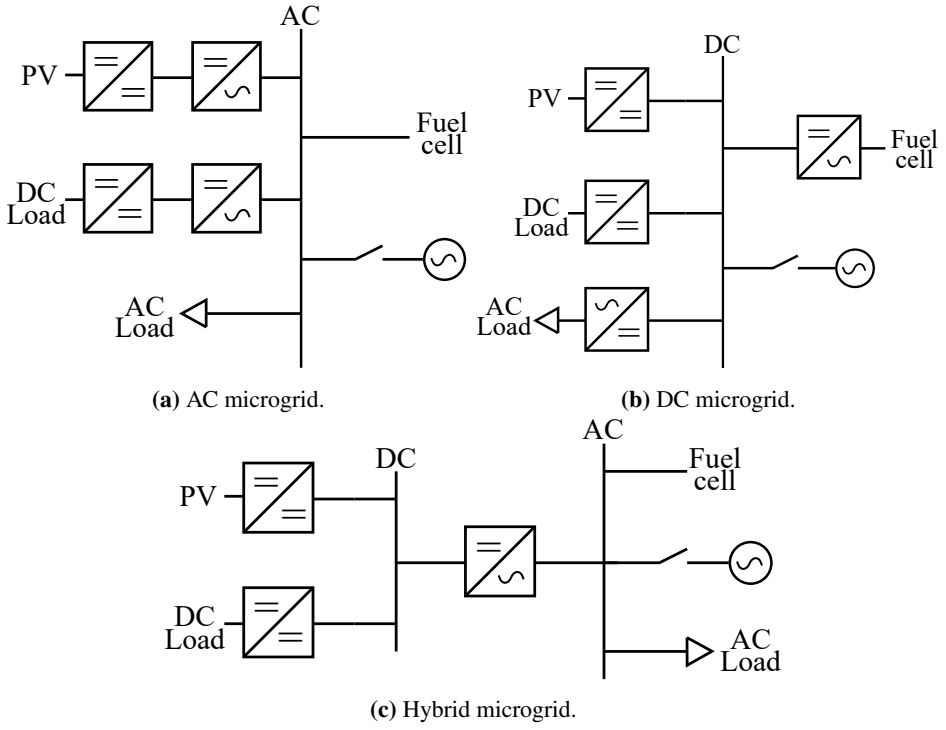


**(a)** AC microgrid.

**(b)** DC microgrid.

**(c)** Hybrid microgrid.

**Figure 2.1:** Types of microgrids. (a) AC microgrid; (b) DC microgrid; (c) Hybrid microgrid.

## 2.5 Control of Microgrid

### 2.5.1 Converter Control

When the microgrid is connected to the grid, the microgrid usually follows the voltage and frequency from the main grid. However, when the microgrid is in islanded mode, it has to dictate the voltage and frequency [16]. Because of this, there is a need for different types of converters in a grid with an AC bus. The types of converters are grid-forming,grid-feeding, and grid-supporting [21].

**Grid-forming converter:** The grid-forming converter is an ideal voltage source and sets the reference voltage and frequency, V* and f*. This converter is often connected to a reliable source, for example, energy storage. Typical control systems include current control and/or voltage control.

**Grid-feeding converter:** This is typically a current source like wind power or solar power. This control is often a high-level controller, which sets the reference active and reactive power, P* and Q*. This controller can, for example, be a maximum power point tracker.

**Grid-supporting converter:** This converter contributes to regulating the voltage and frequency by regulating the active and reactive power delivered to the microgrid. The converter can be controlled as a voltage source or a current source.

A grid-forming converter is essential to operate a microgrid in islanded mode. It is not enough with a grid-feeding and a grid-supporting converter. For example, the voltage source converter is ideally a grid-forming converter when the microgrid is in islanded mode and a grid-supporting converter when the microgrid is grid-connected.

### 2.5.2 Microgrid Control

The control of a microgrid can be studied as a hierarchy of four levels. At the bottom, there is the inner control, then the primary control, above there is secondary control, and on top tertiary control [21][27], see fig.2.2.

**Inner control loops/level 0:** Voltage and current regulations, here goes the different types of control loops.

**Primarily control/level 1:** Local control. To control local frequency, voltage, and current to make the system stable. Local control can be, for example, a droop controller or virtual impedance.

**Secondarily control/level 2:** Correcting errors in voltage and frequency. It is responsible for keeping the voltage between the accepted limits. These are communication systems such as WAMS.

**Tertiary control/level3:** The part of the control that optimizes the microgrid's performance by controlling the active- and reactive power reference for the DERs and the flow to or from the main grid.

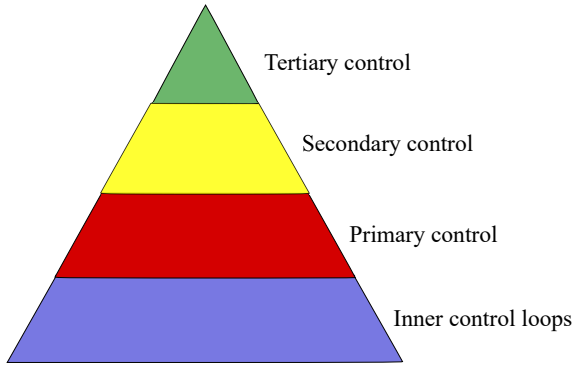


**Figure 2.2:** Hierarchical control.

The microgrid control can also be split into low-level control and high-level control. The low-level control is the control of each converter, and the high-level control is the control of the whole microgrid.

## 2.6 Power Management

Power management strategies for microgrids are essential to secure the operation of a microgrid. Power management is for microgrids with two or more DERs [28] and ensures that the wanted power, voltage, current, and frequency are obtained [29]. Unlike the energy management of microgrids, power management does not consider the economic aspect and is short-term management. Power management ensures that the specific limits are not exceeded, such as capacity limits, to ensure the microgrid's stable operation and reduce power losses and keep an efficient power-sharing. Power management is done by assigning both real and reactive power references for the DERs. Power management strategies should [28]:

- Keep efficient load sharing between DERs.
- Consider limits of DERs, for example, load limits, costs, environmental impact.
- Maintain the power quality, for example, keeping a good voltage profile, avoid voltage fluctuations.
- Improve the dynamic response due to transients.

Power management can be classified into two groups: active power-sharing and droop control. Examples of active power-sharing are centralized controllers, master-slave, and average load sharing. Common for active sharing techniques is that the DERs are close

to each other and use communication systems for control. The other strategy is droop control. Droop control is implemented in grid-supporting converters and does not use communication channels [21][30]. The active load sharing has a faster response, but communication is critical. The droop control does not need communication links and is thus more reliable but slower. For further readings about power management strategies, see [30].

The power management strategy for this thesis is the centralized controller. The centralized controller is a secondary control strategy that takes in information from the microgrid units, processes the information, and sends information back to the units [5]. The information the controller input is the time, state of charges, solar irradiation, load and whether the electric vehicle is connected or not. The output is the active power reference to the voltage source converter, current reference to the EV and the grid switch reference. The inputs, outputs and control strategy will also be explained in later chapters. Because the controller sends references to the grid switch, the controller is also a tertiary control strategy. A drawback with this type of controller is the reliability of the communication link and the lack of easily adding or removing units. An artificial neural network centralized controller can hopefully eliminate these drawbacks.

## 2.7 Microgrid Model

The microgrid for this thesis is presented in fig.2.3. The microgrid is a low voltage, hybrid microgrid, and thus it consists of a DC bus and an AC bus. There is one solar PV connected with a boost converter on the DC bus, one battery energy storage system connected with a bi-directional converter, and an electric vehicle system also connected with a bidirectional converter. On the AC bus, there are two AC loads, one constant load and one variable load. On the AC bus, the microgrid can connect to the main grid through a switch. The connection between the AC and DC bus goes through a voltage source converter.

The PV's task is to deliver power and is considered the primary power source. It is renewable but unfortunately not controllable. A battery energy storage system is implemented in the microgrid to secure power delivery on days and times when there is no sun. An electric vehicle (EV) is implemented to work as an additional power source. The electric vehicle switches on when it can supply or receive power and is off when the power source is unavailable. For simplifications, the EV does not discharge when it is disconnected.

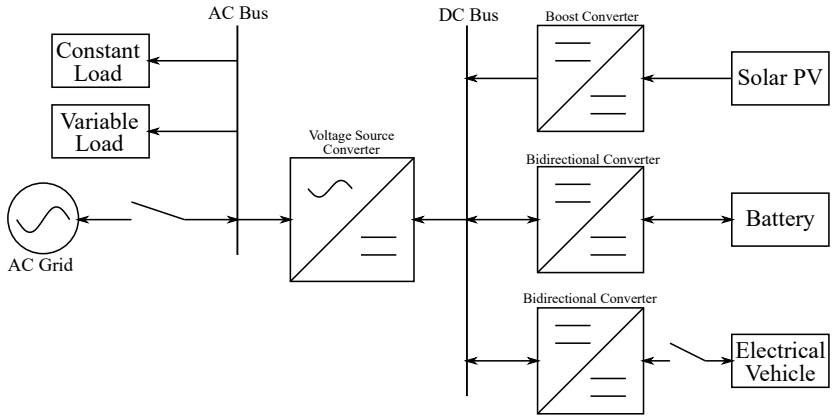


**Figure 2.3:** A hybrid microgrid model for this thesis.

The BESS converter will work as a grid-forming converter on the DC side, setting the voltage. The same will the VSC on the AC side when the microgrid is in islanded mode. Ch.3 presents the topology of the converters, the converter's control systems, and related system values.

For power management, an artificial neural network is presented as a centralized controller in ch.5. The ANN will both be a secondary and tertiary control strategy, as it controls the microgrid performance by giving references to the converter controllers and the grid switch.

### 2.7.1 System Values

This microgrid test system is built in Simulink/MATLAB, Appendix A.1. Some general nominal values for the microgrid are given in tab.2.1.

**Table 2.1:** Nominal values for the AC bus and DC bus. The nominal AC voltage is the instantaneous line-to-line voltage.

| Parameter | Value |
|---|---|
| $f_n$ | 50 Hz |
| $V_{AC,n}$ | 400 V |
| $V_{DC,n}$ | 400 V |
| $R_{grid}$ | 1.2 m$\Omega$ |
| $L_{grid}$ | 0.51 $\mu$H |

### Solar PV

The values for the solar arrays are given in tab.2.2. The solar array used is the Fire EnergyFE5P-240M with a maximum power of 243.5 W. The power from one solar PV depends on the solar irradiation level, where 1000 W/m$^2$ is the maximum, eq.2.1. The total power from all the solar arrays is given by eq.2.2. The power out also depends on temperature, but is neglected in this thesis.

$$P_{PV} = \frac{SI}{1000} \cdot P_{PV,max} \tag{2.1}$$

$$P_{PV,tot} = P_{PV} \cdot \textit{Parallel strings} \cdot \textit{Series-connected modules} \tag{2.2}$$

**Table 2.2:** Values for the solar array.

| Parameter | Value |
|---|---|
| $P_{PV,max}$ | 243.5 W |
| Parallel strings | 40 |
| Series-connected modules | 2 |
| $P_{PV,tot,max}$ | 19.48 kW |

### Battery Energy Storage System

The battery energy storage consists of a lithium-ion battery. The values for the battery are given in tab.2.3.

**Table 2.3:** Battery values for the battery energy storage system.

| Parameter | Value |
|---|---|
| $V_{BESS,n}$ | 120 V |
| Capacity | 180 Ah |
| Initial state of charge | 50% |
| Battery response time | 0.1 s |

### Electric Vehicle

The electric vehicle source is a lithium-ion battery, with values given in tab.2.4.

**Table 2.4:** Battery values for the electric vehicle.

| Parameter | Value |
|---|---|
| $V_{EV,n}$ | 120 V |
| Capacity | 180 Ah |
| Initial state of charge | 50% |
| Battery response time | 0.1 s |

### Constant Load

The value for the constant load is provided in tab.2.5.

**Table 2.5:** Value of the constant AC load.

| Parameter | Value |
|---|---|
| $P_{load,c}$ | 8 kW |

### Variable Load

The value for the variable load is given in tab.2.6. The load is changing as the demand for power changes throughout the day.

**Table 2.6:** Value of the variable AC load.

| Parameter | Value |
|---|---|
| $P_{load,v}$ | 0 to 10 kW |

## 2.8 Per Unit

To easier represent and compare the parameters in the system, per unit representation is used. The base value for the apparent power, Sb, is set to be 20 kVA, and the nominal instantaneous value for the voltage and frequency is set to be 400 V and 50 Hz. The instantaneous, line-to-ground base values are found by using the equations given in 2.3 and 2.4. The final base values for this system are given in tab.2.7. Base values for the power sources and loads are presented in tab.2.8. These base values are given by the maximum power they can deliver or demand.

$$V_b = \frac{1}{\sqrt{3}} V_n \qquad I_b = \frac{2}{3} \frac{S_b}{V_b} \qquad \omega_b = 2\pi f_b \tag{2.3}$$

$$Z_b = \frac{V_b}{I_b} \qquad L_b = \frac{Z_b}{\omega_b} \qquad C_b = \frac{1}{\omega_b Z_b} \tag{2.4}$$

**Table 2.7:** Base values for the AC system.

| Parameter | Value |
|---|---|
| $S_b$ | 20 kVA |
| $V_b$ | 230.94 V |
| $I_b$ | 57.74 A |
| $f_b$ | 50 Hz |
| $\omega_b$ | 314.16 rad/s |
| $Z_b$ | 4 Ω |
| $L_b$ | 12.7 mH |
| $C_b$ | 795.77 $\mu F$ |

**Table 2.8:** Base values/maximum values for constant load, variable load, PV, EV, BESS and solar irradiation.

| Parameter | Value |
|---|---|
| $P_{cl}$ | 8 kW |
| $P_{vl}$ | 10 kW |
| $P_{PV}$ | 15 kW |
| $P_{BESS}$ | 9 kW |
| $P_{EV}$ | 9 kW |
| SI | 1000 W/m$^2$ |

# Chapter 3

# Converters and Control Systems in Microgrid

## 3.1 Introduction

Different converters are essential to control the voltage and current in a microgrid and convert from AC to DC power or from DC to AC. This chapter describes the converters necessary for the microgrid presented in ch.2.7. The converters shown are the voltage source converter, bidirectional converter, and boost converter. The control system to each converter is also presented, including system values for the model in Simulink/MATLAB.

## 3.2 AC-DC Switch-Mode Converter

An AC-DC switch-mode converter is needed to transform the voltage from AC to DC. There are two dominant types of converters in the industry: the voltage source converter and the line commutated converter [31]. In this thesis, the voltage source converter (VSC) is used.

### 3.2.1 Voltage Source Converter

The voltage source converter is the most used converter today [32][33] and can give out a controlled voltage with the wanted amplitude and angle [34]. The VSC can handle a black start, which means that it can start up without being connected to the main grid. The black start is an advantage if the microgrid is in islanded mode.

The VSC uses switching devices, such as IGBTs or MOSFETs to control the voltage. However, because of the switching devices, the losses are relatively large, and the amount of power it can handle is limited. Fig.3.1 shows a two-level VSC with six IGBTs con-

nected to the grid through an LCL filter.

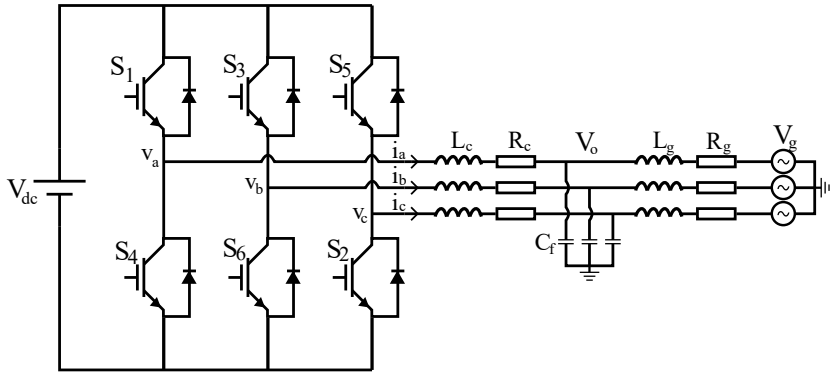


**Figure 3.1:** Two-level voltage source converter with an LCL filter connected to the grid.

A control system and an LCL filter are needed to get a suitable voltage and current quality to the grid.

### LCL filter

Because the VSC uses switching devices to control the voltage to the grid, high-order harmonics and high current ripples can occur. To avoid the harmonics and ripples, an LCL filter is implemented [35]. The LCL filter is a low pass filter consisting of a converter impedance, a capacitor, and a grid impedance. Fig.3.2 shows a circuit diagram of the LCL filter.

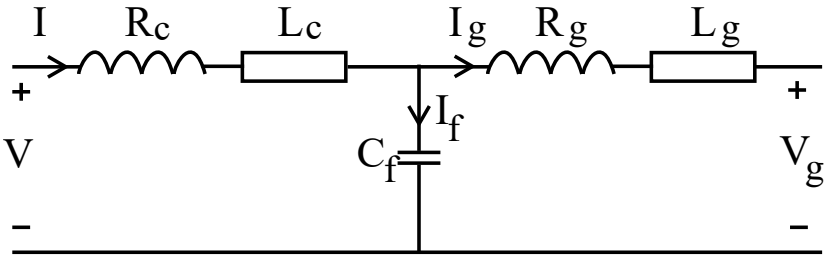


**Figure 3.2:** Circuit diagram of an LCL filter.

Eq.3.1, rewritten to eq.3.2, is used to calculate the converter impedance. The equation decides the converter impedance based on the wanted current ripple out. The wanted current ripple is typically between 15 to 25 percent of the rated current [36].

$$\Delta i_{L_c,max} = \frac{1}{8}\frac{V_{dc}}{L_c f_{sw}} = 15\% - 25\% * i_{rated} \tag{3.1}$$

$$L_c = \frac{1}{8}\frac{V_{dc}}{0.25 \cdot i_{rated} f_{sw}} \tag{3.2}$$

The capacitance and grid impedance to the filter is decided by the fact that the filter's cut-off frequency should be between ten times the grid frequency and 0.5 times the converter's switching frequency, $10 \cdot f_g$ and $0.5 \cdot f_{sw}$ [37]. The transfer function of the filter is found to determine the cut-off frequency, eq.3.3.

$$\frac{i}{v_{in}} = \frac{C_f L_g s^2 + C_f R_g s + 1}{L_c C_f L_g s^3 + (R_c C_f L_g + L_c C_f R_g)s^2 + (L_c + L_g + R_c C_f R_g)s + (R_c + R_g)} \tag{3.3}$$

Current division is used to find the transfer function from the output current to the input current, eq.3.4 and eq.3.5.

$$i_g = \frac{Z_f}{Z_f + Z_g} i \tag{3.4}$$

$$\frac{i_g}{i} = \frac{1}{L_g C_f s^2 + R_g C_f s + 1} \tag{3.5}$$

Inserting eq.3.5 into eq.3.3 gives eq.3.6. The function in eq.3.7 is described by the characteristic function $A(s) = s^2 + 2\zeta\omega_0 + \omega_0^2$, where $\omega_0$ provides the bandwidth and thus the cut-off frequency.

$$\frac{i_g}{v_{in}} = \frac{1}{L_c C_f L_g s^3 + (R_c C_f L_g + L_c C_f R_g)s^2 + (L_c + L_g + R_c C_f R_g)s + (R_c + R_g)} \tag{3.6}$$

$$\frac{i_g}{v_{in}} = \frac{1}{L_c L_g C_f s[S^2 + (\frac{R_g}{L_G} + \frac{R_c}{L_c}) + \frac{R_c R_g C_f + L_c + L_g}{L_c L_g C_f}] + R_c + R_g} \tag{3.7}$$

The bandwidth is provided in eq.3.8. By testing and inserting values for the capacitor and grid inductance, the resulting bandwidth can be found.

$$\omega_0 = \sqrt{\frac{R_c R_g C_f + L_c + L_g}{L_c L_g C_f}} \tag{3.8}$$

### Self-Synchronized Universal Droop Controller

The control system used for the voltage source converter is the self-synchronized universal droop controller (SUDC). The universal droop controller is explained in [38] and is a droop controller stable for output impedances with an angle that changes from $-\frac{\pi}{2}$ to $\frac{\pi}{2}$ rad.

The SUDC is a controller that can achieve synchronization both before and after grid connection. A synchronization unit only for that matter, for instance, a phase-locked loop, is removed. When the converter is in islanded mode, the controller works as a universal droop controller. When the converter is grid-connected, the controller can work in two ways: set mode and droop mode. The set mode makes sure that the desired amount of power is transferred to the grid. The droop mode changes the power according to the grid frequency and/or voltage. In addition to those two modes is a self-synchronizing mode. This control system is further explained in [39]. For further reading, [40] uses this control system with anti-islanding protection, and [41] includes a re-synchronization mechanism. Fig.3.3 gives a block diagram of the SUDC.

The SUDC operates with three different switches to switch modes. Tab.3.1 shows a summary of the modes and switching references. The first switch $S_C$ switches between the virtual current and the grid impedance, eq.3.9. The virtual current is used when the terminal voltage of the microgrid is connected to the grid voltage.

$$i = \begin{cases} \frac{v_0 - v_g}{Ls+R}, & S_c = positions \\ i_g, & S_c = positiong \end{cases} \tag{3.9}$$

The voltage and angle given to calculate the reference voltage to the pulse width modulation are provided by eq.3.10 and 3.11. In eq.3.10, the $V_d$ changes depending on the mode, and the centralized controller gives the active power reference. In eq.3.11, the $\omega_d$ is changing depending on the mode and the reactive power reference is set to 0.

$$E = \frac{1}{s}(V_d + n(P^* - P)) \tag{3.10}$$

$$\theta = \frac{1}{s}(\omega^* - \omega_d - m(Q^* - Q)) \tag{3.11}$$

There are two switches, $S_P$ and $S_Q$, implemented to switch between set mode and droop mode. The switch, $S_P$, is open in set mode and closed in droop mode for the active power. The switch, $S_Q$, is closed in the set mode for the reactive power and open in droop mode. Eq.3.12 and 3.13 give the equations of $V_d$ and $\omega_d$ when the switch is closed or open.

$$V_d = \begin{cases} 0, & S_P = OPEN \\ K_e(E^* - V_0), & S_P = CLOSED \end{cases} \tag{3.12}$$

$$\omega_d = \begin{cases} 0, & S_Q = OPEN \\ \frac{mK}{s}(Q^* - Q), & S_Q = CLOSED \end{cases} \tag{3.13}$$

For $S_Q$, assuming the CLOSED switch gives a pulse 1, and the OPEN switch provides 0.

The voltage E and angle $\theta$ is made to a three-phase voltage presented in eq.3.14. The output is the three-phased voltage minus the current out of the converter times a resistance, eq.3.15.

$$e = \begin{cases} Ecos(\theta) \\ Ecos(\theta - \frac{2\pi}{3}) \\ Ecos(\theta + \frac{2\pi}{3}) \end{cases} \tag{3.14}$$

$$v_g = e - R_v i_c \tag{3.15}$$

**Table 3.1:** Different modes of the SUDC. The modes marked with D is droop mode, the non-marked is set mode.

| **Mode Type** | $S_C$ | $S_P$ | $S_Q$ |
|---|---|---|---|
| Self-synch. mode | s | OPEN | CLOSED |
| P-mode, Q-mode | g | OPEN | CLOSED |
| $P_D$-mode, Q-mode | g | CLOSED | CLOSED |
| P-mode, $Q_D$-mode | g | OPEN | OPEN |
| $P_D$-mode, $Q_D$-mode | g | CLOSED | OPEN |

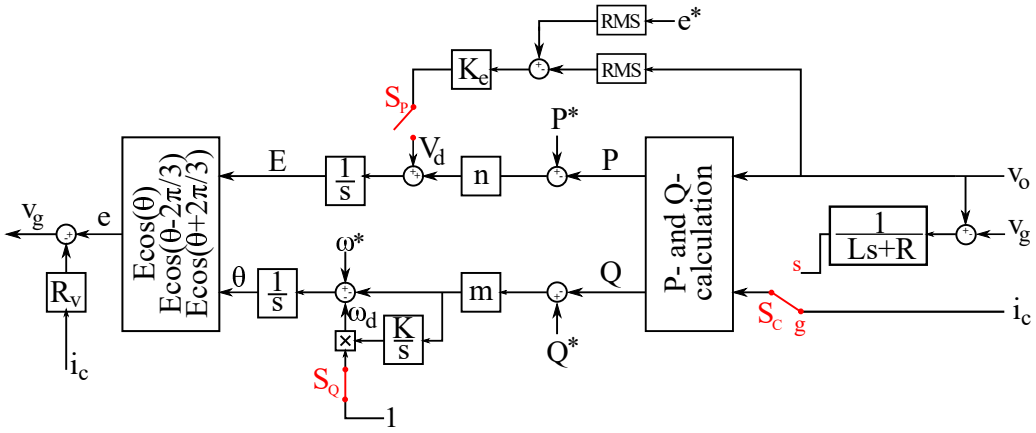


**Figure 3.3:** Self-synchronized universal droop controller in set-mode. The switches are marked in red.

### Pulse Width Modulation

The pulse width modulation (PWM) controls the average output from a converter [42]. The PWM takes a duty cycle D, eq.3.16, and controls the converter by switching on and off according to the duty cycle. The switching frequency is fixed and chosen based on the current ripple and losses [43]. With higher frequency comes a lower ripple but higher losses. Moreover, with lower frequency comes higher ripple but lower losses.

$$D = \frac{V_{out}}{V_{DC}} \tag{3.16}$$

### Voltage Source Converter and SUDC Values

Tab.3.2 gives the values for the converter and LCL filter. By inserting the resistances, inductances and capacitor values in eq.3.8, the bandwidth for the filter can be calculated. The bandwidth when using the grid resistance in tab.2.1 is 12 607.25 rad/s or 2006.5 Hz. This bandwidth is inside the wanted limits.

**Table 3.2:** Values for converter and LCL filter. Inductance number one is the converter inductance, and inductance number two is close to the grid.

| Parameter | Value |
|---|---|
| $S_{VSC}$ | 20 kVA |
| $f_{sw}$ | 5000 Hz |
| $L_{VSC,1}$ | 3.2 mH |
| $R_{VSC}$ | 0.4 Ω |
| $C_{VSC}$ | $14.32\mu F$ |
| $L_{VSC,2}$ | 509.3 $\mu H$ |

The values for the constants in the self-synchronized universal droop controller are given in tab.3.3. The values are collected from [40]. The values of L and R in the controller are the same as the converter inductance and resistance. .

**Table 3.3:** Parameters for the self-synchronized universal droop controller.

| Parameter | Value |
|---|---|
| n | 0.04 |
| m | $0.157 \cdot 10^{-3}$ |
| K | $0.269 \cdot 10^{-3}$ |
| $K_e$ | 10 |
| $R_v$ | 1 |
| L | $3.2 \cdot 10^{-3}$ |
| R | 0.4 |

## 3.3 DC-DC Switch-Mode Converters

DC-DC converters are used for regulating the voltage to make it suit the wanted level [42]. There are many types of dc-dc converters. Some of them are buck, boost, and bidirectional converter. The choosing of converter types depend if it is wanted to regulate the voltage up, down, or both. In the microgrid presented for this thesis, the boost converter and bidirectional converter are used; thus, they are described further. The other types of converters can be found and read more about in [42].

### 3.3.1 Boost Converter

A boost converter, or step-up converter, is used to increase the voltage level. In this thesis, the step-up converter is being used for solar PV. The voltage at the solar array is low and does not match the wanted voltage level at the DC bus. Fig.3.4 gives the circuit of a boost converter. The converter has a switch that closes and opens at a given frequency. When the switch is closed, the input supplies energy to the inductor. When the switch is open, both the inductor and the input give away energy to the output [42]. The switch can be a MOSFET or IGBT that can be controlled. A diode is included to ensure that the current never flows in the opposite direction. Two capacitors (one on the input and one on the output) are included to filter out the voltage ripple.

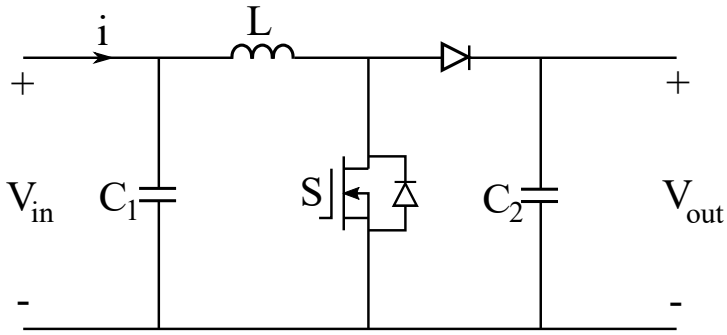


**Figure 3.4:** Circuit diagram of a boost converter.

### Maximum Power Point Tracking Control

A maximum power point tracking (MPPT) control is included to control the switch in the boost converter. The MPPT is needed to extract the maximum power from the module [44] and is widely used in solar power systems. The MPPT forces the PV to operate at the voltage closest to the maximum power point, fig.3.5. That ensures a system with high efficiency and is needed because the maximum power varies with solar radiation and temperature. There are several different ways of modelling the MPPT. Some of the types are the hill-climbing method, perturb and observe method, and fuzzy logic control. In this thesis, the incremental conductance method is used. The incremental conductance method and several other methods are explained in [45], [46] ,and [47]. The choosing of the method is based on implementation, type of sensors, costs, and application.

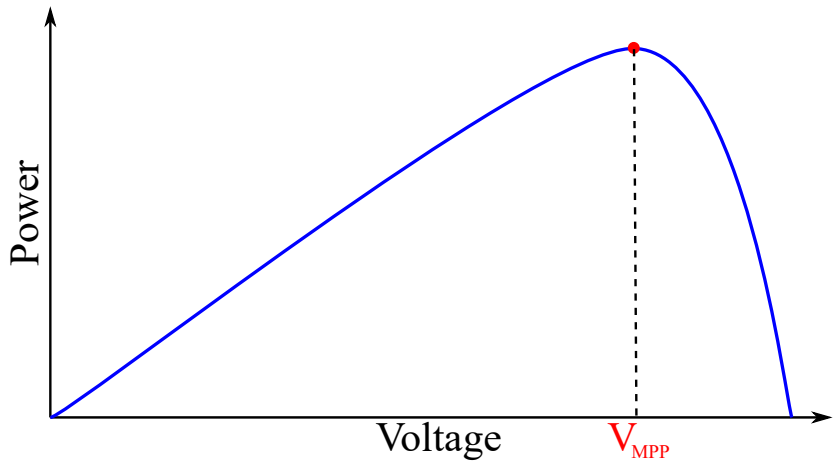


**Figure 3.5:** Figure of a PV curve, showing the maximum power point for the voltage.

The incremental conductance method changes the duty cycle to the pulse width modulation (PWM) by calculating the voltage and current changes. Based on the changes, the slope of the PV curve is zero at the maximum power point (MPP) [45]. A figure explaining the incremental conductance method is given in fig.3.6. First, the change in voltage is measured. If there is no change, the change in current is measured. If there is no change in current, the duty cycle remains the same. However, if the current has been increasing or decreasing, the duty cycle is decreased or increased a given step. If the voltage has changed, the change in voltage and change in current is compared to the measured voltage and current, making the duty cycle decrease, increase, or remain the same.

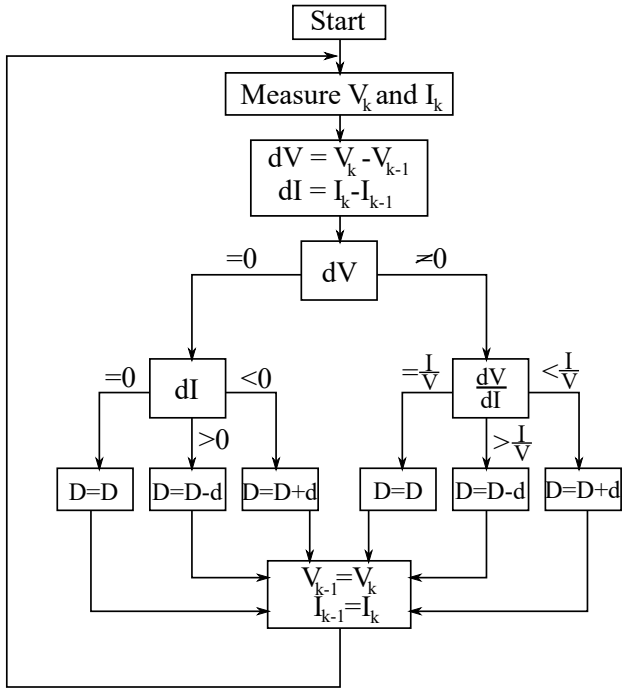


**Figure 3.6:** Flow chart showing the incremental conductance method.

### System Values PV Converter

The values for the boost converter connected to the solar PV are given in tab.3.4. The control system used is the incremental conductance, with a step of d = 0.00005. The Simulink model of the solar PV and control system is given in Appendix A.2.

**Table 3.4:** Values for the boost converter connected to the solar array. Capacitor number one is on the solar array side, and capacitor number two is on the DC bus side.

| Parameter | Value |
|---|---|
| $L_{PV}$ | 25 mH |
| $R_{PV}$ | 0.01 Ω |
| $C_{PV,1}$ | 8 mF |
| $C_{PV,2}$ | 10.1 mF |
| $f_{switch}$ | 5000 Hz |

### 3.3.2 Bidirectional Converter

A bidirectional converter, or buck-boost converter, can make the power flow in both directions. That means that the power can flow in one direction and boost the voltage, and it can also flow in the opposite direction and buck the voltage [42]. The bidirectional converter is especially suitable for energy storing devices such as batteries, super-capacitors, and electric vehicles [48]. These are all elements that can draw power and supply power.

A circuit diagram of a bidirectional converter is given in fig.3.7. The converter is non-isolated as it is expected to be connected to low power isolation. The positive direction of the power is, in this thesis, set to go from left to right in boost mode, and the negative direction of the power is set to go from right to left in buck mode. In the circuit, two switches are controlled by a control system. When switch 1 receives a signal, the converter is working as a boost converter. Furthermore, when switch 2 receives a signal, the converter is working as a buck converter. The switches can, for example, be IGBTs or MOSFETs.

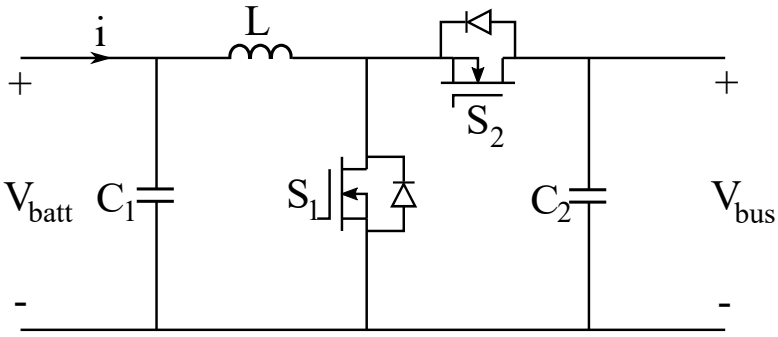


**Figure 3.7:** Circuit diagram of a bidirectional converter.

Two ways of controlling a bidirectional converter are presented: voltage control and current control.

#### Voltage Control

A converter with voltage control is needed to control the voltage at the DC bus. This voltage-controlled converter can work as a grid-forming converter. Fig.3.8 presents a block diagram of the voltage control for the bidirectional converter.

The voltage control system takes in the measured voltage at the DC-bus side and a reference voltage. The error is found and goes through a PI-controller to get a duty cycle. Because the switch only understands 0's and 1's, the saturation block sets the signal to 0 or 1 and compares it to a sawtooth block to get pulses. Out is a duty cycle for the buck converter and a duty cycle for the boost converter. The measured voltage is compared

to the reference voltage to know if the converter should be bucking or boosting. If the measured voltage is higher than the reference voltage, the control system sends a signal 0 to switch 1 and the duty cycle to switch 2, making the converter buck. If the measured voltage is lower than the reference voltage, the control system sends the duty cycle to switch 1 and 0 to switch 2, making the converter boost. This control system is found in [49] and [50].

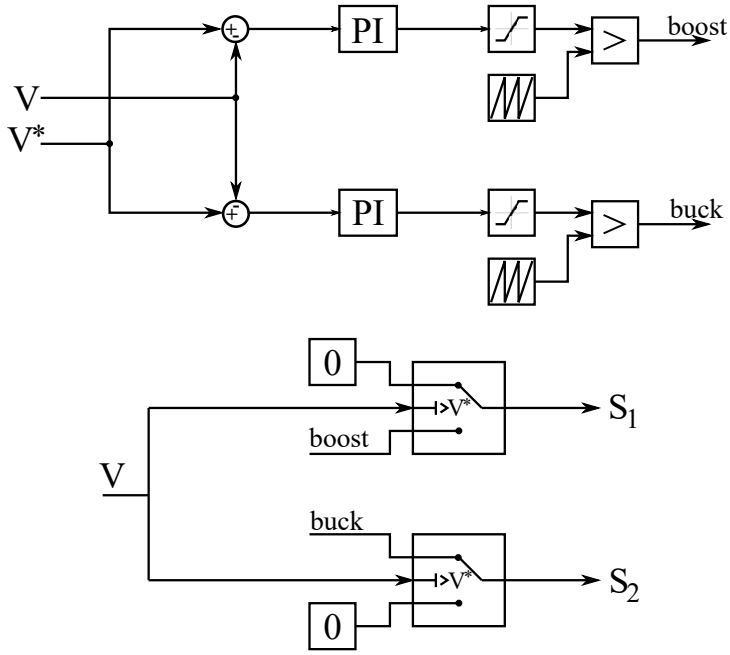


**Figure 3.8:** Block diagram of voltage control for the bidirectional converter.

### System Values BESS Converter

The BESS is connected to the DC bus through a bidirectional converter with voltage control. The converter and control system values are given in tab.3.6 and tab.3.5 and are based on [49] and [50]. The reference voltage for the control system is 400 V and is constant throughout the simulations. The Simulink model of the BESS and control system is given in Appendix A.3.

**Table 3.5:** Values bidirectional converter connected to the BESS. Capacitor number one is on the BESS side, and capacitor number two is on the DC bus side.

| Parameter | Value |
|---|---|
| L | 0.5 mH |
| $C_1$ | 1200 uF |
| $C_2$ | 1200 uF |
| R | 0.01 Ω |
| $f_{switch}$ | 5000 Hz |

**Table 3.6:** Values control system for the bidirectional converter connected to the BESS.

| Parameter | Value |
|---|---|
| $K_{p,boost}$ | 0.02 |
| $K_{i,boost}$ | 3 |
| $K_{p,buck}$ | 0.02 |
| $K_{i,buck}$ | 110 |

### Current Control

A current control system is implemented to control the current flowing through the bi-directional converter. This converter is very similar to the voltage controller explained above. Because the current can be both positive and negative depending on the current flow, two blocks with a gain of $-1$ are implemented at the buck-control part. The positive reference is set to when the current goes from left to right in fig.3.7, boosting. Hence, when the converter is bucking, both the measured current and the reference current is negative. Two $-1$ gain blocks are implemented to make the rest of the control system work. Out is a duty cycle for the boost part and the buck part. The reference current is compared to the value 0 to decide whether the system should be boosting or bucking. If the reference current is positive, the boosting duty cycle is sent to switch 1, and 0 is sent to switch 2, making the converter boost. If the reference current is negative, the buck duty cycle is sent to switch 2, and 0 is sent to switch 1, making the converter buck. This control system is also presented in [49] and [50].

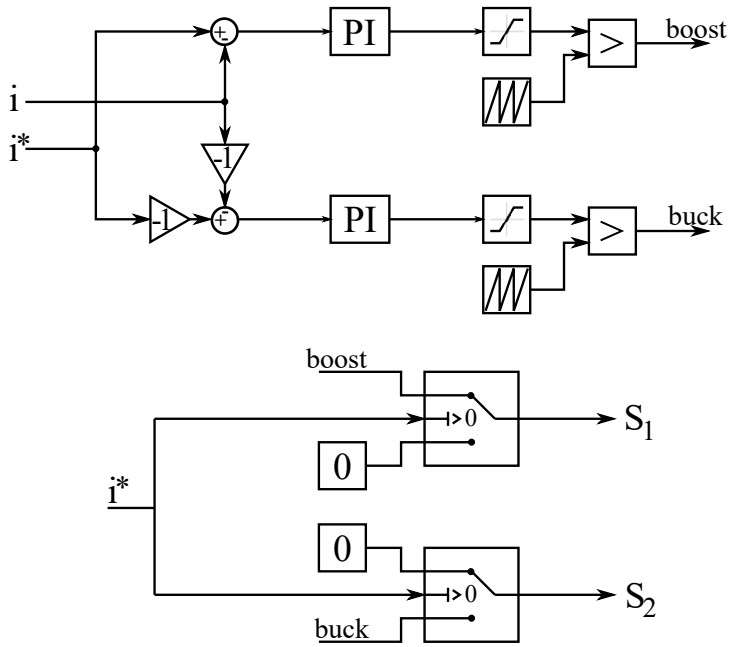


**Figure 3.9:** Block diagram of current control for bidirectional converter.

### System Values EV Converter

The EV is connected to the DC bus through a bidirectional converter with current control. The converter and control system values are given in tab.3.7 and tab.3.8 and are based on [49] and [50]. On the EV side of the converter is a switch, which connects and disconnects the EV to the microgrid. The reference current to the control system is given by the centralized controller and changes throughout the day. The Simulink model of the EV and control system is given in Appendix A.4.

**Table 3.7:** Values bidirectional converter connected to the EV. Capacitor number one is on the EV side, and capacitor number two is on the DC bus side.

| Parameter | Value |
|---|---|
| L | 9 mH |
| $C_1$ | 1200 $\mu F$ |
| $C_2$ | 1200 $\mu F$ |
| R | 0.01 $\Omega$ |
| $f_{switching}$ | 5000 Hz |

**Table 3.8:** Values control system for the bidirectional converter connected to the EV.

| Parameter | Value |
|---|---|
| $K_{p,boost}$ | 0.02 |
| $K_{i,boost}$ | 3 |
| $K_{p,buck}$ | 0.02 |
| $K_{i,buck}$ | 110 |

# Chapter 4

# Microgrid Power Management Based on Optimum Power Flow Algorithm

## 4.1 Introduction

This chapter explains the basis behind optimal power flow. Moreover, an OPF model is derived. The OPF model will work as a centralized controller in the microgrid model given in ch.2.7. It will receive inputs, predict and process information and give outputs. Lastly, simulations are done in Simulink to see how this centralized controller works. This OPF model gives samples to the training of the artificial neural network in ch.5.

## 4.2 Optimal Power Flow

Optimal power flow algorithms want to optimize solutions for performance [51] and secure a stable operation of power systems [52]. Examples of solutions to optimize are the need for minimizing losses or costs. When doing optimal power flow, different constraints have to be satisfied [53]. The constraints can, for example, be loading limits and voltage limits. Eq.4.1 gives a general expression to the optimal power flow problem [54]. $f$ is the function to be optimized and minimized, $g$ is the power balance equations, and $h$ is the constraints. $x$ is the state variable vector, and $u$ is the control variable vector.

$$\begin{aligned} \textit{min } J &= f(x,u) \\ \textit{subject to } & g(x,u) \\ & h(x,u) \end{aligned} \tag{4.1}$$

However, there are a few challenges to the optimal power flow problem [52]. Conventional OPF solutions have a long computing time typically. The computing time can be a problem as the load and generated power changes throughout the day and year. Especially in microgrids with DERs, can the changes be fast and great. Another problem is measuring the secure operation and stability of the system, as stability is a dynamic problem and difficult to quantify. As a solution, [55] proposes a real-time OPF algorithm, and in [56], the OPF problem, including the stability, is discussed.

Many different optimization methods can be used. Some examples are linear programming, dynamic programming, Newton-based techniques and particle swarm optimization [53], [57], [58]. This thesis uses dynamic linear programming, as the predictions and input values are time-dependent and changing, and the power flow calculations are linear.

## 4.3 Optimal Power Flow Model

This thesis's optimal power flow model is based on minimizing the power losses in the microgrid and keeping a stable voltage and frequency. Firstly, it is explained how the microgrid works. Then the predictions and optimal power flow are described. In the predictions and optimal power flow, the values from time $t$ are sampled, then the following values, $t + \Delta t$, are predicted. The values sampled are the state of charge for the EV and BESS, the load, switch value for the EV and the solar irradiation level. The predicted values then go through the optimal power flow algorithm. The values wanted to optimize are $S_{grid}$, $P_{VSC,ref}$ and $I_{EV,ref}$. All the inputs and outputs are in per unit, but calculated back to real value in the beginning of the OPF code. The objective function, predictions and programming are explained. Fig.4.1 shows the flow chart of how the centralized controller works.

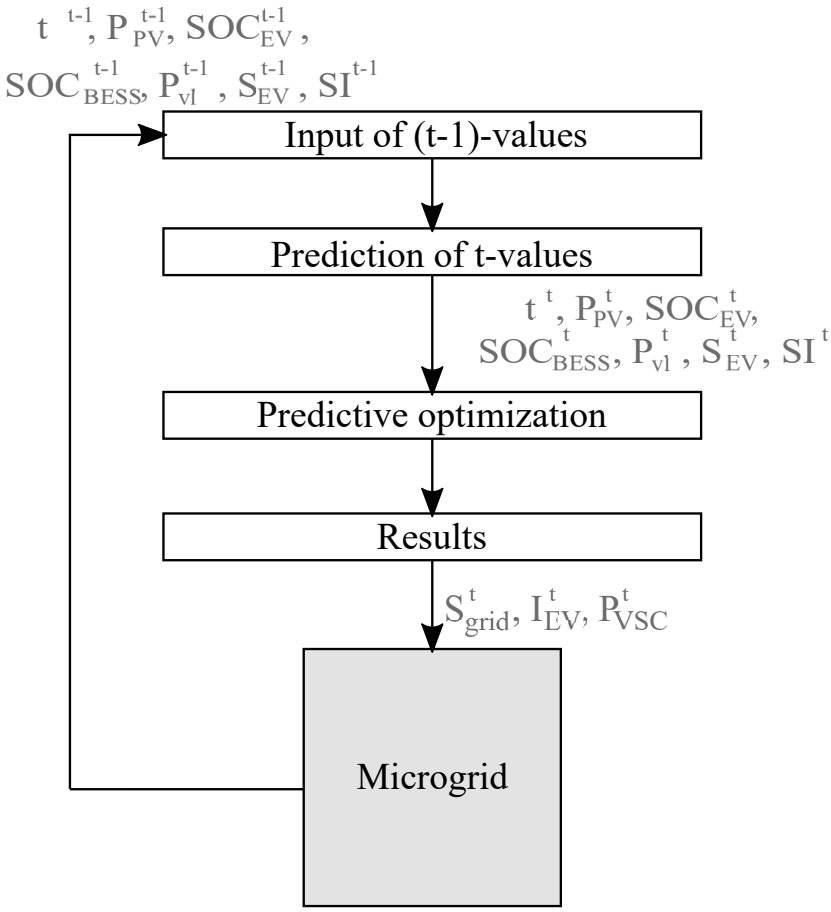


**Figure 4.1:** Flow chart of microgrid power management.

### 4.3.1 Systems Working

It is essential to know how the system works to make an optimal power flow algorithm. All the features of the microgrids units are summarized in tab.4.1.

| | |
|---|---|
| **Grid Switch** | • Is in general open, it is wanted that the microgrid can supply itself as much as possible.<br>• Only closed when the generated power (included power from batteries) is lower than the total load and when fault and disturbances occur (thus, faults and disturbances are not considered in the OPF). |
| **BESS** | • The battery is charged with power from the PV.<br>• In grid-connected mode, the battery does not deliver power to the AC load.<br>• The maximum power delivered from the BESS is 9000 W. |
| **EV** | • The EV has a switch that disconnects it from the microgrid. When it is disconnected, it cannot deliver or consume power from the microgrid.<br>• For simplifications, when the EV is disconnected, it does not charge/discharge.<br>• The maximum power delivered from the EV is 9000 W. |
| **PV** | • The PV generates power based on the solar irradiance. The temperature level is neglected.<br>• In grid connected mode, the PV does not deliver power to the AC-load. |
| **Variable Load** | • A load that is changing throughout the day. |
| **Constant Load** | • Constant and most critical load. |

**Table 4.1:** Table explaining the features of different parts of the microgrid.

### 4.3.2 Objective Function for Islanded Microgrid

The goal of the OPF in this thesis is to minimize the difference between generated power and load, eq.4.11. All the generation units are summarized, and all the load units are summarized. The types of generation units and loads are given in eq.4.3 and 4.4.

$$min(J) = min(\sum_{i=1}^{N} P_i^G - \sum_{i=1}^{M} P_i^L) \tag{4.2}$$

$$P^G = [P_{PV}, P_{EV}, P_{BESS}] \tag{4.3}$$

$$P^L = [P_{cl}, P_{vl}, P_{EV}, P_{BESS}, P_{VSC,loss}] \tag{4.4}$$

The systems constraints are given in eq.4.5-4.9 and tab.4.2.

$$0 \leq S_{VSC} \leq S_{VSC,max} \tag{4.5}$$

$$SOC_{BESS,min} \leq SOC_{BESS} \leq SOC_{BESS,max} \tag{4.6}$$

$$SOC_{EV,min} \leq SOC_{EV} \leq SOC_{EV,max} \tag{4.7}$$

$$-P_{BESS,max} \leq P_{BESS} \leq P_{BESS,max} \tag{4.8}$$

$$-P_{EV,max} \leq P_{EV} \leq P_{EV,max} \tag{4.9}$$

**Table 4.2:** Values for system constraints.

| Parameter | Value |
|---|---|
| $S_{VSC,max}$ | 20 000 MVA |
| $SOC_{BESS,min}$ | 1% |
| $SOC_{BESS,max}$ | 99% |
| $SOC_{EV,min}$ | 1% |
| $SOC_{EV,max}$ | 99% |
| $P_{BESS,max}$ | 9000 W |
| $P_{EV,max}$ | 9000 W |

The control variables are given in eq.4.10.

$$u = [S_{grid}, P_{VSC,ref}, I_{EV,ref}] \tag{4.10}$$

### 4.3.3 Objective Function for Grid-Connected Microgrid

When the microgrid is grid-connected, the DC-bus and the AC-bus does not share power. Thus, it is now desired to minimize the difference between generated power and load on the DC bus, eq.4.11. The generation unit and load units are given in eq.4.12 and 4.13.

$$min(J) = min(\sum_{i=1}^{N} P_i^G - \sum_{i=1}^{M} P_i^L) \tag{4.11}$$

$$P^G = [P_{PV}] \tag{4.12}$$

$$P^L = [P_{EV}, P_{BESS}] \tag{4.13}$$

The system constraints are given in eq.4.14-4.17 and tab.4.2.

$$SOC_{BESS,min} \leq SOC_{BESS} \leq SOC_{BESS,max} \tag{4.14}$$

$$SOC_{EV,min} \leq SOC_{EV} \leq SOC_{EV,max} \tag{4.15}$$

$$-P_{BESS,max} \leq P_{BESS} \leq 0 \tag{4.16}$$

$$-P_{EV,max} \leq P_{EV} \leq 0 \tag{4.17}$$

The control variables are given in eq.4.18.

$$u = [S_{grid}, P_{VSC,ref}, I_{EV,ref}] \tag{4.18}$$

### 4.3.4 Predictions of Dynamic Variables

The dynamic values of the microgrid are the state of charge for the BESS and EV, EV switch, the variable load and the solar irradiance. Thus, the values needed to be predicted to give the most correct output value and prediction of the $S_{grid}$, $P_{VSC,ref}$ and $I_{EV,ref}$. The input values are given in eq.4.19, and the predicted values are given in eq.4.20.

$$Z(t) = \begin{bmatrix} SOC_{EV}(t) & SOC_{BESS}(t) & P_{vl}(t) & S_{EV}(t) & SI(t) \end{bmatrix} \tag{4.19}$$

$$Z(t+\Delta t) = \begin{bmatrix} SOC_{EV}(t+\Delta t) & SOC_{BESS}(t+\Delta t) & P_{vl}(t+\Delta t) & S_{EV}(t+\Delta t) & SI(t+\Delta t) \end{bmatrix} \tag{4.20}$$

### Solar Irradiance Prediction

The solar irradiance prediction is based on values for April, where the sun starts shining at around 6 o'clock and goes down at around 18 o'clock [59]. The sun rises slowly until 8 o'clock, and then it arises faster. At 12, it shines brightest, and then it goes down slowly. The predictions are partly linear. These are the assumptions for one day where it is predicted that the sun will shine. On other days, the sun might not shine at all. For more detailed predictions, see [60].

$$SI(t+\Delta t)[W/m^2] = \begin{cases} 0, & t = [0,6) \\ SI(t) + 50 \cdot \Delta t, & t = [6,8) \\ SI(t) + 100 \cdot \Delta t, & t = [8,12) \\ SI(t) - 50 \cdot \Delta t, & t = [12,18) \\ 0 & t = [19,24) \end{cases} \tag{4.21}$$

Using eq.2.1 and 2.2, the resulting equation for the power delivered from the PV is $P_{pv}(t+\Delta t) = \frac{SI(t+\Delta t)}{1000} \cdot P_{max} \cdot N_s \cdot N_p$.

### Load

The variable load is predicted with two tops and two bottoms. The first top is at 8 o'clock and the second is at 17 o'clock and lasts until 21. The bottoms are at 14 o'clock and 24 o'clock. The predictions are based on values from the 8th of April 2021 from [61]. It is assumed that most of the days in April looks like this day.

$$P_{vl}(t+\Delta t)[w] = \begin{cases} P_{vl}(t) + 200 \cdot \Delta t, & t = [0,8) \\ P_{vl}(t) - 200 \cdot \Delta t, & t = [8,14) \\ P_{vl}(t) + 200 \cdot \Delta t, & t = [14,17) \\ P_{vl}(t) & t = [17,21) \\ P_{vl}(t) - 200 \cdot \Delta t, & t = [21,24) \end{cases} \tag{4.22}$$

### State of Charge

The state of charge equation for the EV and BESS from $t$ to $t + \Delta t$ is given in eq.4.23. Because the load, solar irradiation and SOC from the time t before is given, the SOC at time $t + \Delta t$ can be found mathematically.

$$SOC(t+\Delta t) = SOC(t) + \frac{\int_t^{t+\Delta t} I\, dt}{C_{ref}} * 100\% \tag{4.23}$$

If the EV is connected, the current from both the batteries is given in eq.4.24. Thus, the current on the battery side can not exceed $I = \frac{9000W}{120V} = 75A$. If the microgrid is grid-connected, the loads and loss are neglected from the equations.

$$I = \frac{P_{PV} - P_{VSC,loss} - P_{vl} - P_{cl}}{2 \cdot V_{BESS}} \tag{4.24}$$

If the EV is disconnected, $I_{EV} = 0$ and $I_{BESS}$ is given in eq.4.25.

$$I = \frac{P_{PV} - P_{VSC,loss} - P_{vl} - P_{cl}}{V_{BESS}} \tag{4.25}$$

**EV Switch**

The EV is assumed to be disconnected to the microgrid from 8 o'clock to 16 every day and between 6 o'clock to 20. This is always predicted even though the previous value can be different from normality.

$$S_{EV}(t + \Delta t) = \begin{cases} 1, & t = [0, 8) \\ 0, & t = [8, 16) \\ 1, & t = [16, 18) \\ 0, & t = [18, 20) \\ 1 & t = [20 - 23) \end{cases} \tag{4.26}$$

**Losses**

The losses considered are the losses through the VSC. Other losses are neglected. This value is predicted to be the same always, even though it depends on the current flowing, eq.4.27. The per-unit value for the current from tab.3.2 is used here. That gives a loss of 1333.33 W.

$$P_{VSC.loss} = R_{VSC} \cdot I^2_{VSC,n} \tag{4.27}$$

### 4.3.5 Optimal Power Flow

The control variables of this system are $P_{VSC,ref}, S_{grid}$ and $I_{EV,ref}$. $P_{VSC,ref}$ is the active power reference of the control system to the VSC. $S_{grid}$ is the switch that switches

the microgrid from grid-connected mode to islanded mode and back. $I_{EV,ref}$ is the reference current that decides how much current is going into or out of the EV. The optimal power flow MATLAB code including predictions is given in Appendix B.1.

### Grid Switch

The net power is considered to decide whether the switch to the grid should be in grid-connected mode or islanded. If the net power in eq.4.28 is negative, the microgrid cannot supply itself with power and need help from the grid. If the net power is positive, the microgrid can supply itself.

$$P_{net} = P_{gen} - P_{load} \tag{4.28}$$

Firstly, it is checked if the PV can supply the load itself. If the power from the PV is less than the load, $P_{PV} < P_{vl} + P_{cl} + P_{VSC,loss}$, the batteries have to supply power. The batteries conditions have to be checked to know if they can supply power eq.4.29.

$$P_{gen} = \begin{cases} P_{PV} + P_{EV,max} + P_{BESS,max}, & SOC_{EV} \neq 0 \wedge S_{EV} = ON, SOC_{BESS} \neq 0 \\ P_{PV} + P_{EV,max}, & SOC_{EV} \neq 0 \wedge S_{EV} = ON, SOC_{BESS} = 0 \\ P_{PV} + P_{BESS,max}, & SOC_{EV} = 0 \vee S_{EV} = OFF, SOC_{BESS} \neq 0 \\ P_{PV}, & SOC_{EV} = 0 \vee S_{EV} = OFF, SOC_{BESS} = 0 \end{cases} \tag{4.29}$$

If the PV-generated power is more than the AC-load, $P_{PV} > P_{vl} + P_{cl} + P_{VSC,loss}$, the batteries will draw power if they are connected and not fully charged. In some instances, the generated power can be more than what is needed if both batteries are fully charged. As it is desired to get $P_{net}$ to 0, this is not good for the system.

Based on the net power, the microgrid is set either in islanded mode (OFF) or in grid-connected mode (ON), eq.4.30.

$$S_{grid} = \begin{cases} ON, & P_{net} < 0 \\ OFF, & P_{net} \geq 0 \end{cases} \tag{4.30}$$

### Grid-Connected Mode

When it is known that the microgrid is grid-connected, the other variables $I_{EV,ref}$ and $P_{VSC,ref}$ can be found. The EV has no load to discharge power to, so it is only charging, eq.4.31. The power to the EV is now negative as it works as a load.

$$P_{EV} = \begin{cases} -\frac{P_{PV}}{2}, & SOC_{EV} \neq 100, SOC_{BESS} \neq 100, S_{EV} = ON \\ -P_{PV}, & SOC_{EV} \neq 100, SOC_{BESS} = 100, S_{EV} = ON \\ 0, & SOC_{EV} = 100, SOC_{BESS} \neq 100, S_{EV} = ON \\ 0, & SOC_{EV} = 100, SOC_{BESS} = 100, S_{EV} = ON \\ 0, & S_{EV} = OFF \end{cases} \tag{4.31}$$

The reference current to the EV is given in eq.4.32.

$$I_{ref,EV} = \frac{P_{EV}}{V_{EV}} \tag{4.32}$$

In grid-connected mode, the reference power for the grid always 0, as no power is going through it, eq.4.33.

$$P_{ref,VSC} = 0 \tag{4.33}$$

**Islanded Mode**

When the microgrid is in islanded mode, the EV and BESS can both be charged and discharged. If the power from the PV is less than the AC-load and loss, $P_{PV} < P_{vl} + P_{cl} + P_{VSC,loss}$, the batteries are discharging. When the power from the PV is greater than the AC-load and loss, $P_{PV} > P_{vl} + P_{cl} + P_{VSC,loss}$, the batteries are charging. Whether the load is charging or discharging depends on the sign of the $P_{EV}$ in eq.4.34. A negative sign is charging, positive is discharging.

$$P_{EV} = \begin{cases} \frac{P_{vl}+P_{cl}+P_{VSC,loss}-P_{PV}}{2}, & SOC_{EV} \neq 0, SOC_{BESS} \neq 0, S_{EV} = ON \\ P_{vl} + P_{cl} + P_{VSC,loss} - P_{PV}, & SOC_{EV} \neq 0, SOC_{BESS} = 0, S_{EV} = ON \\ 0, & SOC_{EV} = 0, SOC_{BESS} \neq 0, S_{EV} = ON \\ 0, & SOC_{EV} = 0, SOC_{BESS} = 0, S_{EV} = ON \\ 0, & S_{EV} = OFF \end{cases} \tag{4.34}$$

The resulting reference current to the EV is given in eq.4.35, and the resulting active power reference for the VSC is given in eq.4.36.

$$I_{ref,EV} = \frac{P_{EV}}{V_{EV}} \tag{4.35}$$

$$P_{VSC} = P_{vl} + P_{cl} + P_{VSC,loss} \tag{4.36}$$

## 4.4 Simulation Results

This chapter gives the results from running simulations of the microgrid in Simulink/MATLAB, including the optimal power flow algorithm as a centralized controller. The simulations are done for four different scenarios:

- Base case.
- One scenario with abnormal behaviour of the load.
- One scenario where the sun disappears when the irradiation is at its strongest.
- One scenario when the state of charge at both the EV and BESS is 0% in the beginning.

The reference values from the OPF, $S_{grid}$, $P_{VSC,ref}$ and $I_{EV,ref}$, are presented and examined for all the simulations. After that is the power from the units in the microgrid presented, and lastly, the voltage at PCC and DC bus, and current form the VSC is presented. At the end of the chapter is a complete discussion of all the simulations.

The base case data for the solar irradiance, total power consumption and EV switch for the microgrid simulations are given in Appendix C.1, C.3 and C.5, respectively. The data for solar irradiance is retrieved in [59], and the power data is retrieved from [61]. The state of charge for the BESS and EV starts at 50%.

### 4.4.1 Base Case

This simulation present the results when using optimal power flow for base case values.

The output parameters for the grid switch, active power reference for the SUDC and current reference for the EV is given in fig.4.2. It can be seen from the grid switch reference that the microgrid goes to grid-connected mode two times. The power reference follows after. The EV current reference is disconnected a lot during the day.

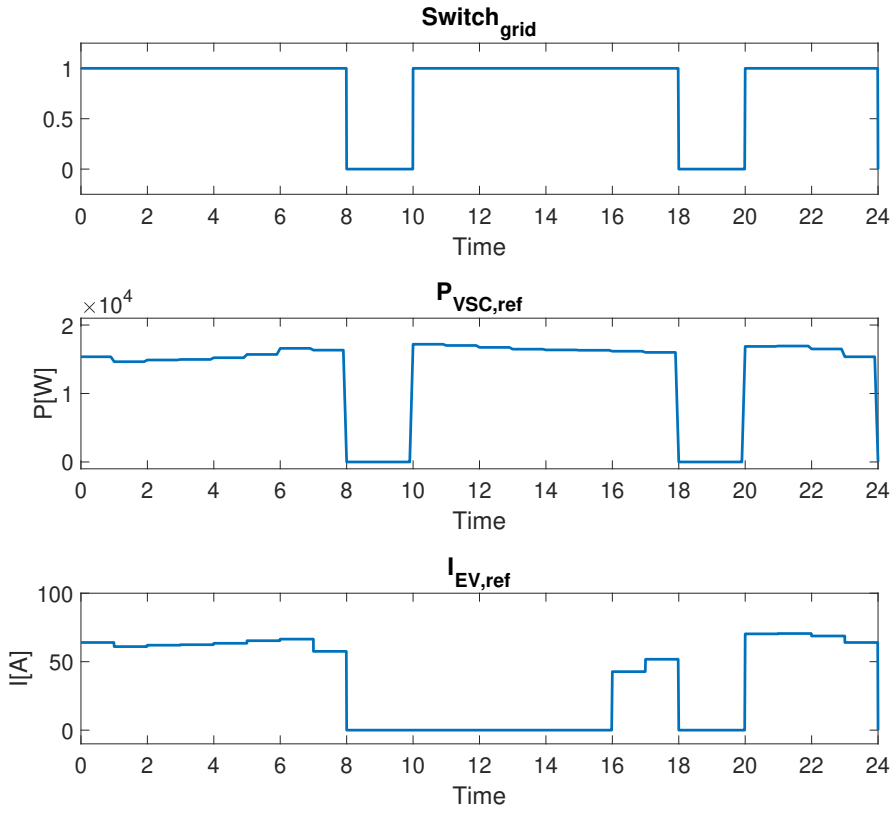


**Figure 4.2:** Output parameters from the centralized controller for the OPF base case. The grid is islanded at 1 (switch OFF) and grid-connected at 0 (switch ON).

The plots for the power to and from different units are given in fig.4.3. When the microgrid is islanded a large ripple occurs in active and reactive load power. Also the PV experiences a larger ripple as the power generated increases. The BESS and EV has occasionally a large ripple. Lastly, the grid power changes according to the mode of the microgrid.

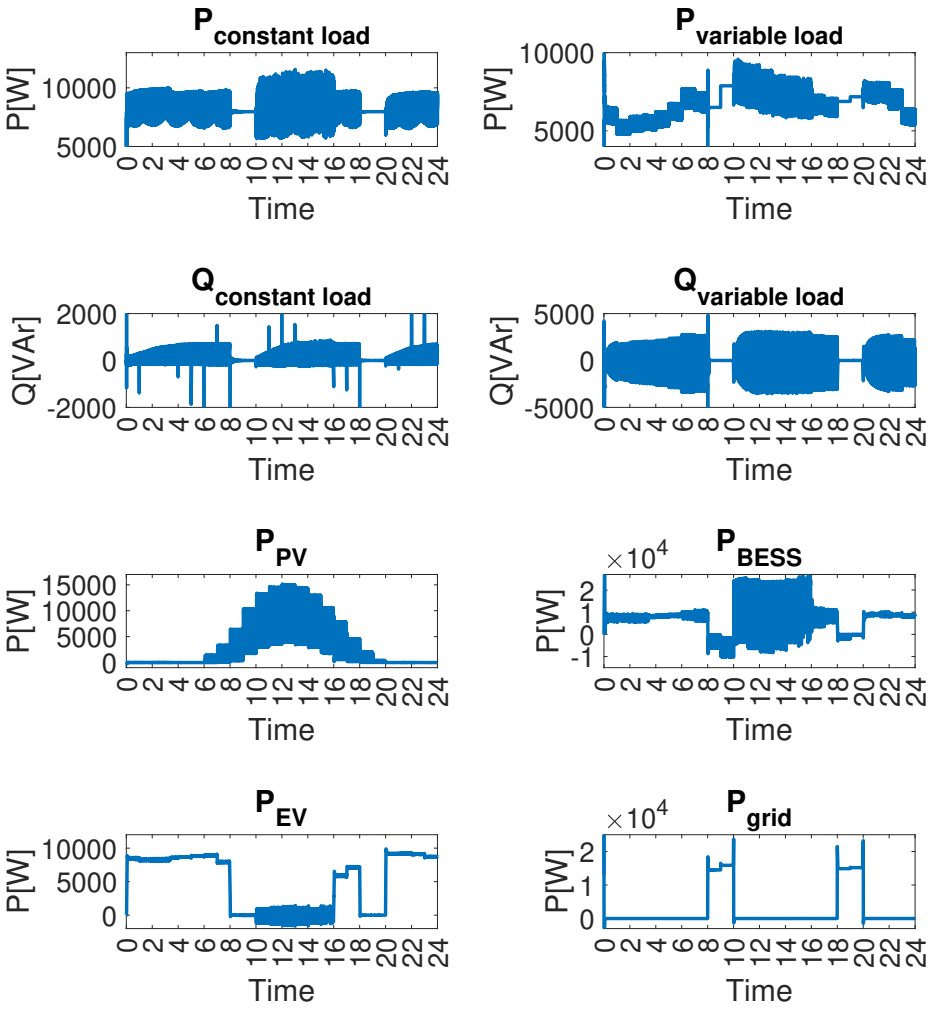


**Figure 4.3:** Active and reactive power drawn or generated from units in the microgrid for OPF base case.

The voltage at PCC, current from the VSC and DC bus voltage is presented in fig.4.4. The voltage experiences transients and an unstable condition from 10 to 16 seconds. The current follows the flow of power from the DC bus to the AC bus. Lastly, the DC bus voltage has a low ripple most of the time, but from 10 to 16 seconds it is high.

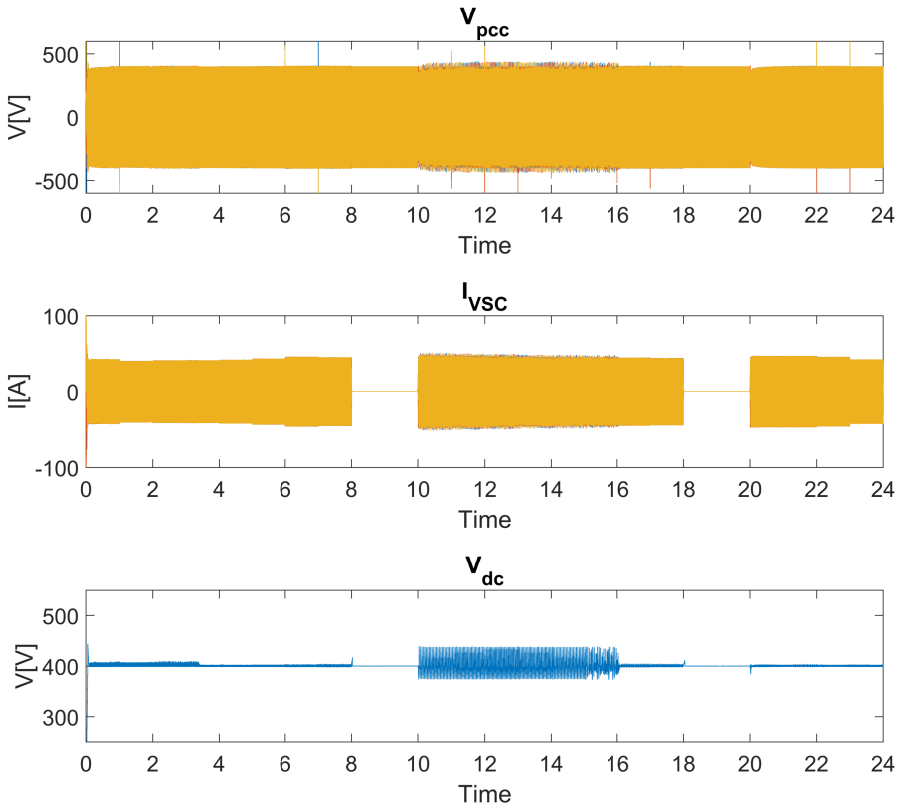


**Figure 4.4:** Voltage at the PCC, current from the VSC and DC bus voltage for OPF base case.

### 4.4.2 Abnormal Load

Figures are presented for a scenario where the load reaches a low point at 8 and a high top at 21. The values are given in Appendix C.4.

The output parameters for the grid switch, active power reference for the SUDC and current reference for the EV is given in fig.4.5. With the new load, the switching from islanded mode to grid-connected mode is different from the base case. The power from and to the units in the microgrid is given in fig.4.6. All the power has the same trend as the base case. The voltage in PCC and at the DC bus, and the VSC current is shown in fig.4.7. This results are also very similar as the base case, except for a different switching time and load demand.

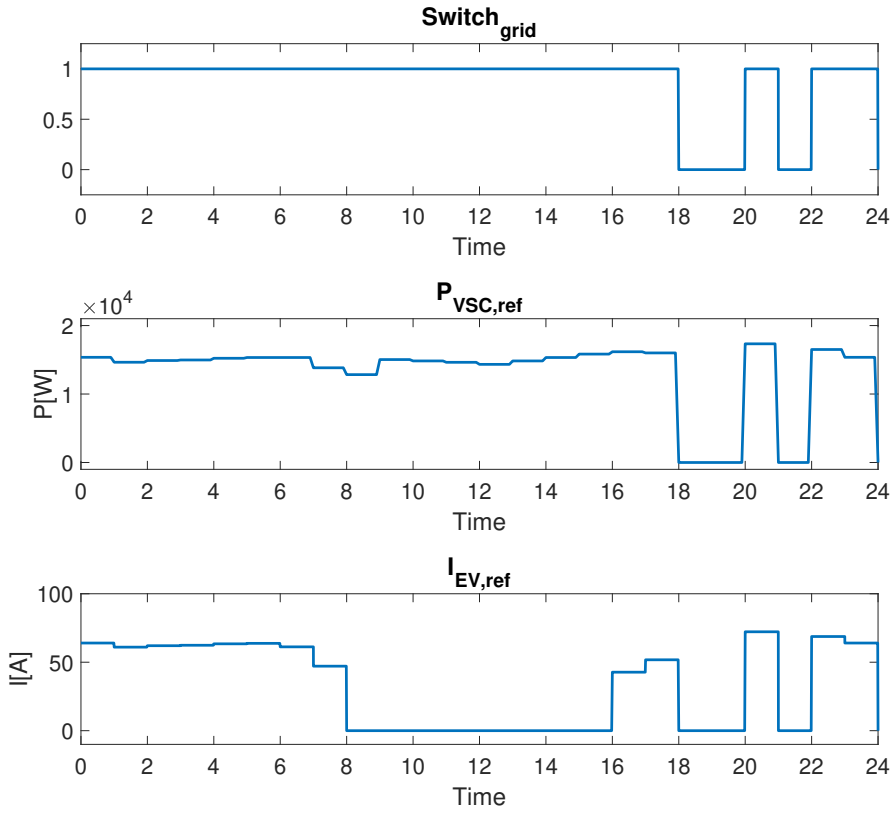


**Figure 4.5:** Output parameters from the centralized controller for the OPF abnormal load case. The grid is islanded at 1 (switch OFF) and grid-connected at 0 (switch ON).

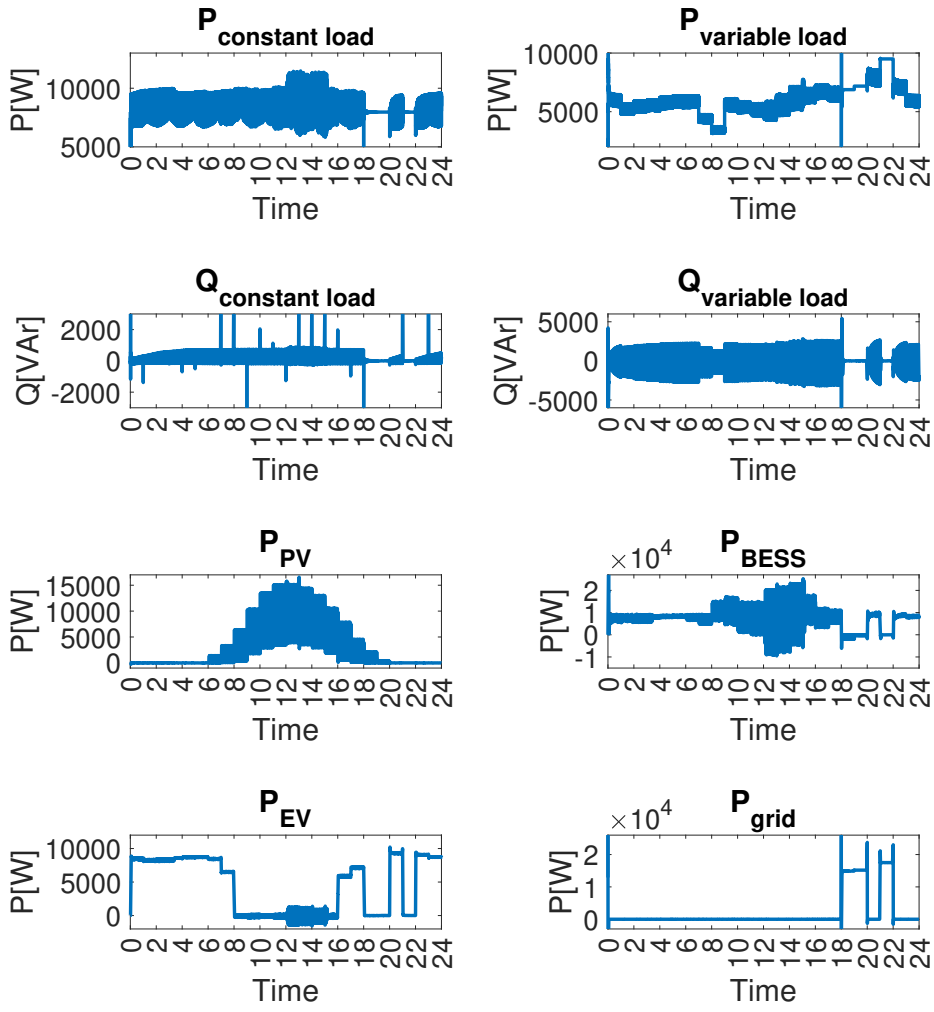


**Figure 4.6:** Active and reactive power drawn or generated from units in the microgrid for OPF abnormal load case.

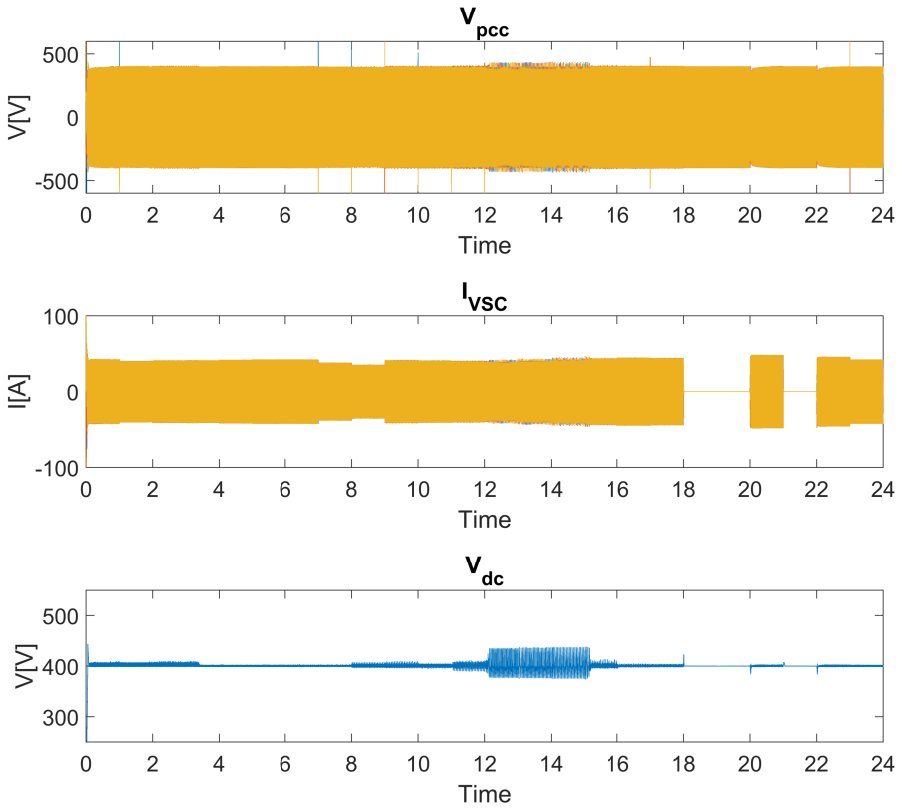


**Figure 4.7:** Voltage at the PCC, current from the VSC and DC bus voltage for OPF abnormal load case.

### 4.4.3 Abnormal Solar Irradiance

This chapter presents the plots when the sun irradiance follows the base case conditions until 12 o'clock. After 12 o'clock, the solar irradiance is zero the rest of the day. The solar irradiance values are given in Appendix C.2.

The output parameters for the grid switch, active power reference for the SUDC and current reference for the EV is given in fig.4.8. It is clearly shown that the solar irradiation disappears after 12 seconds as the microgrid connects to the grid. The power from and to the units in the microgrid is given in fig.4.9. Also here, large ripples occurs when the microgrid is islanded. The voltage in PCC and at the DC bus, and the VSC current is shown in fig.4.10. Also here, transients happens in the PCC voltage, and a large ripple occur in the DC bus voltage.

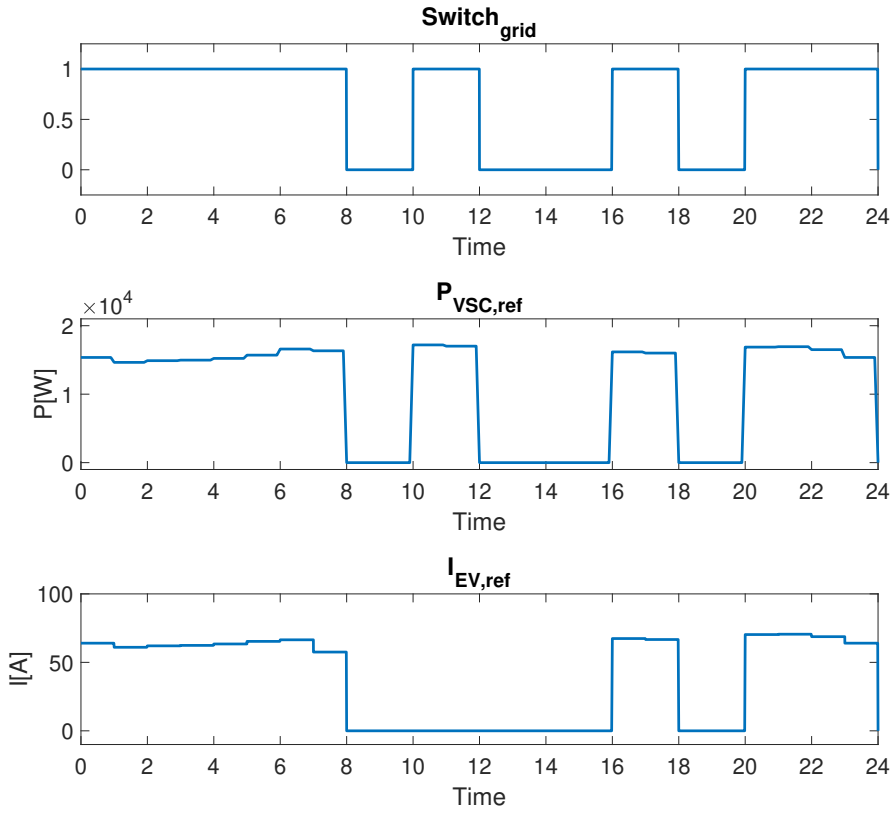


**Figure 4.8:** Output parameters from the centralized controller for the OPF abnormal solar irradiation case. The grid is islanded at 1 (switch OFF) and grid-connected at 0 (switch ON).

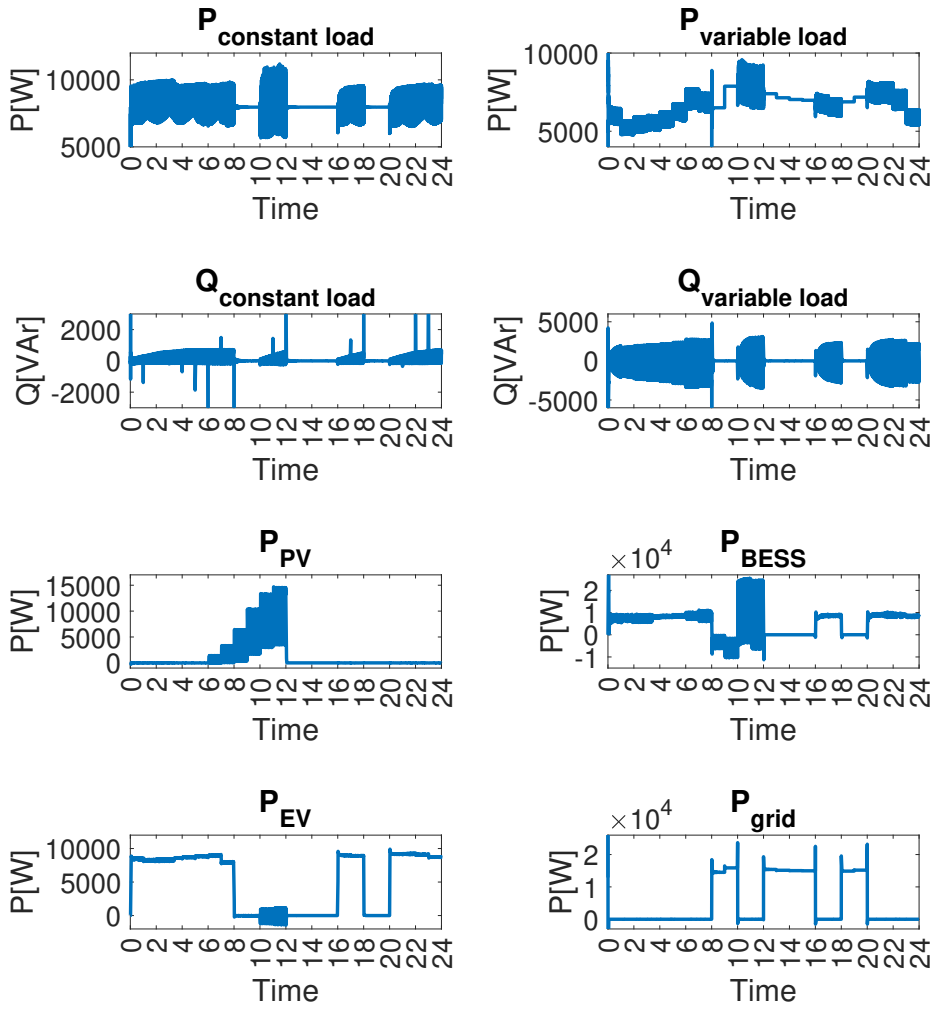


**Figure 4.9:** Active and reactive power drawn or generated from units in the microgrid for OPF abnormal solar irradiation case.

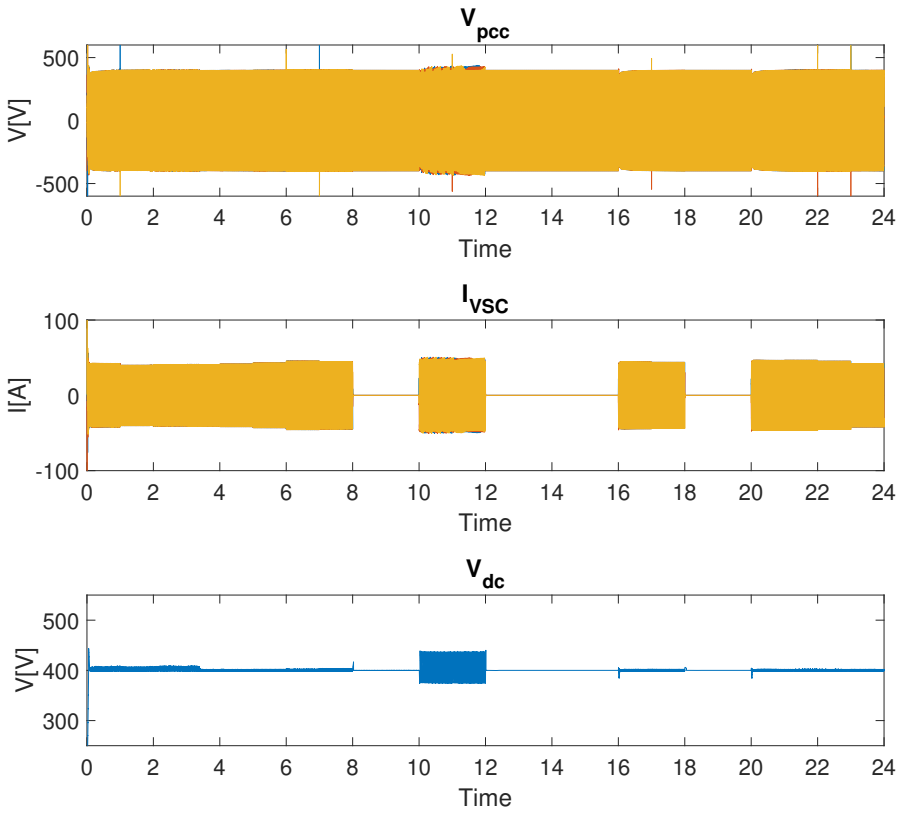


**Figure 4.10:** Voltage at the PCC, current from the VSC and DC bus voltage for OPF abnormal solar irradiation case.

### 4.4.4 BESS and EV State of Charge 0%

In this chapter, the EV and BESS start with a state of charge at 0%.

The references for the grid switch, active power to the SUDC and current to the EV current controller is given in fig.4.11. Here, it can be seen that the switch is on throughout the simulation. The current reference and power reference is thus zero most of the time. The plots for the power to and from different units are given in fig.4.12. The power to the grid is excellent. A large ripple in the PV can be noticed, which also affects the BESS power ripple. The voltage at PCC, current from the VSC and DC bus voltage is presented in fig.4.13.

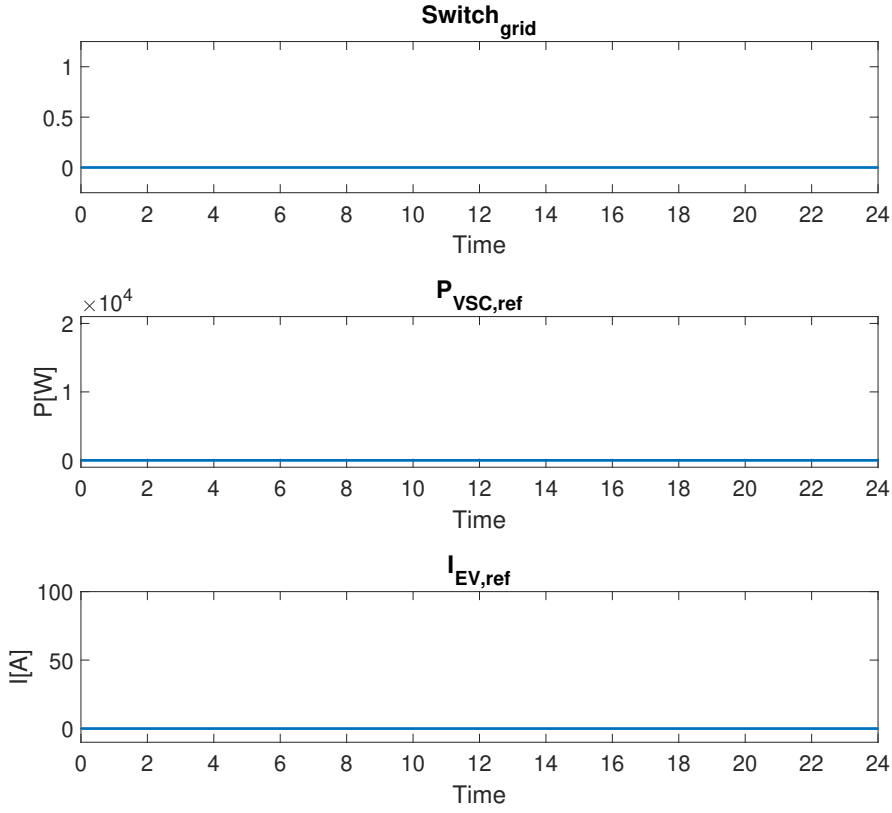


**Figure 4.11:** Output parameters from the centralized controller for the OPF state of charge case. The grid is islanded at 1 (switch OFF) and grid-connected at 0 (switch ON).

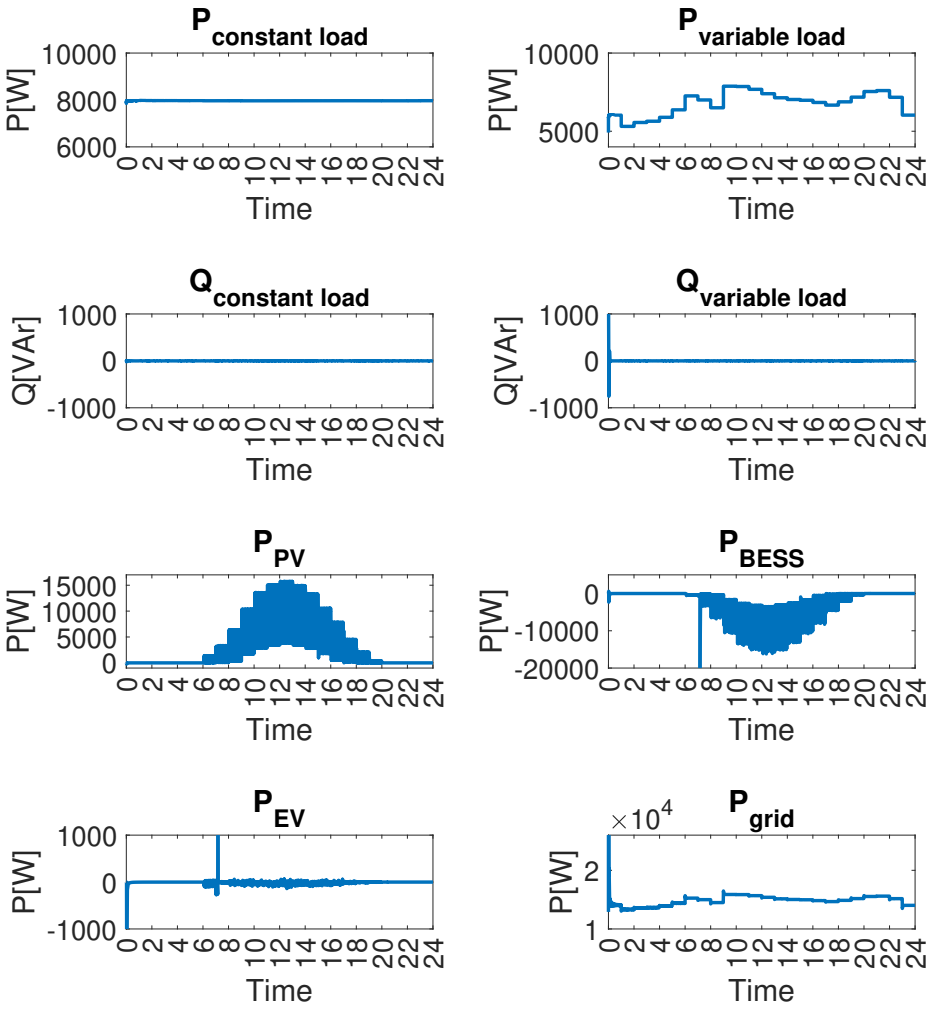


**Figure 4.12:** Active and reactive power drawn or generated from units in the microgrid for OPF state of charge case.

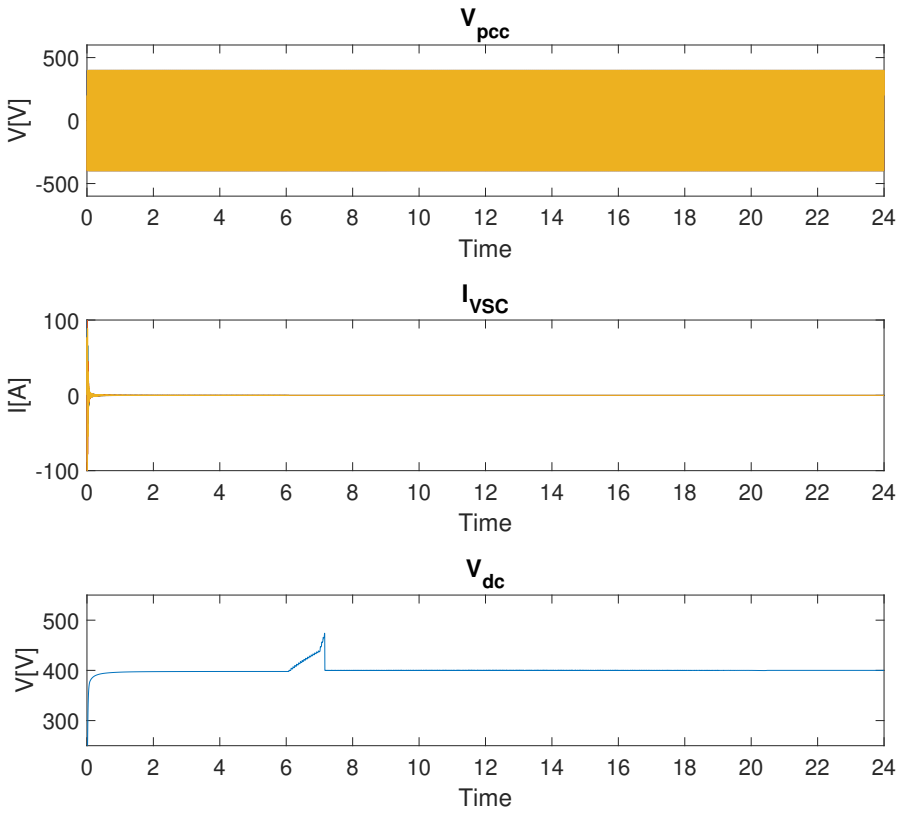


**Figure 4.13:** Voltage at the PCC, current from the VSC and DC bus voltage for OPF state of charge case.

### 4.4.5 Discussion of Results

The criteria a power management strategy should fulfil is given in ch.2.6. These criteria look at power-sharing, power quality, limitations of the system, and dynamic behaviour.

The OPF manages to share power well between the units; one example is the power from the grid "on" when needed to secure a power delivery to the loads, fig.4.3. However, the power quality and dynamic behaviour of the system is not satisfying. Fig.4.6 shows a power going into the loads with a large ripple. The voltage at the PCC in fig.4.7 experiences transients and a disturbance, especially between 12 and 15 seconds. The last criteria are to make sure the limits of the system is withheld. Limitations of the system is the power to and from the EV and BESS and the power going through the VSC. Fig.4.12 shows that the BESS receives a large amount of power which is above the acceptable limit.

Based on these simulations, only one out of four criteria is fulfilled for the OPF to succeed as a power management strategy. A more detailed discussion about power management strategy is presented in ch.5.8.5.

# Chapter 5

# Microgrid Power Management Based on Artificial Neural Network Algorithm

## 5.1 Introduction

This chapter explains the basis behind artificial neural networks. It explains how it works, what areas one can use it and how it learns. An artificial neural network centralized controller is proposed, and a training model is made. The training is done by using samples from the OPF model in ch.4. The controller is simulated for four different cases in Simulink and compared to the OPF simulations. In the end, is a discussion of the results.

## 5.2 How Does An Artificial Neuron Work?

Biological neurons can learn, draw parallels, process information and see it in a context, compute and structure information—all of this using very little energy. Artificial neural networks are trying to inherit some of these characteristics to solve tasks [62]. Tasks that are interesting to solve are problems regarding classification, prediction, categorization, approximation, or, as in this thesis, problems regarding optimization and control.

One example: the human brain can see one cat and one dog and can not classify them. By learning, the human now knows the difference and can easily recognize which animal is a cat and a dog. In additions, the human knows that the cat and the dog is an animal. The neurons in the brain processed the information, learned and put the information in a context and category. The goal is to get an ANN, a computer, to do the same but with

values that can control a microgrid.

An artificial neuron takes in n inputs, multiplied by a weight, summaries the weights and the bias and takes the sum through an activation function. The process is shown in eq.5.1 and 5.2 and fig.5.1. This is known as the McCulloch-Pitts model and can be read more about in [63].

$$v = \sum_{i=1}^{n} x_i w_i + b \tag{5.1}$$

$$y = \phi(v) \tag{5.2}$$

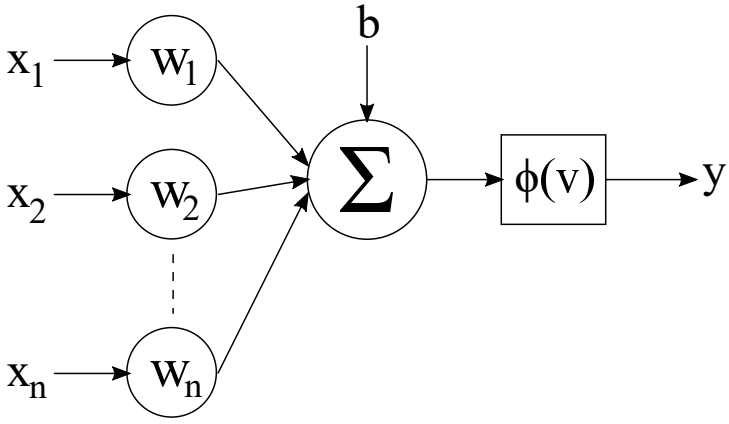


**Figure 5.1:** The "inside" of one artificial neuron.

**Input:** The input can come from an input given or measured, for example, a given day or measured temperature, or it can come from other neurons. It can be one input or many inputs.

**Weights:** Each input is multiplied by a weight. The weight tells how much this input should be considered and the importance. If one input has a significant weight and the others have low weights, the one with a significant weight will contribute the most to the output [64].

**Bias:** This allows shifting the function left or right.

**Summation:** The summation, or adder, summaries the inputs and weights and the bias.

**Activation function:** Limits the output [65]. The output can be limited to a value between, for example, 0 and 1 or 0 and infinity [66]. It can also give out only one of

two values, for example, 0 or 1. The activation function can be a step-function, a linear function or a non-linear function [67]. Eq.5.3 shows three different often used activation functions, and fig.5.2 shows the plot of the functions. $\phi_a(x)$ is a threshold function that only gives out 0 or 1. $\phi_b(x)$ is the rectifier linear unit (ReLU) function [68], which is partly linear. It gives out 0 if the value is negative and the number x if the value is positive. The last function, $\phi_a(x)$, is the Sigmoid function, which is non-linear.

$$\phi_a(x) = \begin{cases} 1, & x \geq 0 \\ 0, & x < 0 \end{cases} \qquad \phi_b(x) = max(0, x) \qquad \phi_c(x) = \frac{1}{1 + e^{-x}} \tag{5.3}$$

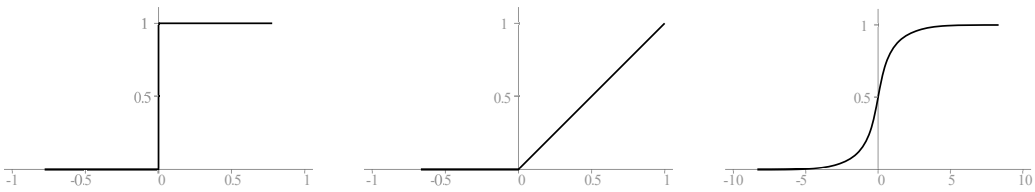


**Figure 5.2:** Plot of activation functions. (a) threshold function; (b) ReLU function; (c) Sigmoid function.

**Output:** The output is the value gotten from the activation function. It can be the final output value, or it can go to other neurons.

## 5.3 ANN Architecture

There are two types of neural networks, feed-forward and recurrent (feedback). Feed-forward is considered a static system, and the recurrent is considered dynamic [62]. Fig.5.3 shows a figure of a feed-forward and a recurrent neural network.

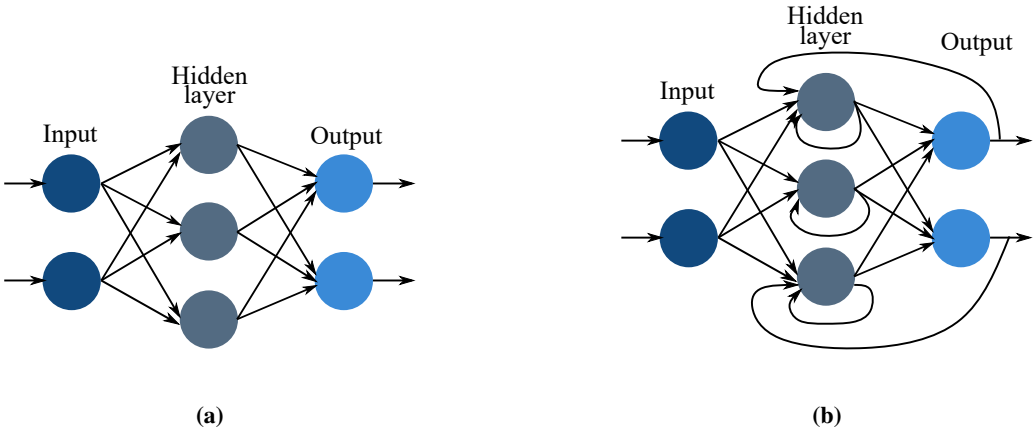


**Figure 5.3:** Types of neural networks. (a) Feed-forward; (b) Recurrent.

A neural network can be a single layer network or a multilayer network. A single layer neural network consists of one layer of neurons, and a multilayer neural network consists of two or more layers of neurons in parallel [69]. A multilayer neural network architecture can be described as $m - h - n$, where m is the number of input nodes, h is the number of nodes in the hidden layer(s), and n is the number of output nodes. Fig.5.4 has, for example, an $m - i - j - n$ architecture.

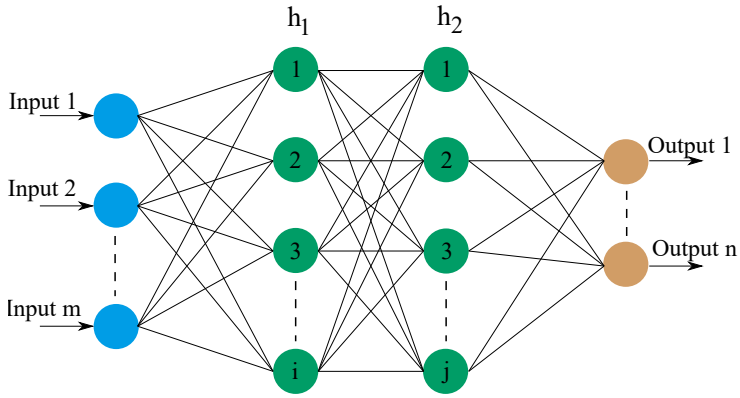


**Figure 5.4:** Neural network illustrated with n inputs (blue), two hidden layers (green) and m outputs (orange).

## 5.4 Learning

To get an ANN to perform a specific task, it has to learn. Learning means that the weights, bias and/or architecture is updated. By learning, the network does not need to follow a set of given rules (for example, optimal power flow equations) but learns the patterns [62]. There are three forms of learning paradigms: supervised learning, unsupervised learning and hybrid learning.

**Supervised learning:** The ANN has been given the correct answers to the inputs.

**Unsupervised learning:** The ANN has not been given the correct answers but learns by looking at the structure and pattern and categorizes the data.

**Hybrid learning:** Parts of the ANN is learning by supervised learning, and parts are learning from unsupervised learning.

There are also four different learning rules: Error correction, Boltzmann, Hebbian and Competitive. For more information about the learning rules, see [62]. The error correction learning is further used in this thesis with the backpropagation algorithm. The backpropagation algorithm is well suitable for supervised learning of both single- and multilayered ANNs. Thus, the ANN needs inputs and given outputs/targets. The learning algorithm of backpropagation is given in fig.5.5 [70].

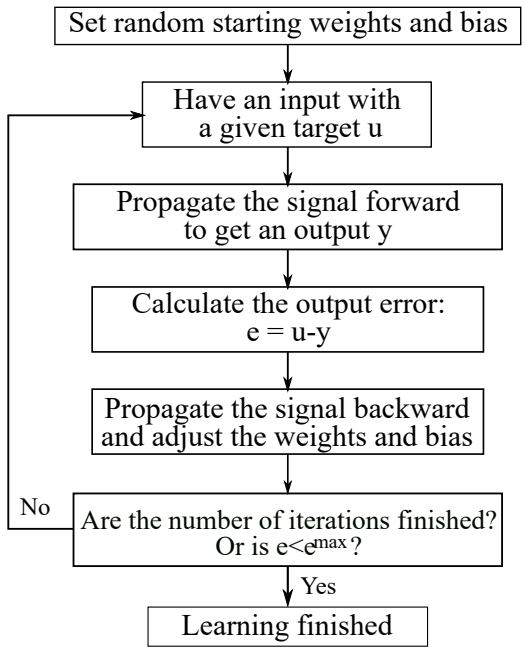


**Figure 5.5:** Flow chart of the backpropagation algorithm.

## 5.5 Verification

To avoid overfitting the ANN, or to train the ANN too much, verification is used [7]. Overfitting means that the error of the training samples is decreasing, but the error of other samples are increasing. The ANN gets too good at the training samples and bad at other samples. Fig.5.6 shows an example of overfitting where the weights and bias from epoch six should be used even though the training samples errors are decreasing.

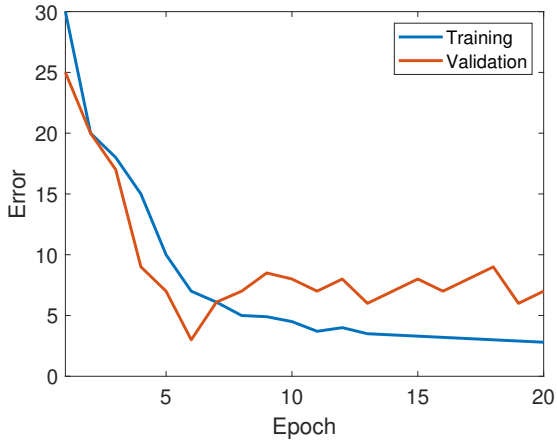


**Figure 5.6:** Example plot of training error and validation error.

To avoid overfitting, early stopping can be used [7]. Early stopping means that the ANN training stops when the error of the validation set increases through, for example, six epoch. One epoch means going through all the samples one time.

One type of error commonly used when validating the network is the mean square error (MSE) [7]. The errors from all the samples in one epoch are summarized and divided by the number of samples Q, eq.5.4.

$$MSE = \frac{1}{Q}\sum_{q=1}^{Q} e_q \tag{5.4}$$

## 5.6 ANN Model

The architecture chosen for this thesis is a 6-10-10-3 feed-forward network. The ANN has one input layer with six inputs, two hidden layers with ten neurons, and one output layer with three outputs. The inputs are given in eq.4.19 plus time, and the outputs are $S_{grid}$, $P_{ref,VSC}$ and $I_{ref,EV}$. Both the input and output is in per unit, a number between 0 and 1. The full ANN training, verification and testing MATLAB-code is given in Appendix B.2.

Neural network training is divided into three parts: training, verification and testing. Samples are obtained from the optimal power flow algorithm in ch.4, and the ANN is going to try to follow this. Thus, the training is supervised with given inputs and targets. The samples are put in random order and divided into training samples, verification samples and testing samples.

**Training:** 70% of samples. To train the network, updating weights and bias.

**Verification:** 15% of samples. To verify when the training is done, to avoid overfitting.

**Testing:** 15% of samples. For testing the network.

Further in this chapter, the vectors are marked with small, bold letters and matrices are marked with large, bold letters. The forward propagation, error and back propagation is presented.

### 5.6.1 Forward Propagation

The forward propagation for the ANN model is presented. This forward propagation algorithm is used in training, validation, testing, and simulations in Simulink, where the ANN works as a centralized controller. The algorithm starts with taking in the inputs, $\boldsymbol{a^0}$, the first weights and bias, and propagating through the activation function, 5.5a, 5.5b and 5.6. The Sigmoid function is the activation function chosen, as it gives an output between 0 and 1. The weights and bias are set to random uniform numbers between -0.5 and 0.5 the first iteration when training.

$$\boldsymbol{n^1} = \boldsymbol{W^1 a^0} + \boldsymbol{b^1} \tag{5.5a}$$

$$\boldsymbol{a^1} = f^1(\boldsymbol{n^1}) \tag{5.5b}$$

$$f^1(n) = \frac{1}{1+e^{-n}} \tag{5.6}$$

The input and output of the second hidden layer are given in eq.5.7a and 5.7b, and the activation function is given in eq.5.8. Here, the Sigmoid function is also chosen as the activation function.

$$\boldsymbol{n^2} = \boldsymbol{W^2 a^1} + \boldsymbol{b^2} \tag{5.7a}$$

$$\boldsymbol{a^2} = f^2(\boldsymbol{n^2}) \tag{5.7b}$$

$$f^2(n) = \frac{1}{1+e^{-n}} \tag{5.8}$$

The last propagation is given in eq.5.9a and 5.9b, with the activation function given in eq.5.10. The activation function used is the identity function. For the grid switching reference output in Simulink, the value has to be 0 or 1 as the switch only "understands" those values. A threshold activation function could have been used for this output, but because the derivative of the threshold function is 0 and needed for the backpropagation algorithm, it is not chosen. Instead is an extra function added to the output. If the output value is more than 0.5, the output is 1, and else it is 0. This extra function is only for the simulations in Simulink.

$$\boldsymbol{n^3} = \boldsymbol{W^3 a^2} + \boldsymbol{b^3} \tag{5.9a}$$

$$\boldsymbol{a^3} = f^3(\boldsymbol{n^3}) \tag{5.9b}$$

$$f^3(n) = n \tag{5.10}$$

Eq.5.11 gives the final output written with only inputs, weights and bias. Fig.5.7 shows the block diagram of the forward propagation.

$$\boldsymbol{a^3} = f^3(\boldsymbol{W^3} f^2(\boldsymbol{W^2} f^1(\boldsymbol{W^1 a^0} + \boldsymbol{b^1}) + \boldsymbol{b^2}) + \boldsymbol{b^3}) \tag{5.11}$$

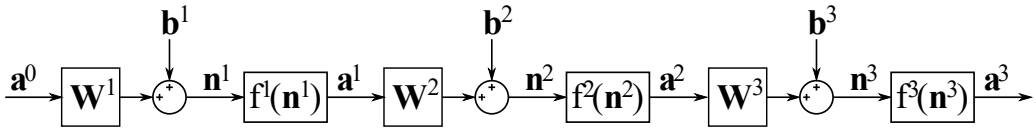


**Figure 5.7:** Block diagram of the forward propagation.

### 5.6.2 Mean Square Error

When training, verifying and testing the ANN, an error has to be calculated. In this thesis, the mean square error is used. First, the error between the target from the OPF and the output of the ANN is found, eq.5.12. Then, the square error is found in eq.5.13. All

the samples' errors are summated for each epoch and divided by the number of samples, eq.5.4.

$$\boldsymbol{e} = \boldsymbol{t} - \boldsymbol{a^3} \tag{5.12}$$

$$e_q = \boldsymbol{e^T} \cdot \boldsymbol{e} \tag{5.13}$$

The mean square error indicates how good the ANN is. If the mean square error is high, the ANN has a high error and does not work well. Moreover, if the MSE is low, the error is low, and the ANN works well. However, if the MSE is too low, it can mean that the ANN works perfectly for the training data but not other data. Therefore, early stopping is implemented. Early stopping happens if the validation error increases six times in a row.

### 5.6.3 Backpropagation

Backpropagation is used to train and update the weights and bias of the neural network. The algorithm is described with equations. Firstly is the sensitivity of each layer found, eq.5.14, going backwards from the output. The first sensitivity uses the derivative of the activation function and the error, eq.5.14a. The following sensitivities do not use the error, but the weights and previous sensitivity, eq.5.14b and eq.5.14c.

$$\boldsymbol{s^3} = -2\dot{\boldsymbol{F}}^{\boldsymbol{3}}(\boldsymbol{n}^3)\boldsymbol{e} \tag{5.14a}$$

$$\boldsymbol{s^2} = \dot{\boldsymbol{F}}^{\boldsymbol{2}}(\boldsymbol{n^2})\boldsymbol{W^{3,T}}\boldsymbol{s^3} \tag{5.14b}$$

$$\boldsymbol{s^1} = \dot{\boldsymbol{F}}^{\boldsymbol{1}}(\boldsymbol{n^1})\boldsymbol{W^{2,T}}\boldsymbol{s^2} \tag{5.14c}$$

The derivatives of the activation functions are given in eq.5.15a and 5.15b, and are placed in a Jacobi matrix, eq.5.16.

$$\dot{f}^3(n) = 1 \tag{5.15a}$$

$$\dot{f}^2(n) = \dot{f}^1(n) = \frac{1}{1+e^{-n}}\left(1 - \frac{1}{1+e^{-n}}\right) \tag{5.15b}$$

$$\dot{\boldsymbol{F}}^{\boldsymbol{m}}(\boldsymbol{n^m}) = \begin{bmatrix} \dot{f}^m(n_1^m) & 0 & \cdots & 0 \\ 0 & \dot{f}^m(n_2^m) & ... & 0 \\ \vdots & \vdots & \ddots & \vdots \\ 0 & 0 & \cdots & \dot{f}^m(n_p^m) \end{bmatrix} \tag{5.16}$$

After finding the sensitivities, the weights and bias can be updated. The change in weights are given in eq.5.17. Here, a training parameter $\alpha$, the sensitivities and the input are included. $\alpha$ is set to 0.1 and decides how fast the network is training. The new weights are given in eq.5.18.

$$\Delta \boldsymbol{W^3} = \alpha \boldsymbol{s^3 a^{2,T}} \tag{5.17a}$$
$$\Delta \boldsymbol{W^2} = \alpha \boldsymbol{s^2 a^{1,T}} \tag{5.17b}$$
$$\Delta \boldsymbol{W^1} = \alpha \boldsymbol{s^1 a^{0,T}} \tag{5.17c}$$

$$\boldsymbol{W^3} = \boldsymbol{W^3} - \Delta \boldsymbol{W^3} \tag{5.18a}$$
$$\boldsymbol{W^2} = \boldsymbol{W^2} - \Delta \boldsymbol{W^2} \tag{5.18b}$$
$$\boldsymbol{W^1} = \boldsymbol{W^1} - \Delta \boldsymbol{W^1} \tag{5.18c}$$

The change in bias is given in eq.5.19. Here, only the training parameter and sensitivities are included. The updated bias is given in eq.5.20.

$$\Delta \boldsymbol{b^3} = \alpha \boldsymbol{s^3} \tag{5.19a}$$
$$\Delta \boldsymbol{b^2} = \alpha \boldsymbol{s^2} \tag{5.19b}$$
$$\Delta \boldsymbol{b^1} = \alpha \boldsymbol{s^1} \tag{5.19c}$$

$$\boldsymbol{b^3} = \boldsymbol{b^3} - \Delta \boldsymbol{b^3} \tag{5.20a}$$
$$\boldsymbol{b^2} = \boldsymbol{b^2} - \Delta \boldsymbol{b^2} \tag{5.20b}$$
$$\boldsymbol{b^1} = \boldsymbol{b^1} - \Delta \boldsymbol{b^1} \tag{5.20c}$$

## 5.7 Verification of Model

When training, the mean square error for the training set, validation set and test set is found. The training is done with 426 888 samples from the OPF code and has been done several times with different numbers of epochs. This training was found to be the best. The error for each epoch is plotted in fig.5.8. The validation set does not increase significantly. Therefore is the last epoch, epoch number 1000, used for simulations. The training MSE is 0.03174, the verification MSE is 0.04064, and the test MSE is 0.04079.

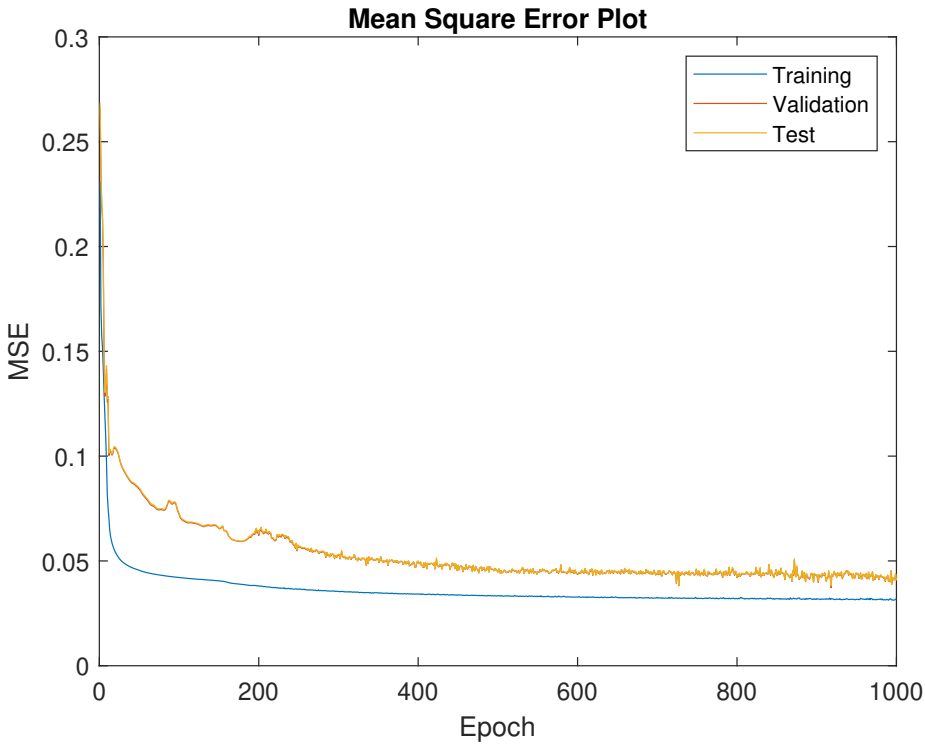


**Figure 5.8:** Plot of the mean square error for the training (blue), validation (red) and test (yellow). The validation MSE and test MSE follow each other closely.

## 5.8 Simulation Results

This chapter gives the results from running simulations of the microgrid in Simulink/MATLAB, including the artificial neural network as a centralized controller. The simulations are done for four different scenarios, similar as in ch.4.4:

- Base case.
- One scenario with abnormal behaviour of the load.
- One scenario where the sun disappears when the irradiation is at its strongest.
- One scenario when the state of charge at both the EV and BESS is 0% in the beginning.

The reference values from the OPF, $S_{grid}$, $P_{VSC,ref}$ and $I_{EV,ref}$, are presented and examined for all the simulations. After that is the power from the units in the microgrid presented, and lastly, the voltage at PCC and DC bus, and current form the VSC is presented. At the end of the chapter is a complete discussion the results from the simulations regarding to power management and performance of the ANN compared to the OPF simulations in ch.4.4.

The base case data for the solar irradiance, total power consumption and EV switch for the microgrid simulations are given in Appendix C.1, C.3 and C.5, respectively. The data for solar irradiance is retrieved in [59], and the power data is retrieved from [61]. The state of charge for the BESS and EV starts at 50%.

### 5.8.1 Base Case

These figures present the results when using artificial neural network centralized controller for base case values.

The output values from the centralized controller are given in fig.5.9. The plots shows the references for the grid switch, active power to the SUDC and current to the EV current controller. The grid switch switches on two times. The power reference follows after, and the current reference is affected by the fact that most of the time during the day, the EV is disconnected.

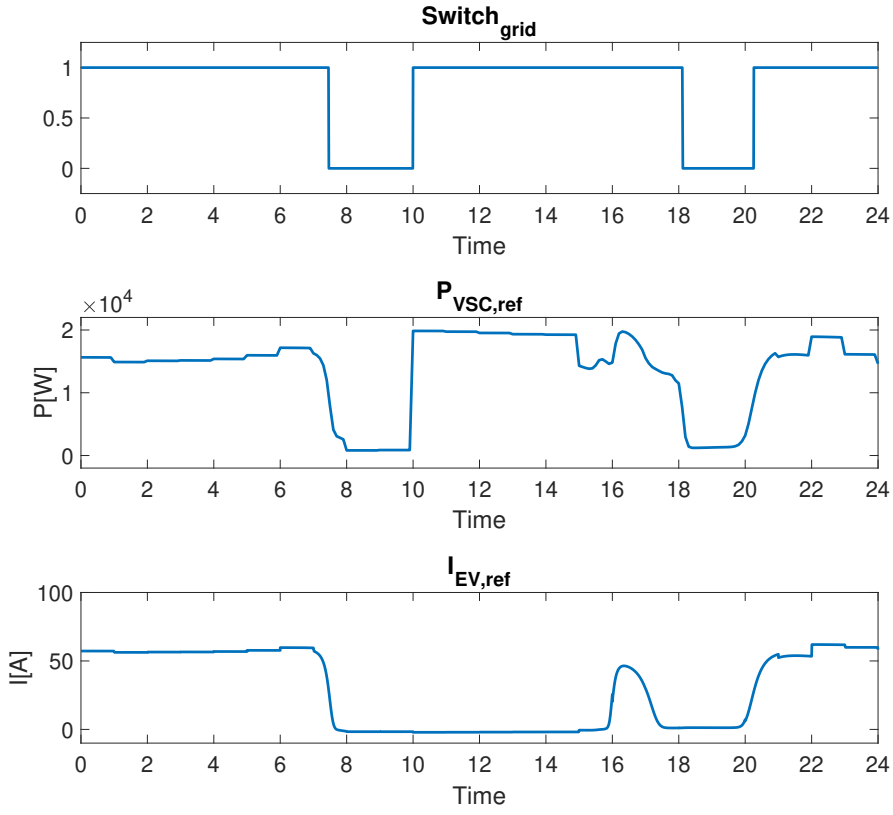


**Figure 5.9:** Output parameters from the centralized controller for the ANN base case. The grid is islanded at 1 (switch OFF) and grid-connected at 0 (switch ON).

Fig.5.10 shows the power going in and out of units in the microgrid, including the power from the grid when it is connected. When the microgrid is grid-connected, the power qualtiy to the AC loads are good. When it is disconnected, the power quality is not suitable. The DC units also experiences large ripples. And the grid power is changing as the grid is connected or not.

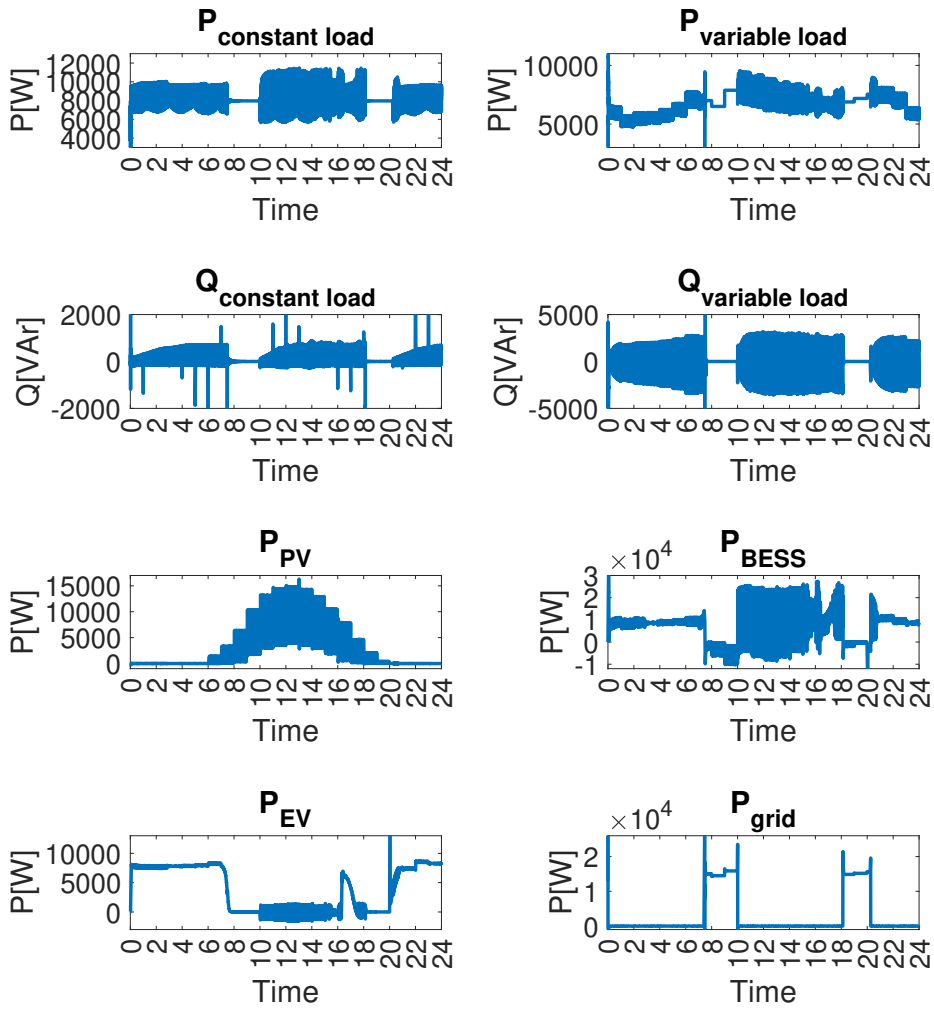


**Figure 5.10:** Active and reactive power drawn or generated from units in the microgrid for ANN base case.

Lastly, fig.5.11 shows the voltage in PCC, the current from the VSC and the DC bus voltage. The voltage in PCC experiences transients, and the voltage has a bad quality between 10 and 16 seconds. The current follows the references and the DC bus voltage experiences a large ripple occasionally.

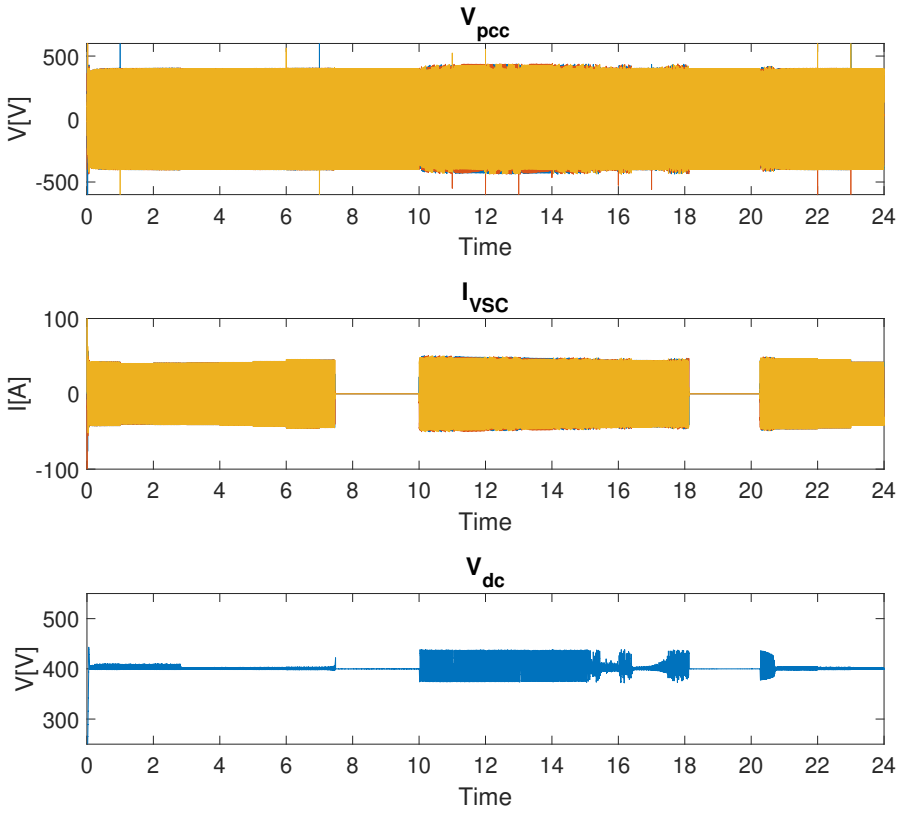


**Figure 5.11:** Voltage at the PCC, current from the VSC and DC bus voltage for ANN base case.

### 5.8.2 Abnormal Load

Figures are presented for a scenario where the load reaches a low point at 8 and a high top at 21. The values are given in Appendix C.4.

Fig.5.12 shows the output values from the centralized controller, including grid switch reference, active power reference to the SUDC and current reference to the EV current controller. The grid is grid-connected two times, and the rest of the references are following the trend. The power for all units in the microgrid, including the power from the main grid, is given in fig.5.13. The power shows the same drift as the base case, but with a difference because of the switching and load demand. Furthermore, the voltage in PCC, current from the VSC and the DC bus voltage is shown in fig.5.14. These elements also has the same tendencies as the base case.

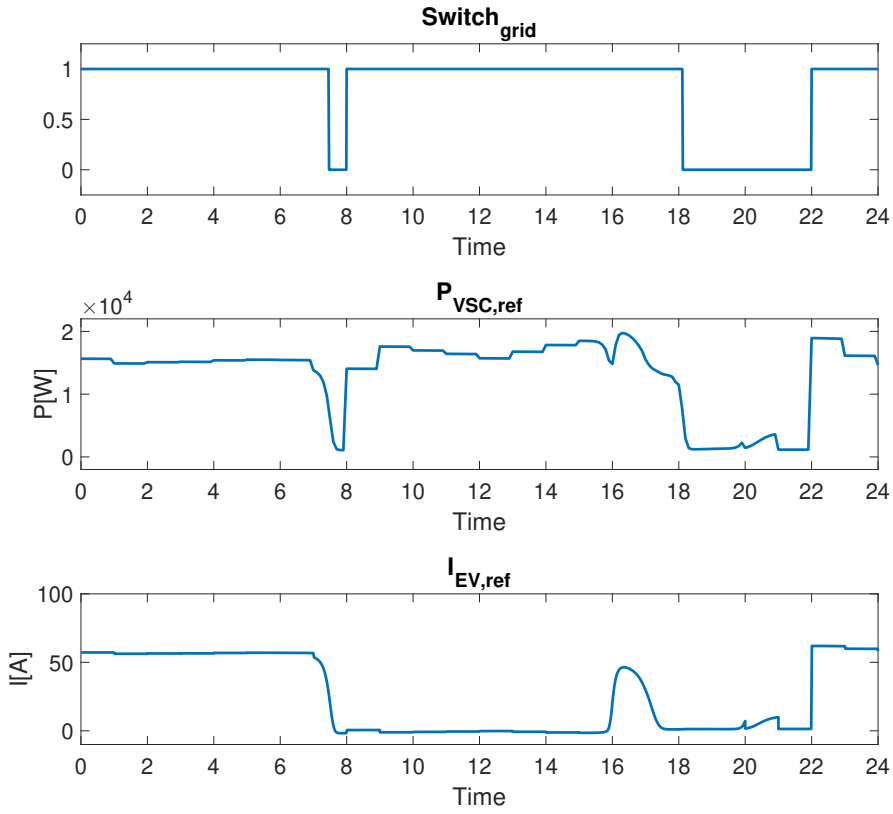


**Figure 5.12:** Output parameters from the centralized controller for the ANN abnormal load case. The grid is islanded at 1 (switch OFF) and grid-connected at 0 (switch ON).

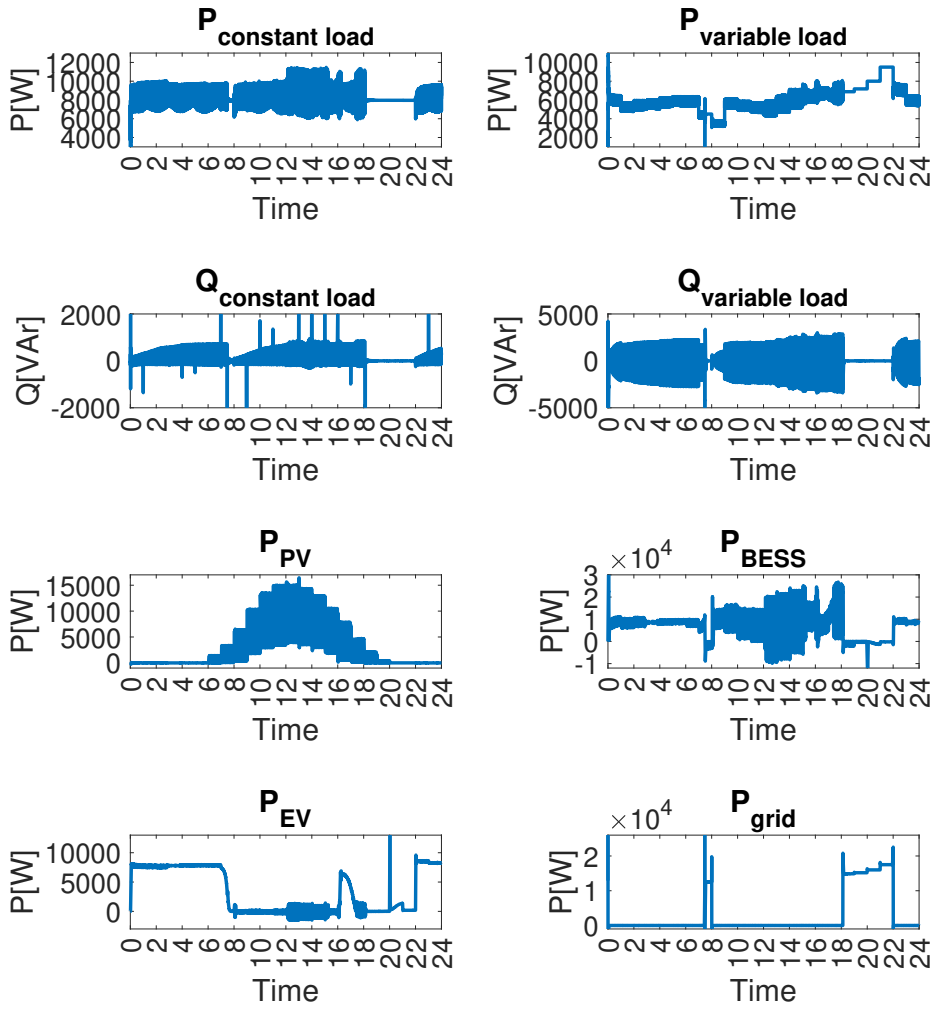


**Figure 5.13:** Active and reactive power drawn or generated from units in the microgrid for ANN abnormal load case.

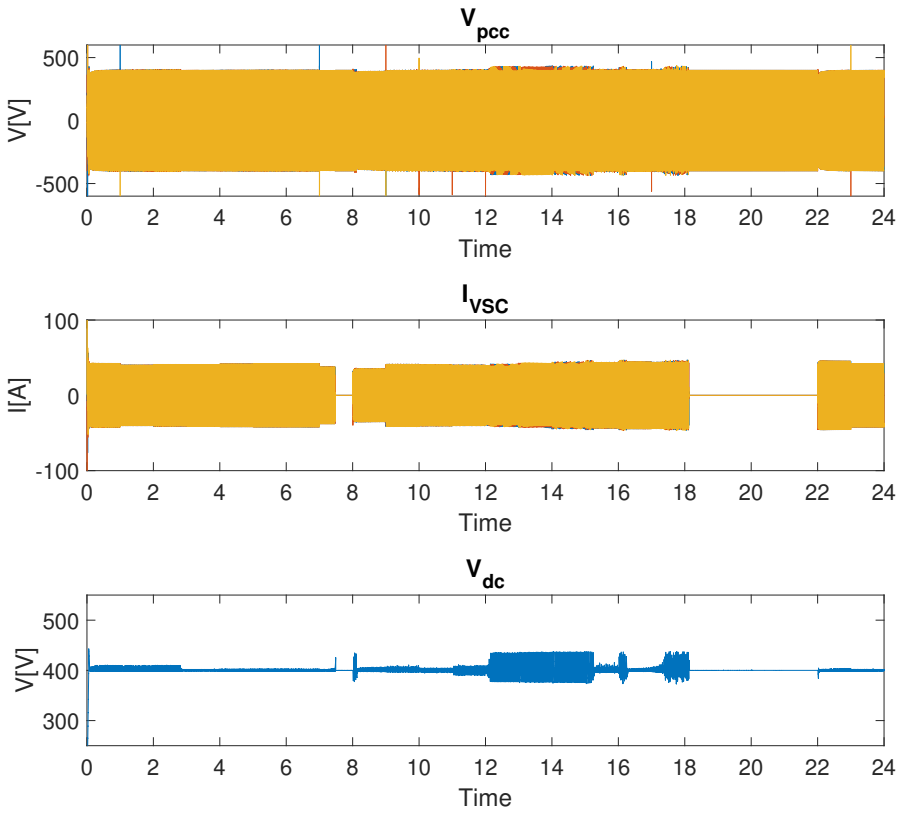


**Figure 5.14:** Voltage at the PCC, current from the VSC and DC bus voltage for ANN abnormal load case.

### 5.8.3 Abnormal Solar Irradiance

This chapter presents the plots when the sun irradiance follows the base case conditions until 12 o'clock. After 12 o'clock, the solar irradiance is zero the rest of the day. The solar irradiance values are given in Appendix C.2.

The output parameters for the grid switch, active power reference for the VSC and current reference for the EV is provided in fig.5.15. Now, the microgrid is grid-connected three times. The power reference is following well, and the current reference is similar as the base case because the EV is diconnected when the large change is happening. The power from and to the units in the microgrid is given in fig.5.16. The voltage in PCC and at the DC bus and the VSC current is presented in fig.5.17. Both the power, voltages and currents has the same trends as previous cases.

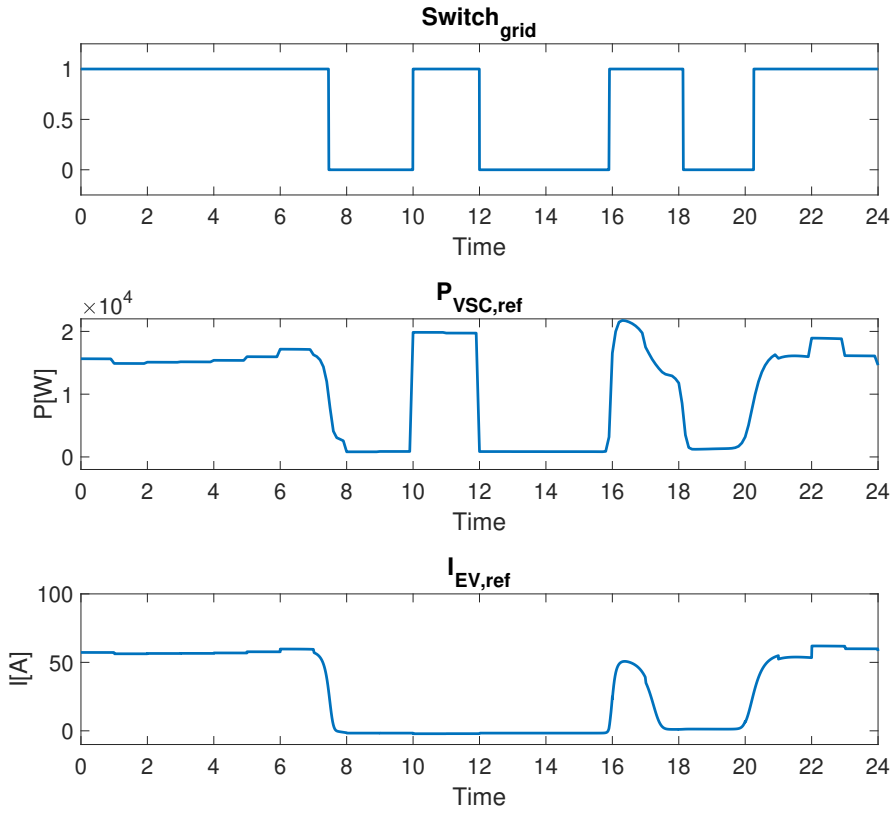


**Figure 5.15:** Output parameters from the centralized controller for the ANN abnormal solar irradiation case. The grid is islanded at 1 (switch OFF) and grid-connected at 0 (switch ON).

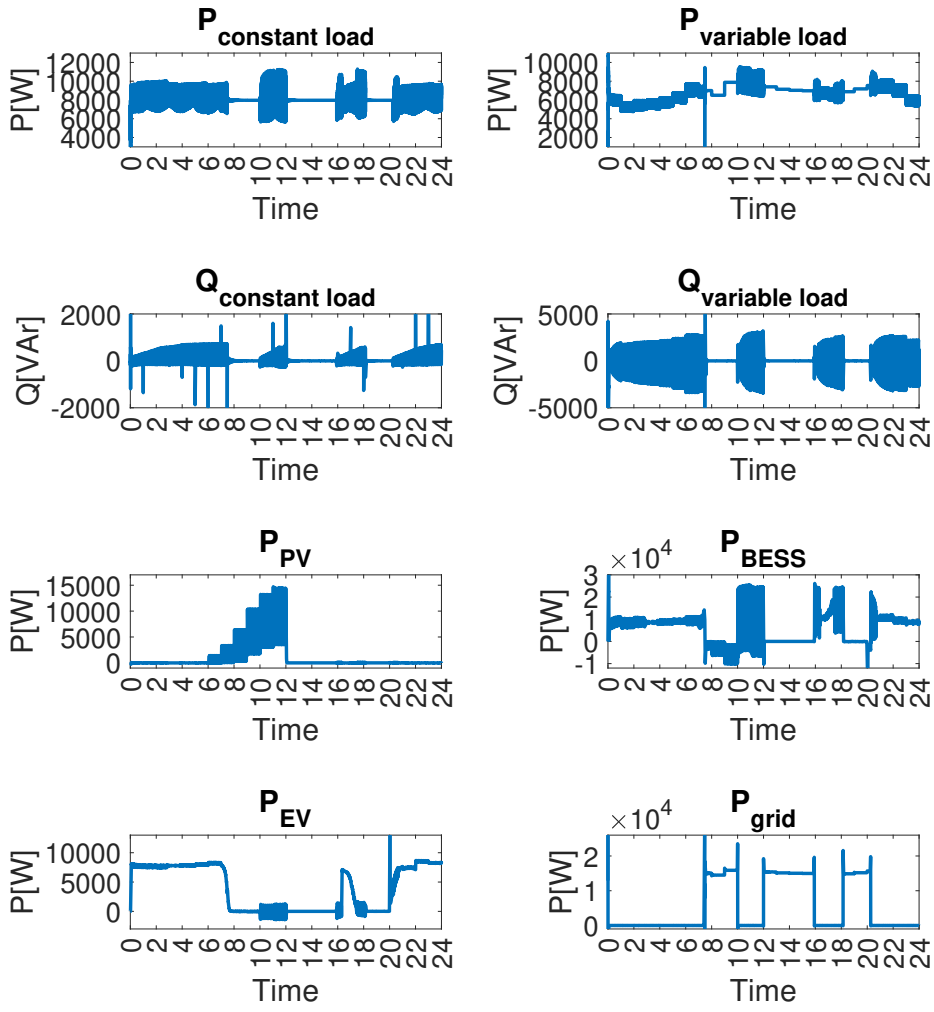


**Figure 5.16:** Active and reactive power drawn or generated from units in the microgrid for ANN abnormal solar irradiation case.

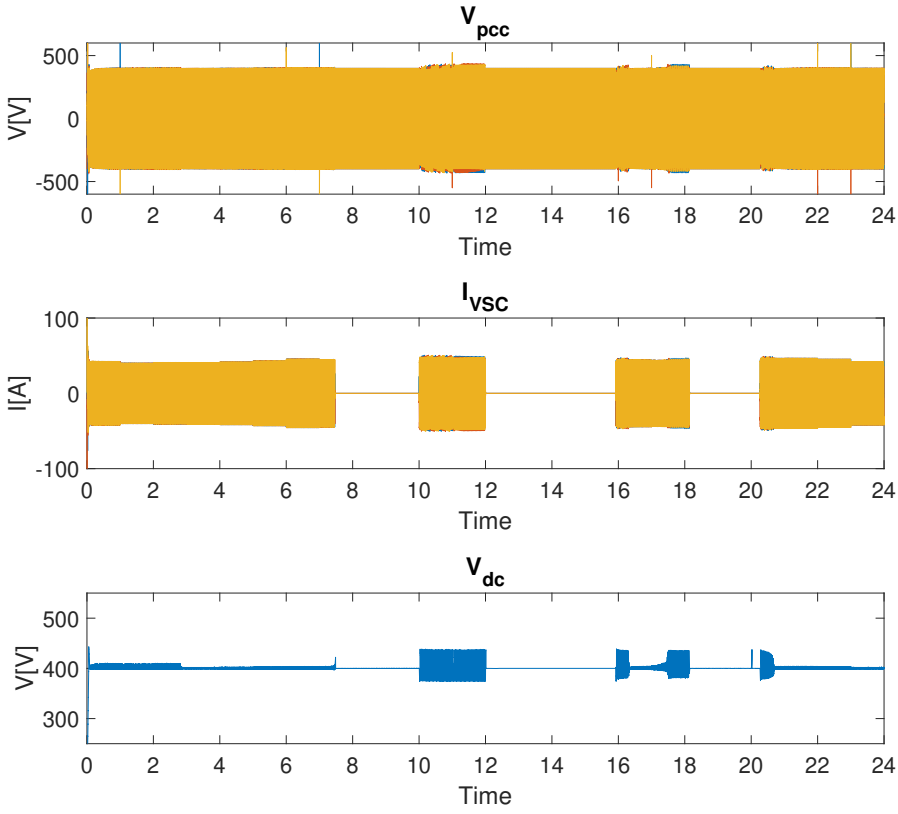


**Figure 5.17:** Voltage at the PCC, current from the VSC and DC bus voltage for ANN abnormal solar irradiation case.

### 5.8.4 BESS and EV State of Charge 0%

In this chapter, the EV and BESS start with a state of charge at 0%.

In this last simulation case, the output reference values are presented in fig.5.18. The microgrid is grid-connected throughout the simulation, which also affects the power and current references. The power from the generating units and the power going to the loads are given in fig.5.19. The quality is good for the AC powers, but the PV and EV experiences a larger ripple as the power increases. And lastly, fig.5.20 displays the voltage in PCC, current from the VSC, and the DC bus voltage. The plots shows a current that is zero and voltages with good quality.

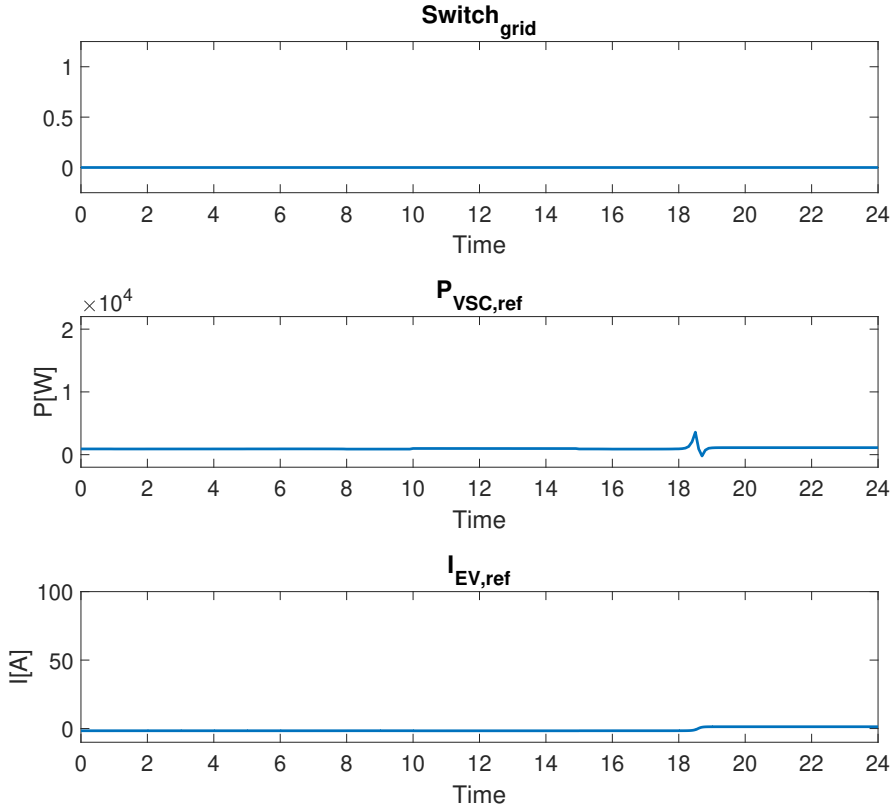


**Figure 5.18:** Output parameters from the centralized controller for the ANN state of charge case. The grid is islanded at 1 (switch OFF) and grid-connected at 0 (switch ON).

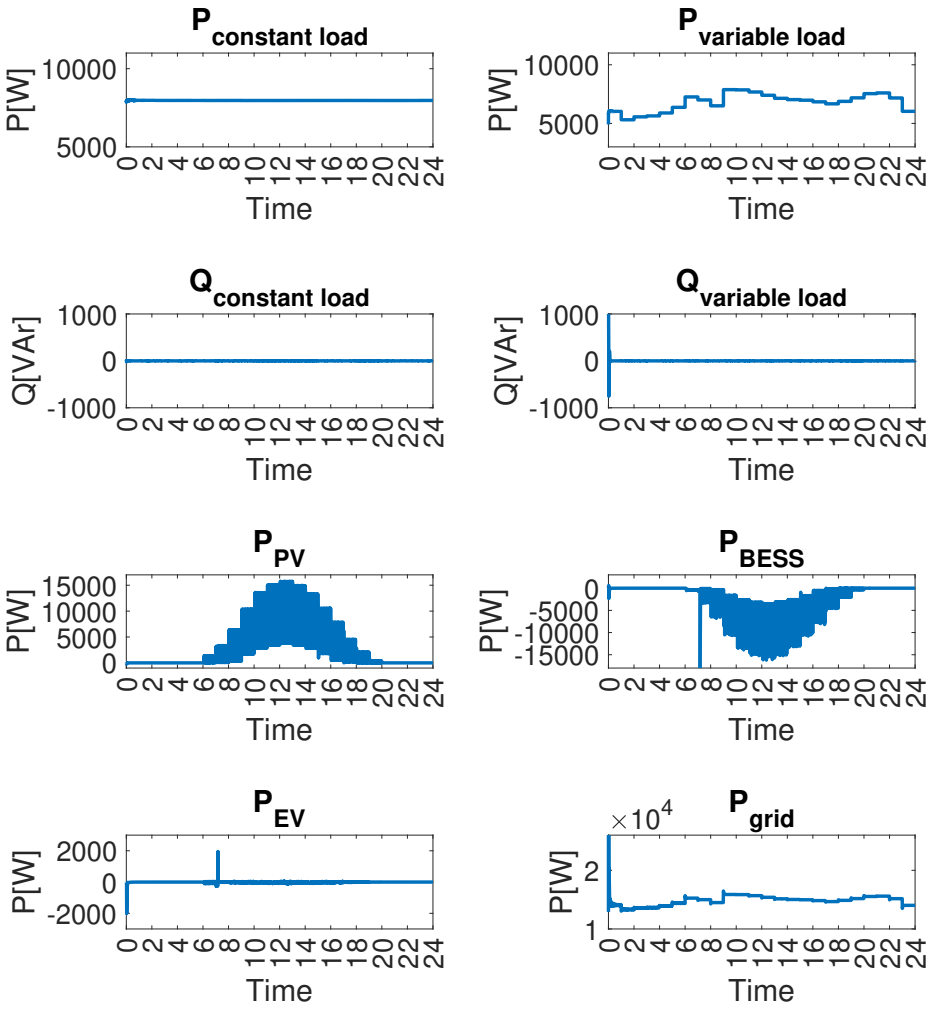


**Figure 5.19:** Active and reactive power drawn or generated from units in the microgrid for ANN state of charge case.

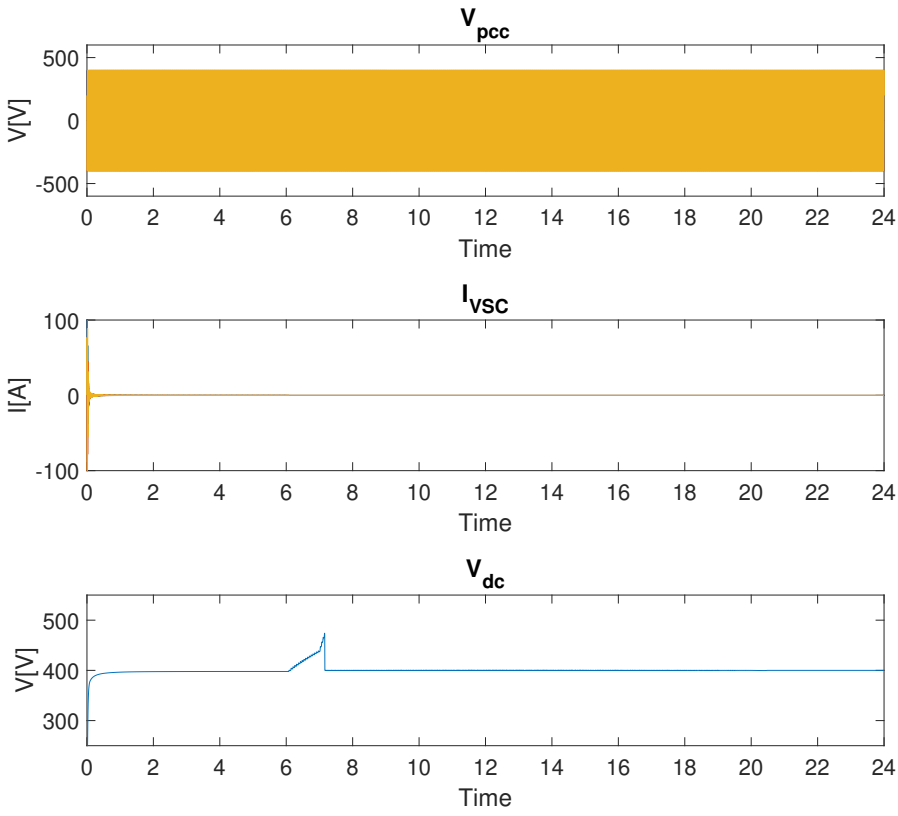


**Figure 5.20:** Voltage at the PCC, current from the VSC and DC bus voltage for ANN state of charge case.

### 5.8.5 Discussion of Results

Four cases using artificial neural networks as a centralized controller has been presented. Ch.2.6 raised four points of what a power management strategy should do. This discussion part is firstly discussing the power management strategy and if the points are achieved. Lastly, the performance of the artificial neural network compared to the optimal power flow is concerned.

**Power Management**

The first point in ch.2.6 is that a power management strategy should keep an efficient load sharing between DERs. In all the cases, the criteria are fulfilled. The microgrid is changing according to the references from the ANN. One example is the base case power in fig.5.10. When the network realizes that the power from the microgrids units is not enough to satisfy the load demand, a change in power-sharing happens. The main grid connects, and the power from the BESS decreases. It can also be noted that the power from the EV follows the same trend as the current reference to the EV. This yields for all the cases.

The second point is to consider the limits of the DERs. Three specific limitations are noted from ch.4.4: the power limit for the BESS, the power limit for the EV and the power limit from the VSC. In this case, the batteries state of charge limits is not focused as they use a very long time to charge and discharge. Firstly, when looking at the EV, the power never exceeds the limit of 9 kW. However, transients above that value occur, see, for example, fig.5.16 at 20 seconds. The power from or to the BESS experiences large ripple midday in all the cases. However, the power limits are not withheld in the state of charge case in fig.5.19. When the generated power from the PV increases, the power going to the BESS increases. However, this is a weakness in the system, as the power has nowhere else to go when the microgrid is grid-connected, and the EV is disconnected. The power limits of the VSC is 20 kVA, and the current limit is thus 57.74 A. The current from all the cases is below the wanted value.

The third point is to maintain the power quality. When the microgrid is grid-connected, the microgrids power quality is good, except for a large ripple from the PV and into the BESS, fig.5.19. The voltage profile is good. When the microgrid is islanded, the power quality is not satisfying. In, for example, fig.5.11, the voltage in PCC experiences disturbances, and the voltage at the DC bus experiences large ripples. The active power going to the loads also receives a large ripple, and the reactive power is not constant at zero, fig.5.10. This point is not fulfilled. However, to improve the power quality, the controllers in the lower hierarchy should be considered. The reason is that the bad quality occur most of the time, and not only when the load and generated power is changing. Perhaps they need a retuning or to be changed. The inductor and capacitance values

in the converters can also be investigated, the same can the switching frequency of the IGBTs.

Lastly, a power management strategy should improve the dynamic response. In fig.5.14, the voltage experiences transients. The transients occur at whole seconds, which is the time the load and generated power changes. Fig.5.13 also presents powers with transients. One example is the EV power at 20 seconds and the grid power around 8 seconds. This point is also not fulfilled.

The ANN manages to keep a good load sharing between DERs and the grid. But the limitations, power quality and dynamic response are not acceptable for a microgrid. However, to improve the system, the control methods down in the hierarchy should firstly be considered. If the first levels in a hierarchy are not fulfilled, the following levels will also fail. Lastly, the capacitor and inductor values in the different converter should be examined and the switching frequency.

**Artificial Neural Network Performance**

The results from the ANN simulations are compared to the OPF simulations. Fig.5.21 shows the reference values given from the centralized controller with OPF and ANN. This is for the base case simulations. Looking at the switch in fig.5.21(a), the ANN follows the OPF good, except for some errors around 7-8 seconds. The power reference in fig.5.21(b) shows an ANN that follows the trends of the OPF but overshoots some places, for example, from 10 to 14 seconds. Furthermore, the current reference in fig.5.21(c) shows an ANN that follows the same trends as the OPF but undershoots in most areas, for example, from 0 to 6 seconds.

The total results of these simulations are that the ANN follows the OPF model, but the values are not entirely correct. Suggestions for improvements are listed below:

- In this ANN model, both predictions and OPF are included. Splitting the predictions into separate neural networks could help to decrease the error.
- The architecture of the ANN could be changed. For example, by adding more neurons and hidden layers to decrease the error. Also, instead of having a feed-forward network, a recurrent network could be implemented. Because these simulations depend on time, it is believed that a recurrent network could work better as it is dynamic.
- More training data could be used. This training already uses over 400 000 samples, but having more or new samples could improve the network performance.
- New training method. Including a new training method could help to decrease

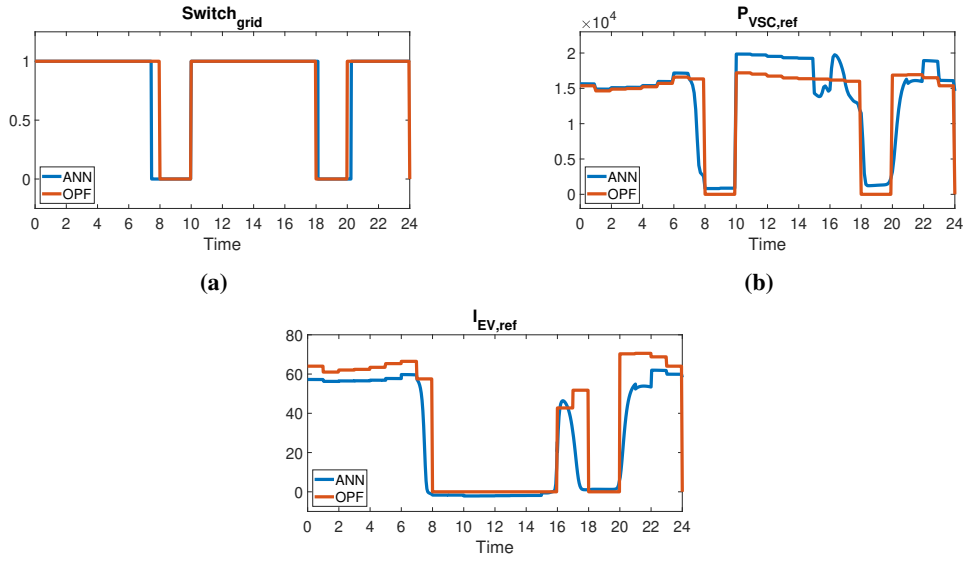


**Figure 5.21:** ANN simulation compared to OPF simulation for the base case. (a) Grid switch; (b) Active power reference for the VSC; (c) Current reference for the EV.

the error faster. For example, the Levenberg-Marquant algorithm could have been implemented.

This study shows that an ANN succeeds to follow the trends of an OPF model but with an error. By improving the ANN, it is believed that it will work very well as a replacement for the OPF. In these simulations, both ANN and OPF results give large ripples and bad power quality. Results show that the ANN itself is not a cause of that. However, if the pros of having an ANN is worth the cons is to decide. An ANN can easily add new units to the system, keep learning new patterns, have a short computation time, and still work even if some information is missing, making the controller more robust. Nevertheless, on the other side, the ANN will need a massive amount of data that will take much time to train and demand a lot of power and costs. It also behaves like a black box, so unexpected behaviour can happen, which means that the microgrid must be robust enough to handle that.

# Chapter 6

# Conclusion

This chapter is concluding the work that has been done in this thesis. It is also pointing out further work.

## 6.1 Conclusion

Because of the increasing use of renewable energy sources, the power management strategy has to be improved. Renewable energy sources can experience rapid and unexpected changes, and it is essential to have energy systems that can handle these changes. In previous studies, artificial neural networks have shown to be well suited for predictions and control and have therefore been suggested as a centralized controller for a hybrid microgrid. Thus, this thesis has focused on using artificial neural networks as a power management strategy. The focus has also been researching if an ANN can be used for optimal power flow of a microgrid.

The hybrid microgrid included two loads, one constant and one variable, one solar PV, one EV and one BESS. The ANN presented was a feed-forward microgrid with two hidden layers with ten neurons each. There were six inputs and three outputs. The inputs were measurements from the microgrid. The outputs were reference values sent to the self-synchronized universal droop controller, EV current controller and the switch that connected the microgrid to the main grid. The ANN was trained using backpropagation, verified and tested with 426 888 samples from the OPF code. The mean square error of the verification set was 0.04064. The mean square error was found satisfying for this thesis, and simulations were done for four different cases with both the OPF and ANN as a centralized controller.

The ANN and OPF centralized controller was researched in a power management perspective. Common for both strategies was that one power management demand was

fulfilled, and the three others were not. The controllers managed to keep an efficient load sharing between DERs and the grid, for example, by connecting the microgrid to the grid when needed. However, the operating limits of the BESS were not withheld, and the power quality was poor with a large ripple. The ripples from the DC sources were significant and should be reduced. The voltage and power also experienced transients that occurred when the load and generated power changed. Based on the results, indications are that most of the the problems in this microgrid come from low-level control. The bad power quality does not appear only when changes in load and generated power happens, but all the time. To improve this can, for example, the converter controllers be re-tuned or changed, and also can the converter parameters be investigated. Converter parameters can be switching frequency, inductors and capacitors. The microgrid does not supply the AC load when the main grid is connected, which leads to a weakness in the system. The power from the PV has to go somewhere, and it results in exceeding the limits of the BESS. With an improved microgrid, the findings in this thesis show that the ANN can work well as a centralized controller, because it manages to control the power sharing.

It could be observed that the ANN managed to follow the same trend as the OPF, but in some cases, there was a significant error. However, it was not seen that the microgrid with ANN performed more poorly than the microgrid with OPF. The load sharing and power quality was very alike. Suggestions for improvements for the ANN was proposed. For example, could the model architecture be changed, a new training method could be applied or new training data could be used. Lastly, elements such as costs, time, and reliability must be considered if using an ANN as a centralized controller is wanted.

The findings in this thesis indicates that with improvements, the ANN can be used for optimization and power management of a hybrid microgrid.

## 6.2 Future work

Future work should focus on improving the ANN as a centralized controller. This can be done by increasing the ANN's performance and decrease the error. In addition should the performance of the microgrid in general be improved, this to get a better view of how the ANN improves the load sharing and power quality.

The ANN should also be used as a centralized controller in a broader perspective. For example, implementing the ANN in a system with more buses or many microgrids networked together. In addition should more scenarios be investigated. For example, how the controller works if a fault happens, or if one measurement (input) is missing.

# Appendices

# Appendix A

# Simulink Model

## A.1 Microgrid Simulink Model

The complete Simulink model for this thesis is given in fig.A.1. The model includes one constant load, variable load, solar PV, BESS, EV, a VSC and a connection to the grid.

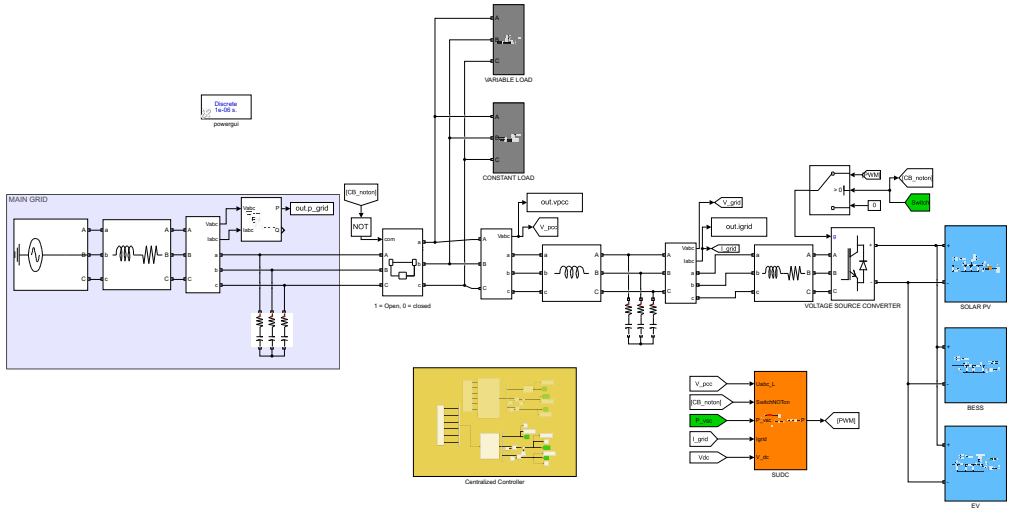


**Figure A.1:** Microgrid model. The purple area marks the main grid, the grey areas mark the loads, the blue regions mark the solar PV, BESS and EV. The centralized controller is given in the yellow box and the SUDC in the orange. The non-marked area is the VSC, LCL filter and switch to the grid. The green "Switch" and "P_vsc" marks the receiving outputs from the centralized controller.

## A.2 Solar PV Simulink Model

The solar PV Simulink model is given in fig.A.2.

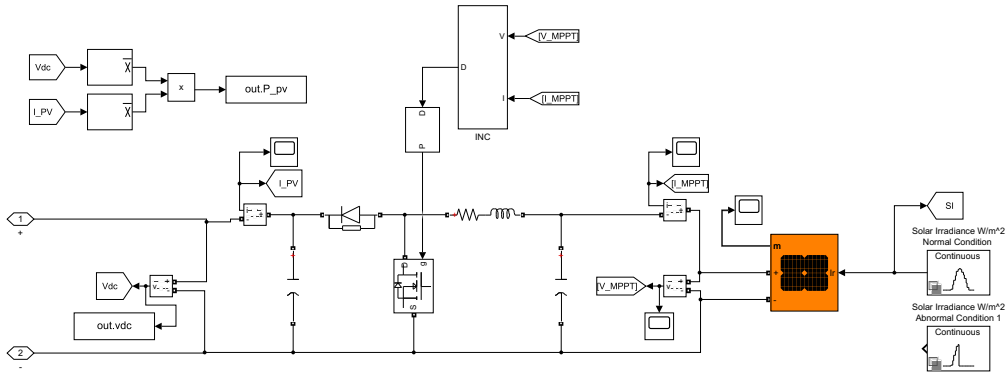


**Figure A.2:** Solar PV Simulink model. The model includes a boost converter, an MPPT controller (marked "INC") and a PV array. To change the solar irradiation from normal conditions to abnormal conditions, the boxes marked with "Solar Irradiance" are switched.

## A.3 BESS Simulink Model

The BESS Simulink model is given in fig.A.3.

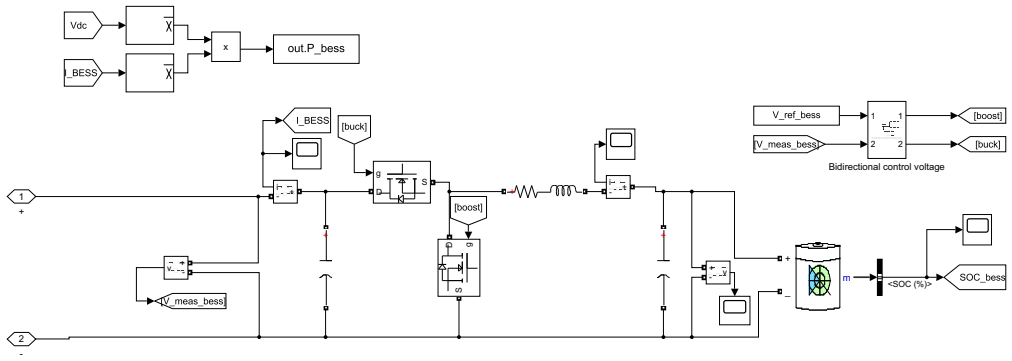


**Figure A.3:** BESS Simulink model. The model includes a bidirectional converter, a voltage controller and a battery.

## A.4 EV Simulink Model

The EV Simulink model is given in fig.A.4.

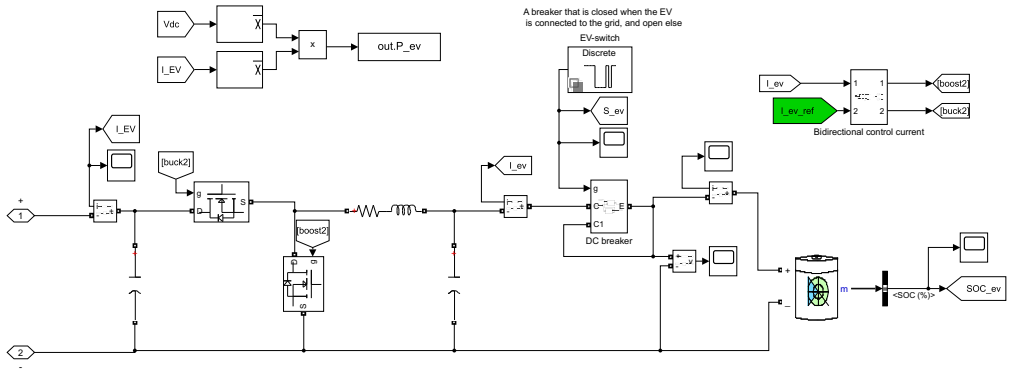


**Figure A.4:** EV Simulink model. The model includes a bidirectional converter, a current controller and a battery. In addition, there is a switch ("DC breaker") consisting of two IGBTs receiving signals from a stair generator. The green "I_ev_ref" marks the receiving output from the centralized controller.

## A.5 Load Simulink Model

The variable load Simulink model and the constant load Simulink model is given in fig.A.5 and A.6, respectively.

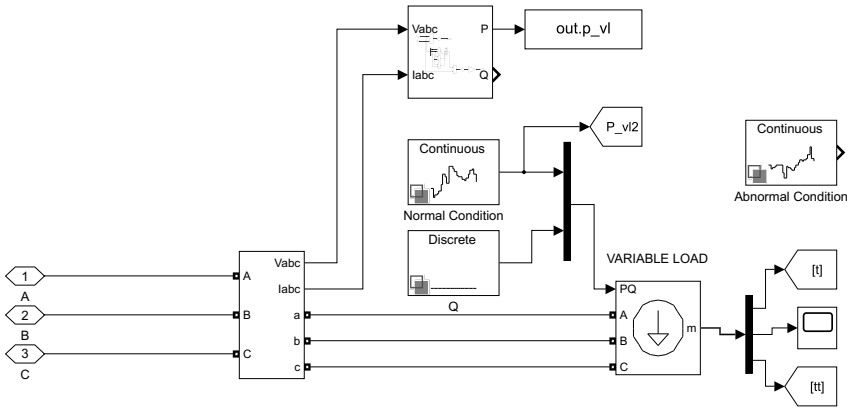


**Figure A.5:** Variable load Simulink model. The blocks marked "Normal Condition" and "Abnormal Condition" are switched to change the load from normal conditions to abnormal conditions.

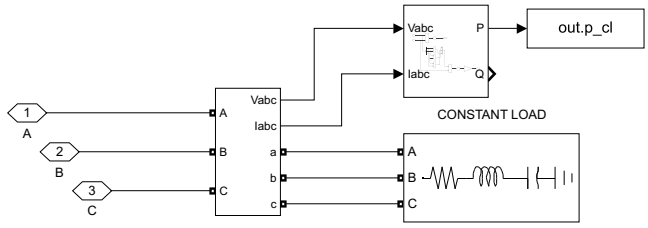


**Figure A.6:** Constant load Simulink model.

## A.6 Centralized Controller Simulink Model

The centralized controller Simulink model is presented in fig.A.7.

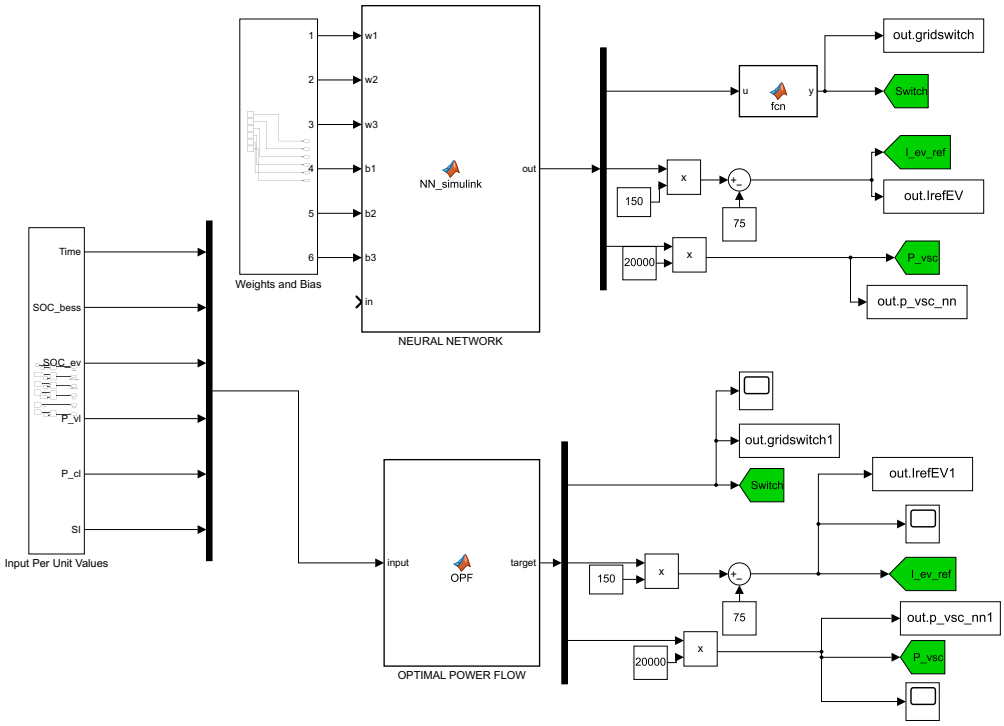


**Figure A.7:** Centralized controller Simulink model. The model includes inputs from the microgrid units, which are transformed to per-unit values, an optimal power flow algorithm, and an artificial neural network algorithm. The output from the OPF algorithm is converted to actual values. The ANN takes in the weights and bias, and on the outputs, the values are converted to actual values. In addition, an extra function block is added to keep the switching values to 0 or 1.

# Appendix B

# MATLAB Code

## B.1 Optimal Power Flow MATLAB Code

```
function [target] = OPF(t, SOC_ev, SOC_bess, P_vl, S_ev, SI)
% Time and values are sampled directly from the microgrid, the
% output is a prediction of delta_T second(hour) after.

delta_T = 1e-6; %time steps, needed for predictions
%% From base values to real values
t = t*24;
SOC_ev = SOC_ev*100;
SOC_bess = SOC_bess*100;
P_vl = P_vl*10000;
SI = SI*1000;

%% Constraints
SOC_max = 99;
SOC_min = 1;
S_VSC_max = 20000;
P_ev_max = 9000;
P_ev_min = -9000;

%% Predictions
%Calculating P_pv
P_pv_max = 243.5;
N_p = 40;
N_s = 2;
```

```
P_pv = SI/1000*P_pv_max*N_p*N_s;

%Calculating constant loads
P_cl = 8000;
P_losses = 57.735^2*0.4;

%Calculating the net power for t
if SOC_bess > SOC_min
    SOC_bess_t = 1;
else
    SOC_bess_t = 0;
end
if SOC_ev > SOC_min
    SOC_ev_t = 1;
else
    SOC_ev_t = 0;
end
P_net_t = P_pv-P_vl-P_cl-P_losses+9000*SOC_ev_t*S_ev...
+9000*SOC_bess_t;
%If this has a positive value, the grid switch was on

%% Predictions
%Time
t = t+delta_T;

%SOC
V_ev = 120; %BESS and EV has the same voltage
if P_net_t >= 0
    if S_ev == 1
        I_ev_t = (P_pv-P_cl-P_vl-P_losses)/(2*V_ev);
        I_bess_t = (P_pv-P_cl-P_vl-P_losses)/(2*V_ev);
    else
        I_bess_t = (P_pv-P_cl-P_vl-P_losses)/V_ev;
        I_ev_t = 0;
    end
else
    if S_ev == 1
        I_ev_t = P_pv/(2*V_ev);
        I_bess_t = P_pv/(2*V_ev);
    else
```

```
65          I_ev_t = 0;
66          I_bess_t = P_pv/V_ev;
67      end
68  end
69
70  SOC_ev = SOC_ev + delta_T*I_ev_t/180*100;
71  SOC_bess = SOC_bess + delta_T*I_bess_t/180*100;
72
73  %Sun irradiance
74  if (t == 6) || (t <= 8)
75      SI = SI+50*delta_T;
76  elseif (t>8)&&(t<=12)
77      SI = SI+100*delta_T;
78  elseif (t>12)&&(t<=18)
79      SI = SI-50*delta_T;
80  else
81      SI = 0;
82  end
83
84  %Load prediction
85
86  if (t>=0)&&(t<=8)
87      P_l = P_cl+P_vl+P_losses+200*delta_T;
88  elseif (t>8)&&(t<=14)
89      P_l = P_cl+P_vl+P_losses-200*delta_T;
90  elseif (t>14)&&(t<=17)
91      P_l = P_cl+P_vl+P_losses+200*delta_T;
92  elseif (t>17) && (t<=21)
93      P_l = P_cl+P_vl+P_losses;
94  elseif (t>21)
95      P_l = P_cl+P_vl+P_losses-200*delta_T;
96  end
97
98
99  %EV switch
100 if (t>=0) && (t<8)||(t>=16) && (t<18) ||(t>=20) && (t<=24)
101     S_ev = 1;
102 else
103     S_ev = 0;
104 end
```

```
105
106 %Net power
107 P_net = P_pv-P_l;
108
109
110
111 %% Optimizing power delivery/consumptions from BESS and EV
112 if P_net<0
113
114     if SOC_bess>SOC_min && SOC_ev>SOC_min && S_ev == 1
115
116         P_bess = -P_net/2;
117         P_ev = -P_net/2;
118
119     elseif SOC_bess>SOC_min && (SOC_ev==SOC_min || S_ev == 0)
120
121         P_bess = -P_net;
122         P_ev = 0;
123
124     elseif SOC_bess==SOC_min && SOC_ev>SOC_min && S_ev == 1
125
126         P_bess = 0;
127         P_ev = -P_net;
128
129     else
130
131         P_bess = 0;
132         P_ev = 0;
133
134     end
135 else
136
137     if SOC_bess<SOC_max && SOC_ev<SOC_max && S_ev == 1
138
139         P_bess = -P_net/2;
140         P_ev = -P_net/2;
141
142     elseif SOC_bess<SOC_max && (SOC_ev==SOC_max || S_ev == 0)
143
144         P_bess = -P_net;
```

```
145         P_ev = 0;
146
147     elseif SOC_bess==SOC_max && SOC_ev<SOC_max && S_ev == 1
148
149         P_bess = 0;
150         P_ev = -P_net;
151
152     else
153
154         P_bess = 0;
155         P_ev = 0;
156     end
157 end
158
159 %Checking power limits on battery
160 if P_ev > P_ev_max
161     if P_bess > P_ev_max
162          P_ev = -P_pv/2; %has to connect to the grid and will
163                          %thus be charging if the PV
164                          %is producing power
165     else
166         P_ev = -P_pv;
167     end
168 elseif P_ev < P_ev_min
169    P_ev = -P_ev_min;
170 else
171    P_ev = P_ev;
172 end
173
174 if P_bess > P_ev_max
175    if P_ev > P_ev_max
176          P_bess = -P_pv/2; %has to connect to the grid and
177                            %will thus be charging if the PV
178                            %is producing power
179     else
180         P_bess = -P_pv;
181     end
182 elseif P_bess < P_ev_min
183    P_bess = P_ev_min;
184 else
```

```
185     P_bess = P_bess;
186 end
187
188 I_ev = P_ev/V_ev;
189
190 %Setting I_ev to a non-negative value between 0 and 1, 75 A is the
191 %maximum current.
192 I_ev = (I_ev+75)/150;
193
194 %Calculating the net power
195 P_net = P_pv+P_bess+P_ev-P_l;
196
197 %% Optimizing the grid switch and VSC power reference
198 %Setting grid switch to on(1) or off(0) and setting the power
199 %reference to the vsc. The power reference to the VSC is
200 %divided by 20 000 to get a value between 0 and 1.
201 if P_net < 0
202     S_grid = 0; %Grid-connected
203     P_vsc = 0;
204 else
205     S_grid = 1; %Islanded
206     P_vsc = P_l/20000;
207 end
208
209 %Because the load never exceeds 18 kW, the power limits of the
210 %VSC are not considered.
211
212 target = [S_grid, I_ev, P_vsc];
213 end
```

## B.2 Artificial Neural Network MATLAB Code

```
function NN_training(input, target, samples)
% ANN with two hidden layers, 6-10-10-3
% The input and target has to be X x Y where X is the number of
% samples, and Y is the number of inputs/targets

%% Initializing weights
%Setting random uniform weights and bias' between -0.5 and 0.5
w1 = 1*rand(10,6)-0.5;
w2 = 1*rand(10,10)-0.5;
w3 = 1*rand(3,10)-0.5;
b1 = 1*rand(10,1)-0.5;
b2 = 1*rand(10,1)-0.5;
b3 = 1*rand(3,1)-0.5;

%% Datasets
%Shuffles the rows in the dataset (input and target)
xi = randperm(samples);
input = input(xi, :);
target = target(xi, :);
Numb_epoch = 500;

%% Training
%70 percent of the values are training values
Numb_train = floor(0.7*samples);
mse_train_tot = 0;
alpha = 0.1;
%Values for verification (random values, keep MSE_val_prev large)
MSE_val_prev = 10;
w1_prev = zeros(10,6);
w2_prev = zeros(10,10);
w3_prev = zeros(3,10);
b1_prev = zeros(10,1);
b2_prev = zeros(10,1);
b3_prev = zeros(3,1);

k = 0;

for epoch = 1:Numb_epoch
for i = 1: Numb_train
```

```
40      input_train = input(i,:);
41      target_train = target(i,:);
42      a0_train = input_train;
43
44      %Feed forward
45      n1_train = w1*a0_train'+b1;
46      a1_train = Sigmoid(n1_train);
47
48      n2_train = w2*a1_train'+b2;
49      a2_train = Sigmoid(n2_train);
50
51      n3_train= w3*a2_train'+b3;
52      a3_train = n3_train; %linear output activation function
53
54      %Calculating the error
55      error = target_train- a3_train';
56      delta = error;
57      mse_train = error*error';
58      mse_train_tot = mse_train_tot + mse_train;
59      %Back propagation
60      s3 = -2*Lin_out(n3_train)*delta';
61
62      s2 = Sigmoid_der(n2_train)*w3'*s3;
63
64      s1 = Sigmoid_der(n1_train)*w2'*s2;
65
66      %Updating the weights
67      adjustment_of_w3 = alpha*s3*a2_train;
68      adjustment_of_w2 = alpha*s2*a1_train;
69      adjustment_of_w1 = alpha*s1*a0_train;
70
71      w1 = w1 - adjustment_of_w1;
72      w2 = w2 - adjustment_of_w2;
73      w3 = w3 - adjustment_of_w3;
74
75      b3 = b3 - alpha*s3;
76      b2 = b2 - alpha*s2;
77      b1 = b1 - alpha*s1;
78  end
79
```

```
80
81  %% MSE
82  MSE_train = mse_train_tot/Numb_train; %error after each epoch
83  MSE_plot_train(epoch) = MSE_train;
84  mse_train_tot = 0;
85
86  %% Validation
87
88  Numb_val = floor(0.15*samples);
89  mse_val_tot = 0;
90
91  for i = 1:Numb_val
92
93      a0_val = input(i+Numb_train,:);
94      target_val = target(i+Numb_train,:);
95
96      n1_val = w1*a0_val'+b1;
97      a1_val = Sigmoid(n1_val);
98
99      n2_val = w2*a1_val'+b2;
100     a2_val = Sigmoid(n2_val);
101
102     n3_val = w3*a2_val'+b3;
103     final_output = n3_val;
104
105     error_val = target_val-final_output';
106     mse_val = error_val*error_val';
107     mse_val_tot = mse_val_tot + mse_val;
108 end %epoch
109
110 MSE_val = mse_val_tot/Numb_val
111 MSE_plot_val(epoch) = MSE_val;
112
113
114 % Checking if the mean square error decreases or increases. When
115 % the error goes up for six iterations, the simulations saves the
116 % weights where the error was at its lowest
117
118 if MSE_val > MSE_val_prev
119     k = k+1;
```

```
    if k == 1
    w1_val = w1_prev;
    w2_val = w2_prev;
    w3_val = w3_prev;
    b1_val = b1_prev;
    b2_val = b2_prev;
    b3_val = b3_prev;
    best_epoch = epoch-1;
    end
    if k == 6
    save('DeepNeuralNet_katrine_BEST', 'w1_val', 'w2_val', ...
        'w3_val', 'b1_val', 'b2_val', 'b3_val', 'best_epoch')
    end
else
    k = 0;
end
%
MSE_val_prev = MSE_val;
w1_prev = w1;
w2_prev = w2;
w3_prev = w3;
b1_prev = b1;
b2_prev = b2;
b3_prev = b3;

%% Testing Network
%To check the accuracy of the NN
Numb_test = floor(0.15*samples);
mse_test_tot = 0;
for i = 1: Numb_test

    a0_test = input(Numb_train+Numb_val+i,:);
    target_test = target(Numb_train+Numb_val+i,:);

    n1_test = w1*a0_test'+b1;
    a1_test = Sigmoid(n1_test);

    n2_test = w2*a1_test'+b2;
    a2_test = Sigmoid(n2_test);

```

```
160     n3_test = w3*a2_test'+b3;
161     final_output = n3_test;
162
163
164     %error
165     error = final_output-target_test';
166     mse_error = error'*error;
167     mse_test_tot = mse_test_tot + mse_error;
168
169 end
170 %Calculating the mean square error
171 MSE_test = mse_test_tot/Numb_test;
172 MSE_plot_test(epoch) = MSE_test;
173
174 end
175 %% Plot
176 figure(1)
177 plot(MSE_plot_train)
178 hold on
179 plot(MSE_plot_val)
180 hold on
181 plot(MSE_plot_test)
182 title('Mean Square Error Plot')
183 ylabel('MSE')
184 xlabel('Epoch')
185 legend('Training', 'Validation', 'Test')
186
187 %% Saving data
188 % Saving the data from the last epoch if the validation error
189 % never increases
190 save('DeepNeuralNet_katrine_END', 'w1', 'w2', 'w3', 'b1', ...
191     'b2', 'b3', 'epoch')
```

# Appendix C

# Simulation Data

## C.1 Solar Irradiation Data

| Time | Solar irradiation [W/m$^2$] |
|---|---|
| 0 | 0 |
| 1 | 0 |
| 2 | 0 |
| 3 | 0 |
| 4 | 0 |
| 5 | 1.36 |
| 6 | 32.87 |
| 7 | 129.69 |
| 8 | 255.11 |
| 9 | 382.03 |
| 10 | 479.82 |
| 11 | 532.87 |
| 12 | 564.82 |
| 13 | 528.08 |
| 14 | 471.21 |
| 15 | 387.35 |
| 16 | 303.88 |
| 17 | 183.7 |
| 18 | 65.58 |
| 19 | 8.11 |
| 20 | 0 |
| 21 | 0 |
| 22 | 0 |
| 23 | 0 |

**Table C.1:** The average solar irradiation per hour for April in the Oslo area under normal conditions.

## C.2 Abnormal Solar Irradiation Data

| Time | Solar irradiation [W/m$^2$] |
|---|---|
| 0 | 0 |
| 1 | 0 |
| 2 | 0 |
| 3 | 0 |
| 4 | 0 |
| 5 | 1.36 |
| 6 | 32.87 |
| 7 | 129.69 |
| 8 | 255.11 |
| 9 | 382.03 |
| 10 | 479.82 |
| 11 | 532.87 |
| 12 | 0 |
| 13 | 0 |
| 14 | 0 |
| 15 | 0 |
| 16 | 0 |
| 17 | 0 |
| 18 | 0 |
| 19 | 0 |
| 20 | 0 |
| 21 | 0 |
| 22 | 0 |
| 23 | 0 |

**Table C.2:** Solar irradiation values when the sun stops shining at 12.

## C.3 Power Consumption Data

| Time | Load |
|---|---|
| 0 | 14.03 |
| 1 | 13.71 |
| 2 | 13.56 |
| 3 | 13.64 |
| 4 | 13.89 |
| 5 | 14.37 |
| 6 | 15.26 |
| 7 | 15.73 |
| 8 | 15.75 |
| 9 | 15.88 |
| 10 | 15.86 |
| 11 | 15.68 |
| 12 | 15.40 |
| 13 | 15.14 |
| 14 | 15.03 |
| 15 | 14.98 |
| 16 | 14.84 |
| 17 | 14.67 |
| 18 | 14.88 |
| 19 | 15.18 |
| 20 | 15.54 |
| 21 | 15.60 |
| 22 | 15.17 |
| 23 | 14.62 |

**Table C.3:** Power consumption data for every hour through out a day under normal conditions. The data is based on power consumption trends for April 2020.

## C.4 Abnormal Power Consumption Data

| Time | Load |
|---|---|
| 0 | 14.03 |
| 1 | 13.31 |
| 2 | 13.56 |
| 3 | 13.64 |
| 4 | 13.89 |
| 5 | 14.00 |
| 6 | 14.00 |
| 7 | 12.50 |
| 8 | 11.5 |
| 9 | 13.70 |
| 10 | 13.5 |
| 11 | 13.30 |
| 12 | 13.00 |
| 13 | 13.50 |
| 14 | 14.00 |
| 15 | 14.50 |
| 16 | 14.84 |
| 17 | 14.67 |
| 18 | 14.88 |
| 19 | 15.18 |
| 20 | 16.00 |
| 21 | 17.50 |
| 22 | 15.17 |
| 23 | 14.62 |

**Table C.4:** Power consumption data for every hour through out a day under random/abnomal conditions.

## C.5 EV-switch

| Time | Load |
|---|---|
| 0 | ON |
| 1 | ON |
| 2 | ON |
| 3 | ON |
| 4 | ON |
| 5 | ON |
| 6 | ON |
| 7 | ON |
| 8 | OFF |
| 9 | OFF |
| 10 | OFF |
| 11 | OFF |
| 12 | OFF |
| 13 | OFF |
| 14 | OFF |
| 15 | OFF |
| 16 | ON |
| 17 | ON |
| 18 | OFF |
| 19 | OFF |
| 20 | ON |
| 21 | ON |
| 22 | ON |
| 23 | ON |

**Table C.5:** Data showing at which times the EV is connected to the microgrid (ON) at at which times the EV is disconnected (OFF) under normal conditions.

# Bibliography


[1] BP p.l.c. bp statistical review of world energy 2020. Technical Report 69, 2020.

[2] Pravin P. Varaiya, Felix F. Wu, and Janusz W. Bialek. Smart operation of smart grid: Risk-limiting dispatch. *Proceedings of the IEEE*, 99(1):40–57, 2011.

[3] Julio Romero Aguero, Erik Takayesu, Damir Novosel, and Ralph Masiello. Modernizing the grid: Challenges and opportunities for a sustainable future. *IEEE Power and Energy Magazine*, 15(3):74–83, 2017.

[4] Benjamin Kroposki, Thomas Basso, and Richard DeBlasio. Microgrid standards and technologies. In *2008 IEEE Power and Energy Society General Meeting - Conversion and Delivery of Electrical Energy in the 21st Century*, pages 1–4, 2008.

[5] Mojaharul Islam, Fuwen Yang, and Mohammad Amin. Control and optimisation of networked microgrids: A review. *IET Renewable Power Generation*, 15(6):1133–1148, 2021.

[6] Stephen Frank, Ingrida Steponavice, and Steffen Rebennack. Optimal power flow: a bibliographic survey i. *Energy systems*, 3(3):221–258, 2012.

[7] Howard B. Demuth, Mark H. Beale, Orlando De Jess, and Martin T. Hagan. *Neural Network Design*. Martin Hagan, Stillwater, OK, USA, 2nd edition, 2014.

[8] Jack V Tu. Advantages and disadvantages of using artificial neural networks versus logistic regression for predicting medical outcomes. *Journal of clinical epidemiology*, 49(11):1225–1231, 1996.

[9] Sharara Rehimi, Rahmatollah Mirzaei, and Hassan Bevrani. Ann-based frequency and tie-line power control in interconnected microgrids. In *2019 6th International Conference on Control, Instrumentation and Automation (ICCIA)*, pages 1–6, 2019.

[10] Shravan Kumar Akula and Hossein Salehfar. Frequency control in microgrid communities using neural networks. In *2019 North American Power Symposium (NAPS)*, pages 1–6, 2019.

[11] Kuldip Singh, P. Swathi, and M. Ugender Reddy. Performance analysis of pv inverter in microgrid connected with pv system employing ann control. In *2014 International Conference on Green Computing Communication and Electrical Engineering (ICGCCEE)*, pages 1–6, 2014.

[12] Shoresh Shokoohi, Foad Sabori, and Hassan Bevrani. Secondary voltage and frequency control in islanded microgrids: online ann tuning approach. In *2014 Smart Grid Conference (SGC)*, pages 1–6, 2014.

[13] Divya R., Gopika N.P., and Manjula G. Nair. Ann based solar power forecasting in a smart microgrid system for power flow management. In *2019 Innovations in Power and Advanced Computing Technologies (i-PACT)*, volume 1, pages 1–6, 2019.

[14] Y Jaganmohan Reddy, Y V Pavan Kumar, V Sunil Kumar, and K Padma Raju. Distributed anns in a layered architecture for energy management and maintenance scheduling of renewable energy hps microgrids. In *2012 International Conference on Advances in Power Conversion and Energy Technologies (APCET)*, pages 1–6, 2012.

[15] Daniel E. Olivares, Ali Mehrizi-Sani, Amir H. Etemadi, Claudio A. Cañizares, Reza Iravani, Mehrdad Kazerani, Amir H. Hajimiragha, Oriol Gomis-Bellmunt, Maryam Saeedifard, Rodrigo Palma-Behnke, Guillermo A. Jiménez-Estévez, and Nikos D. Hatziargyriou. Trends in microgrid control. *IEEE Transactions on Smart Grid*, 5(4):1905–1919, 2014.

[16] Nagaraju Pogaku, Milan Prodanovic, and Timothy C. Green. Modeling, analysis and testing of autonomous operation of an inverter-based microgrid. *IEEE Transactions on Power Electronics*, 22(2):613–625, 2007.

[17] Hossein Lotfi and Amin Khodaei. Ac versus dc microgrid planning. *IEEE Transactions on Smart Grid*, 8(1):296–304, 2017.

[18] Md. Rasheduzzaman, Jacob A. Mueller, and Jonathan W. Kimball. Reduced-order small-signal model of microgrid systems. *IEEE Transactions on Sustainable Energy*, 6(4):1292–1305, 2015.

[19] Robert Lasseter, Abbas Akhil, Chris Marnay, John Stephens, Jeff Dagle, Ross Guttromsom, A Sakis Meliopoulous, Robert Yinger, and Joe Eto. Integration of distributed energy resources. the certs microgrid concept.

[20] Huang Jiayi, Jiang Chuanwen, and Xu Rong. A review on distributed energy resources and microgrid. *Renewable and Sustainable Energy Reviews*, 12(9):2472–2483, 2008.

[21] Joan Rocabert, Alvaro Luna, Frede Blaabjerg, and Pedro Rodríguez. Control of power converters in ac microgrids. *IEEE Transactions on Power Electronics*, 27(11):4734–4749, 2012.

[22] Matthew Clayton Such and Glenn Y. Masada. Bess control on an microgrid with significant wind generation. In *2017 IEEE Power Energy Society General Meeting*, pages 1–5, 2017.

[23] S. X. Chen, H. B. Gooi, and M. Q. Wang. Sizing of energy storage for microgrids. *IEEE Transactions on Smart Grid*, 3(1):142–151, 2012.

[24] Chunguang Ren, Longfeng Liu, Xiaoqing Han, Baifu Zhang, Lei Wang, and Peng Wang. Multi-mode control for three-phase bidirectional ac/dc converter in hybrid microgrid under unbalanced ac voltage conditions. In *2019 IEEE Energy Conversion Congress and Exposition (ECCE)*, pages 2658–2663, 2019.

[25] Reza Rahmani and Ahmad Fakharian. A novel method for connecting the pv unit to hybrid microgrid systems based on smart controlling structure. In *2016 24th Iranian Conference on Electrical Engineering (ICEE)*, pages 1439–1443, 2016.

[26] Xiong Liu, Peng Wang, and Poh Chiang Loh. A hybrid ac/dc microgrid and its coordination control. *IEEE Transactions on Smart Grid*, 2(2):278–286, 2011.

[27] Josep M Guerrero, Juan C Vasquez, José Matas, Luis García De Vicuña, and Miguel Castilla. Hierarchical control of droop-controlled ac and dc microgrids—a general approach toward standardization. *IEEE Transactions on industrial electronics*, 58(1):158–172, 2010.

[28] F. Katiraei and M.R. Iravani. Power management strategies for a microgrid with multiple distributed generation units. *IEEE Transactions on Power Systems*, 21(4):1821–1831, 2006.

[29] Farzam Nejabatkhah and Yun Wei Li. Overview of power management strategies of hybrid ac/dc microgrid. *IEEE Transactions on Power Electronics*, 30(12):7072–7089, 2015.

[30] Josep M. Guerrero, Lijun Hang, and Javier Uceda. Control of distributed uninterruptible power supply systems. *IEEE Transactions on Industrial Electronics*, 55(8):2845–2859, 2008.

[31] Kamran Sharifabadi, Lennart Harnefors, Hans-Peter Nee, Staffan Norrga, and Remus Teodorescu. *Design, control, and application of modular multilevel converters for HVDC transmission systems*. John Wiley & Sons, 2016.

[32] K. Sharifabadi, L. Harnefors, H.-P. Nee, S. Norrga, and R. Teodorescu. *Design, Control, and Application of Modular Multilevel Converters for HVDC Transmission Systems*. Wiley - IEEE Press, 2016.

[33] L. Papangelis, M. Debry, T. Prevost, P. Panciatici, and T. Van Cutsem. Stability of a voltage source converter subject to decrease of short-circuit capacity: A case study. In *2018 Power Systems Computation Conference (PSCC)*, pages 1–7, 2018.

[34] L. A. Lamont, D. Jovcic, and K. Abbott. Fast direct voltage controller for vsc transmission. In *39th International Universities Power Engineering Conference, 2004. UPEC 2004.*, volume 3, pages 1135–1139 vol. 2, 2004.

[35] G. E. Mejía Ruiz, N. Muñoz, and J. B. Cano. Modeling, analysis and design procedure of lcl filter for grid connected converters. In *2015 IEEE Workshop on Power Electronics and Power Quality Applications (PEPQA)*, pages 1–6, 2015.

[36] T. C. Y. Wang, Zhihong Ye, Gautam Sinha, and Xiaoming Yuan. Output filter design for a grid-interconnected three-phase inverter. In *IEEE 34th Annual Conference on Power Electronics Specialist, 2003. PESC '03.*, volume 2, pages 779–784 vol.2, 2003.

[37] A. Reznik, M. G. Simões, A. Al-Durra, and S. M. Muyeen. $lcl$ filter design and performance analysis for grid-interconnected systems. *IEEE Transactions on Industry Applications*, 50(2):1225–1232, 2014.

[38] Q. Zhong and Y. Zeng. Universal droop control of inverters with different types of output impedance. *IEEE Access*, 4:702–712, 2016.

[39] Q. Zhong, W. Ming, and Y. Zeng. Self-synchronized universal droop controller. *IEEE Access*, 4:7145–7153, 2016.

[40] M. Amin, Q. C. Zhong, and Z. Lyu. An anti-islanding protection for vsm inverters in distributed generation. *IEEE Open Journal of Power Electronics*, 1:372–382, 2020.

[41] M. Amin and Q. Zhong. Resynchronization of distributed generation based on the universal droop controller for seamless transfer between operation modes. *IEEE Transactions on Industrial Electronics*, 67(9):7574–7582, 2020.

[42] N. Mohan, T. M. Undeland, and W. P. Robbins. *Power Electronics. Converters, Applications, and Design*. John Wiley and Sons, INC, third edition, 2003.

[43] J. Holtz. Pulsewidth modulation-a survey. *IEEE Transactions on Industrial Electronics*, 39(5):410–420, 1992.

[44] Yeong-Chau Kuo, Tsorng-Juu Liang, and Jiann-Fuh Chen. Novel maximum-power-point-tracking controller for photovoltaic energy conversion system. *IEEE Transactions on Industrial Electronics*, 48(3):594–601, 2001.

[45] T. Esram and P. L. Chapman. Comparison of photovoltaic array maximum power point tracking techniques. *IEEE Transactions on Energy Conversion*, 22(2):439–449, 2007.

[46] B. Subudhi and R. Pradhan. A comparative study on maximum power point tracking techniques for photovoltaic power systems. *IEEE Transactions on Sustainable Energy*, 4(1):89–98, 2013.

[47] M. A. G. de Brito, L. Galotto, L. P. Sampaio, G. d. A. e Melo, and C. A. Canesin. Evaluation of the main mppt techniques for photovoltaic applications. *IEEE Transactions on Industrial Electronics*, 60(3):1156–1167, 2013.

[48] Deepak Ravi, Bandi Reddy, Shimi Sudha Letha, and Paulson Samuel. Bidirectional dc to dc converters: An overview of various topologies, switching schemes and control techniques. *International Journal of Engineering and Technology*, 7:360–365, 09 2018.

[49] M. Saleh, Y. Esa, Y. Mhandi, W. Brandauer, and A. Mohamed. Design and implementation of ccny dc microgrid testbed. In *2016 IEEE Industry Applications Society Annual Meeting*, pages 1–7, 2016.

[50] M. S. Saleh, A. Althaibani, Y. Esa, Y. Mhandi, and A. A. Mohamed. Impact of clustering microgrids on their stability and resilience during blackouts. In *2015 International Conference on Smart Grid and Clean Energy Technologies (ICSGCE)*, pages 195–200, 2015.

[51] R.C. Burchett, H.H. Happ, and K.A. Wirgau. Large scale optimal power flow. *IEEE Transactions on Power Apparatus and Systems*, PAS-101(10):3722–3732, 1982.

[52] J Carpentier. Optimal power flows. *International Journal of Electrical Power & Energy Systems*, 1(1):3–15, 1979.

[53] Mohammad A Abido. Optimal power flow using particle swarm optimization. *International Journal of Electrical Power & Energy Systems*, 24(7):563–571, 2002.

[54] C.N. Lu, S.S. Chen, and C.M. Ing. The incorporation of hvdc equations in optimal power flow methods using sequential quadratic programming techniques. *IEEE Transactions on Power Systems*, 3(3):1005–1011, 1988.

[55] Yujie Tang, Krishnamurthy Dvijotham, and Steven Low. Real-time optimal power flow. *IEEE Transactions on Smart Grid*, 8(6):2963–2973, 2017.

[56] D. Gan, R.J. Thomas, and R.D. Zimmerman. Stability-constrained optimal power flow. *IEEE Transactions on Power Systems*, 15(2):535–540, 2000.

[57] RC Bansal. Optimization methods for electric power systems: An overview. *International Journal of Emerging Electric Power Systems*, 2(1), 2005.

[58] Hermann W. Dommel and William F. Tinney. Optimal power flow solutions. *IEEE Transactions on Power Apparatus and Systems*, PAS-87(10):1866–1876, 1968.

[59] The European Commission. Photovoltaic geographical information system, 2021.

[60] Xiangyun Qing and Yugang Niu. Hourly day-ahead solar irradiance prediction using weather forecasts by lstm. *Energy*, 148:461–468, 2018.

[61] Statnett. Data from the power system, 2021.

[62] A.K. Jain, Jianchang Mao, and K.M. Mohiuddin. Artificial neural networks: a tutorial. *Computer*, 29(3):31–44, 1996.

[63] Tara H Abraham. (physio) logical circuits: The intellectual origins of the mcculloch–pitts neural networks. *Journal of the History of the Behavioral Sciences*, 38(1):3–25, 2002.

[64] IBM Cloud Education. Neural networks. `https://www.ibm.com/cloud/learn/neural-networks`. Accessed: 2021-04-22.

[65] Z. Zhang. *Artificial Neural Network. In: Multivariate Time Series Analysis in Climate and Environmental Research*. Springer, Cham, 2018.

[66] Balázs Csanád Csáji et al. Approximation with artificial neural networks. *Faculty of Sciences, Etvs Lornd University, Hungary*, 24(48):7, 2001.

[67] Kenji Suzuki. *Artificial Neural Networks - Methodological Advances and Biomedical Applications*. 04 2011.

[68] Xiaoheng Jiang, Yanwei Pang, Xuelong Li, Jing Pan, and Yinghong Xie. Deep neural networks with elastic rectified linear units for object recognition. *Neurocomputing*, 275:1132–1139, 2018.

[69] M.A. Sartori and P.J. Antsaklis. A simple method to derive bounds on the size and to train multilayer neural networks. *IEEE Transactions on Neural Networks*, 2(4):467–471, 1991.

[70] David E Rumelhart, Geoffrey E Hinton, and Ronald J Williams. Learning representations by back-propagating errors. *nature*, 323(6088):533–536, 1986.

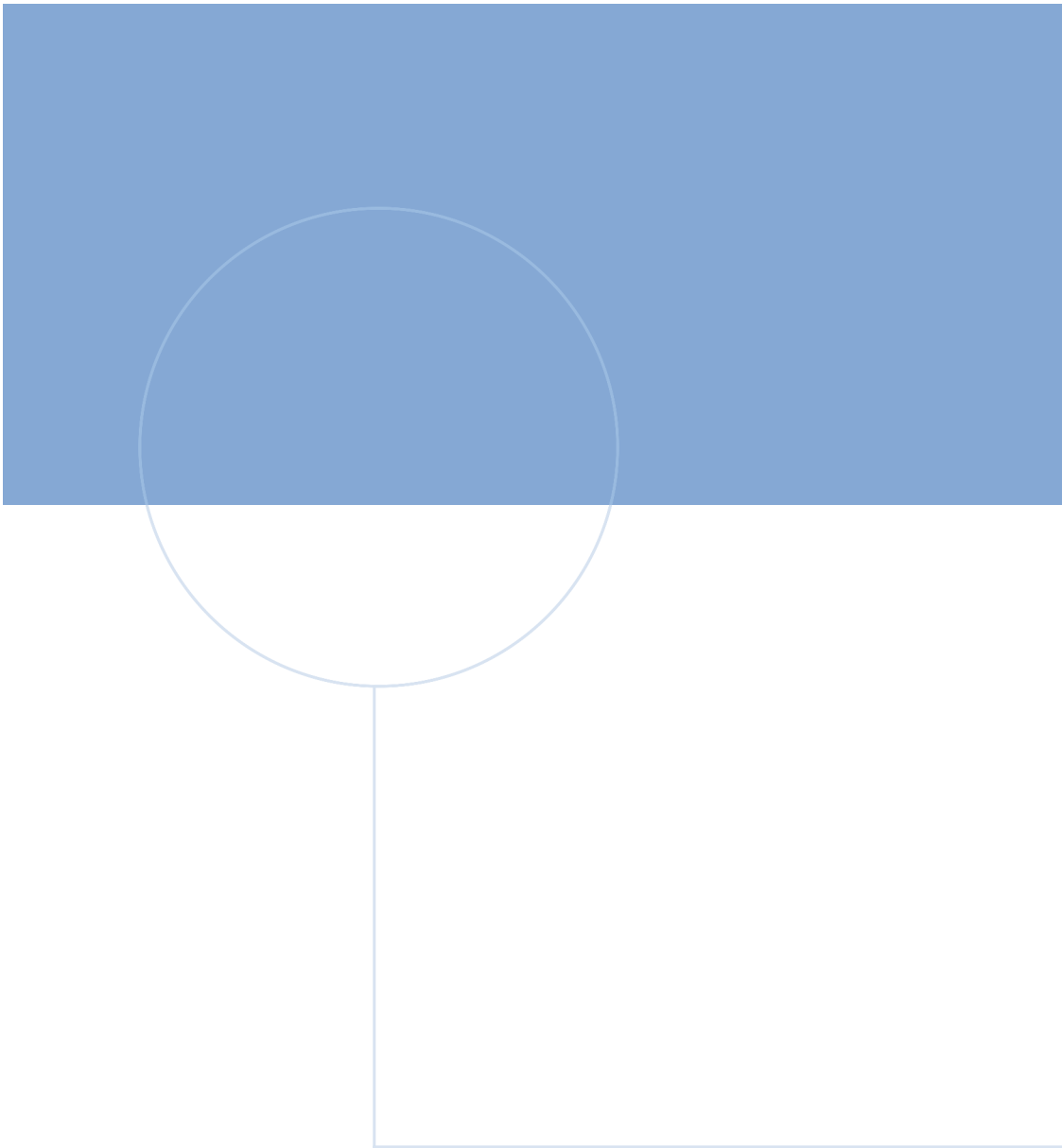

NTNU

Norwegian University of
Science and Technology